BRNO UNIVERSITY OF TECHNOLOGY

FACULTY OF MECHANICAL ENGINEERING
HEAT TRANSFER AND FLUID FLOW LABORATORY

POLYMERIC HOLLOW FIBER HEAT EXCHANGER DESIGN

PhD THESIS

AUTHOR ILYA ASTROUSKI

SUPERVISOR prof. Ing. MIROSLAV RAUDENSKÝ, CSc.

SUPERVISOR-SPECIALIST Ing. PETR KOTRBÁČEK, Ph.D.

BRNO 2016

ABSTRACT

This Ph.D. thesis is focused on theory and experimental investigations developing of new knowledge about polymeric hollow fiber heat exchanger (PHFHE). The state-of-the-art study of plastic heat exchangers shows that their usage is limited by several niches where their advantages significantly dominates, or where the use of non-plastic competitors is not impossible. On the other hand, plastic heat exchangers (and PHFHEs in particular) are devices of increasing interest. It is shown that use of small tubes (fibers) allows PHFHEs to be more competitive than conventional plastic heat exchangers. Small hydraulic diameter of a fiber causes high heat transfer coefficients, reduces thermal resistance of plastic wall and allows it to create light and compact design.

Detailed study of fluid flow and heat transfer inside the hollow fiber showed that conventional approaches for single-phase laminar flow can be utilized. Poiseuille number equal to 64 and Nussel number about 4 are recommended to be used to predict pressure drops and heat transfer coefficient, respectively. Additional attention should be paid to careful determination of fiber diameter and liquid properties (viscosity). Scaling effects, such as axial heat conduction, thermal entrance region and viscous dissipation can be neglected.

The study of outside heat transfer showed that heat transfer on fiber bunches are intense and are competitive to contemporary compact finned-tube heat exchangers. The Grimson approach showed clear correlation with experimental results and, thus is recommended to predict heat transfer coefficients on fiber bunches.

Two types of fouling (particulate- and biofouling) of outer fiber surface were experimentally studied. It was found that particulate fouling by titanium oxide particles is not intense and deposits can be removed relatively easy. However, fouling is much more intense when it is associated with biofouling caused by wastewater. In this case, smooth and low-adhesive surface of plastic is not sufficient precaution to prevent deposit formation.

KEYWORDS

Heat exchanger, microchannels, polymeric hollow fibers, plastics, forced convection, natural convection, heat transfer coefficient, pressure drop, particulate fouling, biofouling

BIBLIOGRAPHIC CITATION

ASTROUSKI, I. Brno: *Polymeric Hollow Fiber Heat Exchanger Design*. Brno University of Technology, Faculty of Mechanical engineering, 2016. 91 pp., Supervisor of doctoral thesis: prof. Ing. Miroslav Raudenský, CSc.

DECLARATION

I declare that the thesis hereby submitted for the Philosophiae Doctor degree at Brno University of Technology is my own work under supervision of prof. Ing. Miroslav Raudenský, CSc., has not been previously submitted at any other University for any degree and all sources were quoted completely and correctly.

Place : .....Brno.....
Date : .....

.....
Author's signature

ACKNOWLEDGEMENTS

Herein, I would like to express my sincere gratitude to my supervisor Prof. Miroslav Raudenský for his continued support of my Ph.D studies, valuable scientific and life advice. I am also very grateful to all my colleagues from the Heat Transfer and Fluid Flow Laboratory. This thesis would not exist without your technical support, discussions and advice. Last but not least, I would like to thank my parents, my sister and all my relatives and friends for supporting me mentally throughout the thesis, and in all aspects of my life.

CONTENT

INTRODUCTION

Different types of heat exchangers are used in many fields of industry. Conventional heat exchangers are made of metals; the most widely used are copper, aluminium and steel. However, some special applications require heat exchangers which are resistant to chemicals and corrosion so plastics were chosen as a convenient material. They are light, chemically resistant and cheaper than corrosion-resistant alloys. Except corrosive applications, plastic heat exchangers are also used in several other fields such as low-temperature water heating, automotive and aerospace industry, food processing industry, biotechnology, etc. Niche application of plastics can be explained by the fact that metal heat exchangers have long history of application, production technologies are well-designed; moreover, companies do not want to depart from well-established practices. Nevertheless, we suppose that the possibility of plastic heat exchangers application need to be reconsidered based on the growth of the overall technological level, and the development in the field of material sciences.

Concept of the polymeric hollow fiber heat exchanger (PHFHE) was proposed about two decades ago. Small diameter of the hollow fibers is the basis to make a heat exchanger with high characteristics because it reduces thermal resistance of the polymer wall, causes high convective heat transfer coefficients and provides possibility to achieve a high ratio of compactness. Since that time, about 20 scientific papers concerning PHFHEs were published. Also worth noting that different types of hollow fibers are commercially available; however, PHFHEs are not produced commercially. It can be explained by the fact that available hollow fibers are not intended to heat transfer applications and are relatively expensive. The connection of hundreds and even thousands of fibers in one heat transfer element is not a simple task too. Furthermore, PHFHEs should be designed taking into account the peculiarity of hollow fibers. A conventional heat exchanger design theory can be applied, but is not completely sufficient and several questions require additional study. This work is intended to choose or develop sufficient approaches for modelling fluid flow and heat transfer in PHFHEs studied in Heat Transfer and Fluid Flow Laboratory (HeatLab). Particularly, the following questions are considered as important for the project and will be studied in the thesis:

- analysis of single-phase fluid flow and heat transfer of liquid inside of polymeric hollow fiber
- heat transfer on the bunch of straight hollow fibers
- particulate and biological fouling of polypropylene hollow fibers

1 GENERAL INFORMATION ABOUT HEAT EXCHANGERS

Heat exchangers are devices that provide the flow of thermal energy between two or more fluids at different temperatures. Heat exchangers are used in a wide variety of applications. These include power production; process, chemical and food industries; electronics; environmental engineering; waste heat recovery; manufacturing industry; and air-conditioning, refrigeration, and space applications [1].

1.1 Basic Heat Exchanger Types and Configurations

Heat exchangers may be classified according different criteria [1]:

- Recuperators and regenerators
- Transfer process: direct contact and indirect contact
- Geometry of construction: tubes, plates and extended surface
- Heat transfer mechanisms: single-phase and two-phase
- Flow arrangements: parallel-, counter- and crossflows.

Recuperator is a heat exchanger which transfers (recuperates) heat between two streams through a separating wall or through the interface (in the case of direct contact type heat exchanger). The biggest part of conventional heat exchangers is recuperators. In regenerators (storage type heat exchangers) fluids flow through the heat exchanger alternately. Thermal energy is accumulating by the heat exchanger mass when hot liquid is flowing through it. This energy will be returned back to cold liquid when it will flow through heat exchanger. Regenerators can be classified as follows: rotary regenerators and fixed matrix regenerators.

In direct contact heat exchangers, heat is transferred between the cold and hot fluids through direct contact between these fluids [1]. There is no wall between two streams, and the heat transfer occurs through the interface between two immiscible liquids, a gas-liquid pair, or solid particle-fluid combination. In indirect contact heat exchangers, the heat energy is exchanged between hot and cold fluid through a heat transfer surface.

By geometry heat exchangers can be divided on tubular, plate and extended surface. Tubular heat exchangers are built out of circular tubes. The most common ones are double-pipe, shell-and-tube and spiral tubular heat exchangers. A typical double pipe heat exchanger consists of one pipe placed concentrically inside another of larger diameter with appropriate fittings to direct the flow from one section to the next. The major use of double-pipe

exchangers is for sensible heating or cooling of process liquids [1]. This design is also extremely suitable for high pressure application.

Shell-and-tube heat exchangers are built out of tubes which are mounted in cylindrical shells with the tubes axis parallel to that of the shell. They are widely used as oil coolers, power plants, steam generators in nuclear plant, in process applications, and in chemical industries. Some of the fluid flows through the tubes while another one flows on the shell side, across or along the tubes. There are a lot of different configurations of tube-and-shell heat exchangers (one-pass or multi-pass configuration, with one or several shells).

Spiral-tube heat exchanger is constructed from a spirally wound coil which is placed inside the shell. The heat transfer coefficient is higher in a spiral tube than in a straight one. This type is suitable for clean fluids, since cleaning is almost impossible [1].

Plate heat exchangers are built out of thin plates forming flow channels. The fluid streams are separated by flat plates or plates with corrugated fins. Plate heat exchangers are used for transferring heat for any combination of gas, liquids, and two-phase streams. Those heat exchangers can be further classified as gasketed plate, spiral plate, or lamella.

Extended surface heat exchangers are devices with fins or appendages on the primary heat transfer surface (tubular or plate) [1]. It is well known that the heat transfer coefficient on the gas side is much lower than those on the liquid side, finned heat transfer surfaces are used on the gas side to increase the heat transfer area. Fins are widely used in gas-to-gas and gas-liquid heat exchangers whenever the heat transfer coefficient on one or both sides is low and there is a need for a compact heat exchanger. The two most common types of extended surface heat exchangers are plate-fin heat exchangers and tube-fin heat exchangers.

According heat transfer mechanism heat exchangers can be classified as: single-phase convection on both sides, single-phase convection on one side and two-phase convection on other side, two-phase convection on both sides. Commonly two-phase convection is associated with phase change processes (boiling, condensing) but it can also occur if mixture flows (e.g. suspension of solid particles in liquid).

There are three basic flow arrangements of heat exchangers: parallel-flow, counter-flow and cross-flow. In parallel-flow heat exchangers, the two fluid streams enter together at one end, flow through in the same direction, and leave together at the other end. In counter-flow heat exchangers, two fluid streams flow in opposite directions. In a single cross-flow heat exchanger, one fluid flows through the heat transfer surface at right angles to the flow path of

the other fluid [1]. In practice, basic flow arrangements are often combined in more complex ones. For example, in a U-baffled tube single-pass shell-and-tube heat exchanger, one fluid flows through the U-tube while the other fluid flows first downwards and then upwards, across the flow path of the other fluid stream. Thus there are two basic arrangements which are realized in this heat exchanger: cross-counter and cross-parallel flow. Moreover, cross-flow can be called mixed and unmixed depending on the design. If fluid flows through the tubes or channels it cannot move in a transverse direction. Thus separated layers of stream cannot mix between each other and the flow should be considered as unmixed. Otherwise flow should be considered as mixed. It should be mentioned that partial mixing conditions may exists in practice and should be properly considered [2].

1.2 Compact Heat Exchangers

Compact heat exchanger is that one which incorporates a large amount of heat transfer surface area per unit volume. According to [3] compact surface it is defined as a surface which has surface area density of 700 m^2/m^3 (gas-side compact surface) or 400 m^2/m^3 (liquid-side compact surface) (see Figure 1).

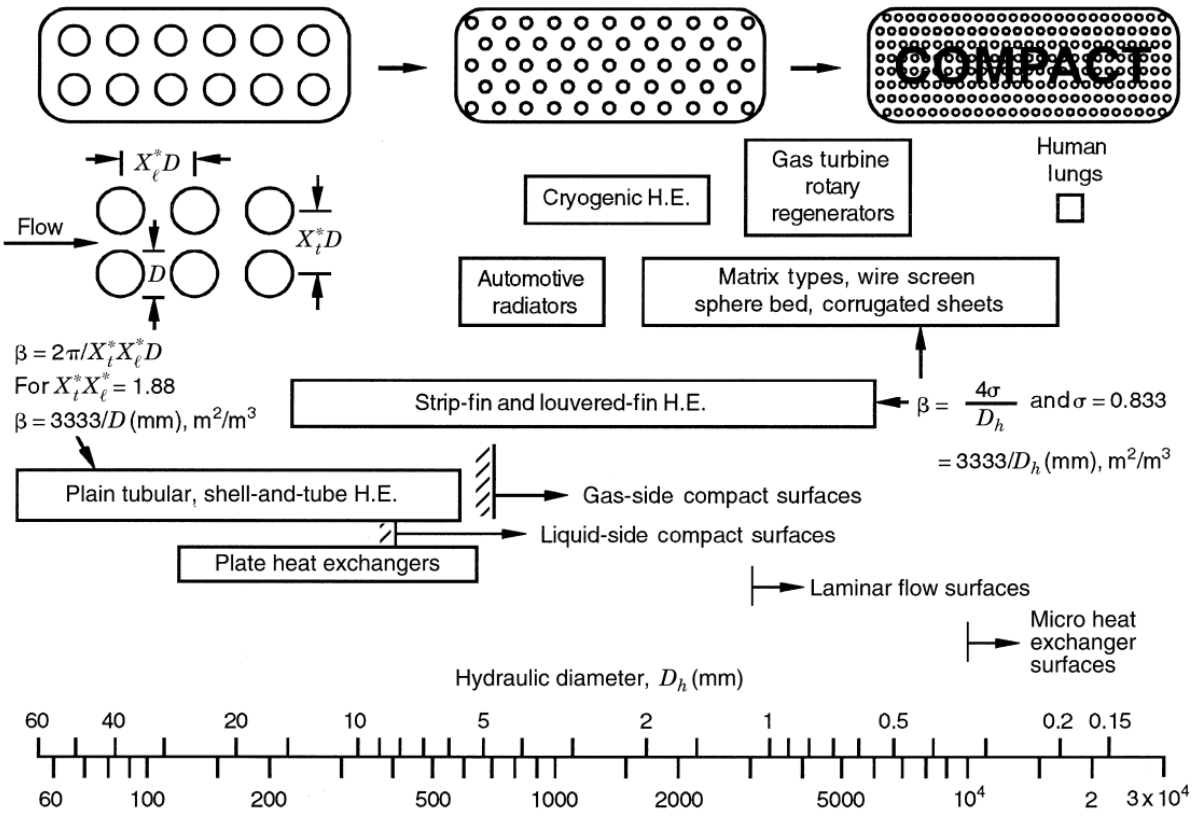

Fig. 1 *Overview of compact heat transfer surfaces [1]*

One of the encouraging aspects of heat exchanger development in the previous decades has been that the historical sectorial divisions utilizing compact heat exchangers have been breaking down. Previously compact heat exchanger were mainly used in refrigeration, power, automotive, aerospace, process and cryogenic industries, but now they have gone beyond these areas (see Fig. 1). PHFHEs seem to be designed as compact mainly and can compete with conventional metal heat exchangers. It will be shown later (see chapter 3.3.4) that structure of fibers of diameter less than 1 mm achieve surface area density of 700 m^2/m^3 and higher. Specific characteristics of compact heat exchangers are discussed in detail in [3]. The following features are mentioned:

- Usually with extended surfaces (fins)
- A high heat-transfer surface area per unit volume of the core
- Small hydraulic diameter
- Usually at least one of the fluids is a gas
- Fluids must be clean and relatively non-fouling because of small hydraulic diameter flow passages and difficulty in cleaning
- The fluid pumping power (i.e., pressure drop) consideration is as important as the heat transfer rate
- Operating pressures and temperatures are limited to a certain extent compared to shell and tube exchangers due to thin fins, plates or tubes
- The use of highly compact surfaces results in an exchanger with a large frontal area and a short flow length; therefore, the header design of a compact heat exchanger is important for a uniform flow distribution.

The fundamental parameter describing compactness is the hydraulic diameter D_h:

$$D_h = \frac{4A_cL}{A_s} \quad (1)$$

where A_c is flow area, L is length of flow and A_s is surface area. For some types of surfaces the flow area A_c varies with flow length, so for these an alternative definition is

$$D_h = \frac{4V_s}{A_s} \quad (2)$$

where V_s is the enclosed (wetted) volume. Next parameter, ratio between enclosed and whole volume, is so-called porosity σ:

$$\sigma = \frac{V_s}{V} \quad (3)$$

And finally the main parameter which is often used as measure of compactness is surface area density:

$$\beta = \frac{A_s}{V} = \frac{4\sigma}{D_h} \quad (4)$$

Overall heat transfer coefficient *U* can be combined together with surface area density to achieve the second parameter of compactness. It is so-called conductance per unit volume (*CUV*) which can be expressed as:

$$CUV = \beta U \quad (5)$$

1.3 Heat Exchanger Performance Criteria

The application of heat transfer principles in the equipment design and achievement of a specific goal is very important, but economic feasibility is important too. Eventually, the economy plays a decisive role in the selection and development of heat transfer equipment, and the designer should take this into consideration when solving a technical problem. Each specific situation dictates its own requirements and criteria that must be observed. For example, the heat exchanger's size and weight are of great importance if used in the aircraft or space industry. These parameters may even be the main criteria for selection in some cases, but in conventional applications the size and weight are just parameters of the cost which should be taken into account. Thermal performance parameters provide a base to obtain size, weight and cost and are of great importance as well.

Thus, the cost (of heat transfer) is main parameter in the majority of application. Rather than talking about the price of the heat exchanger, it is better to talk about the complete costs of the utilization of the heat exchanger. This is because the cost of full life-cycle support of the heat exchanger (design, manufacture, exploitation, recycling) and its net cost may vary significantly. In general, these costs can be split into capital costs (implementation) and operating costs (they depend on time and conditions of operation). Capital cost includes the cost of design, manufacturing, transportation and installation of heat transfer equipment. Operating costs can be roughly estimated proportional to the time of the operation. They include the cost of pumping heat transfer mediums through a heat exchanger and the maintenance costs (monitoring, service, cleaning and repairing).

As already mentioned, the size of the equipment is important. The space available for equipment placed in the vehicle's compartment is significantly limited. It means that compact heat exchanger designs are preferable in this case. In addition, dimensions determine space

requirements in the machine room and affect the cost of transportation and installation. Heat exchanger weight is a very important characteristic if installed in a vehicle, because it increases the overall vehicle weight and, respectively, fuel consumption. Moreover, weight determines the cost of material. Heat exchange equipment are manufactured mainly from steel (stainless steel is most commonly used), copper, aluminium, titanium, nickel alloys, so the cost of the material in the cost of the heat exchanger can be up to 80 percent or more. Thus, weight reduction allows a significant decrease in the manufacturing costs of a heat exchanger. Weight and size are crucial in determining the costs of transportation and installation too.

The next group of parameters describes the thermal performance of heat exchanger. Heat transfer rate Q is basic and most important among them. It is the amount of heat that is transferred by heat exchanger per unit of time in certain conditions. Many factors affecting heat transfer rate can be mentioned. Some of them are directly related to heat exchanger (size, geometry configuration, material). Others are connected with process characteristics (thermophysical properties of mediums, flow rates and temperatures). Thus, heat transfer rate of a heat exchanger cannot be specified by itself, but for the prescribed conditions only.

An essential, and often the most uncertain, part of any heat exchanger analysis is the determination of the overall heat transfer coefficient (OHTC). It is expressed as:

$$U = \frac{Q}{A\,F\,\Delta T_{lm}} \tag{6}$$

where A is heat transfer area, ΔT_{lm} is logarithmic temperature difference (LMTD), F is correction factor for LMTD. On the other hand, OHTC can be determined by accounting thermal resistances to heat transfer (convection and conduction resistances) between fluids. For instance, for heat transfer through a cylindrical wall, the OHTC is expressed as:

$$U = \frac{1}{\frac{1}{h_o}+\frac{D_o ln(D_o/D_i)}{2k_w}+\frac{D_o}{D_i h_i}} \tag{7}$$

It should be mentioned that during normal heat exchanger operation, surface is often the object to fouling and this effect should be taken into account by introducing additional thermal resistance.

Heat exchanger effectiveness ε is defined as a ratio between actual and maximum possible heat transfer rate:

$$\varepsilon = \frac{Q}{Q_{max}} \tag{8}$$

Actual heat transfer rate may be determined based on either the energy lost by the hot fluid or the energy gained by the cold fluid:

$$Q = \dot{m}_h c_{p,h}(T_{h,i} - T_{h,o}) = \dot{m}_c c_{p,c}(T_{c,i} - T_{c,o}) \quad (9)$$

To determine the maximum possible heat transfer for the exchanger, we first recognize that this maximum value could be attained if one of the fluids were to undergo a temperature change equal to the maximum temperature difference present in the exchanger, which is the difference in the entering temperatures for the hot and cold fluids [3]. Evidently, it can be done by liquid with lower heat capacity rate because the energy balance requires that the energy received by one fluid be equal to that given up by the other fluid. Thus maximum possible heat transfer rate is expressed as:

$$Q_{max} = C_{min}(T_{h,i} - T_{c,i}) \quad (10)$$

where C_{min} is equal to $\dot{m}_c c_c$ or $\dot{m}_h c_h$, whichever is smaller. By definition the effectiveness, which is dimensionless, must be in the range $0 < \varepsilon < 1$. It is useful because, if ε, $T_{h,i}$, and $T_{c,i}$ are known, the actual heat transfer rate may be readily determined from the expression:

$$Q = \varepsilon C_{min}(T_{h,i} - T_{c,i}) \quad (11)$$

For any heat exchanger, it can be shown that effectiveness is a function of heat capacity ratio and the grouping of terms UA/C_{min} [3]:

$$\varepsilon = f\left(\frac{UA}{C_{min}}, \frac{C_{min}}{C_{max}}\right) \quad (12)$$

This dimensionless grouping is called number of transfer units (*NTU*) because it indicates the size of the heat exchanger:

$$NTU = \frac{UA}{C_{min}} \quad (13)$$

It is seen that numerator of fraction includes heat transfer area and OHTC and thus presents possibility of heat exchanger to transfer heat. The denominator is a minimum heat capacity rate which represents maximum heat amount which can be transferred. Therefore, *NTU* shows the "size" of heat exchanger related to certain conditions.

2 STATE OF THE ART CONCERNING PLASTIC HEAT EXCHANGERS

2.1 Commercially Available Plastic Heat Exchangers

Plastic tubes are widely used in the construction industry to create heat exchange systems e.g. for underfloor heating. Fig. 2a shows typical tube heating systems. PP-R (polypropylene copolymer) tubes are commonly used for this purpose. Non-isolated Magen eco-Energy panels are designed for heating/cooling applications [13]. For example, Agrimat is a root-zone heating system for greenhouses (see Fig. 2b). It is simple, low-cost and light-height. Its length is unlimited and width is multiple to 30 cm; working pressure is up to 4 bar at 60 ºC.

The largest group of plastic heat exchangers consists of applications for corrosive and aggressive environment in the chemical industry. For example, the plastic heat exchangers are widely used in electroplating, electroforming and electroless plating baths; acidic and alkaline solutions for etching, chemical milling, anodizing, cleaning, stripping, electropolishing, continuous steel pickling applications and other similar operations.

One of the largest world manufacturers, Calorplast [7], produces different types of plastic heat exchangers for a wide range of applications. Depending on type and application, this company produces heat exchangers from polypropylene (PP), standard polyethylene (PE) and polyethylene of raised temperature resistance (PE-RT), polyvinylidene fluoride (PVDF) and perfluoroalkoxy (PFA). Permissible working temperatures of heat exchangers are -30 to +140 °C (depending on the material) and the reliable working pressure is 3-16 bar (depending on the material and the working temperature).

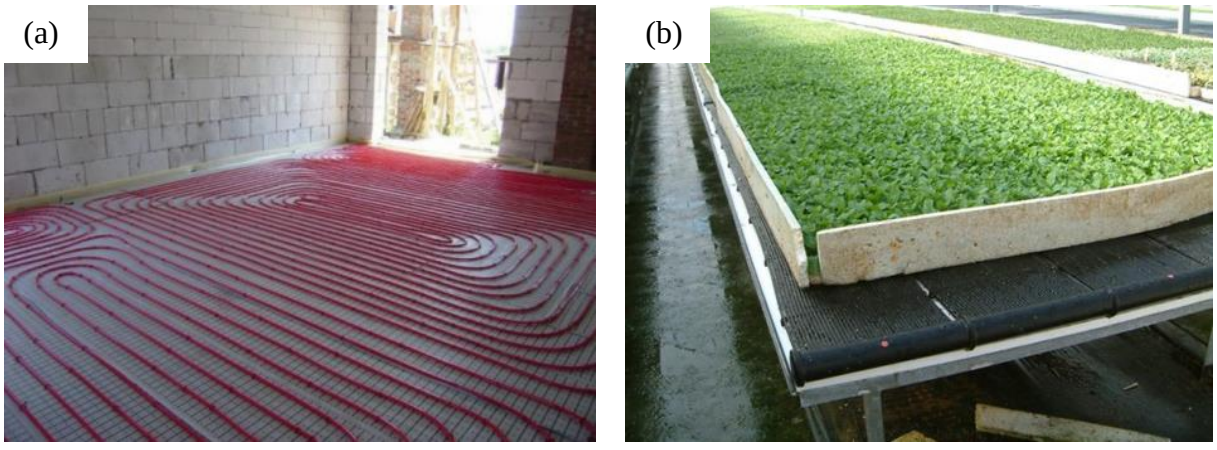

Fig. 2 *Underfloor heating systems made of plastic tubing and (b) Magen eco-Energy Agrimat heating system [13]*

Calorplast immersion-type heat exchangers (see Fig. 3a) are suitable for heating and cooling highly concentrated anorganic acids, high-purity media or aggressive and surface-encrusting fluids in tanks and baths. They are important components in surface technology and the chemical industry. These heat exchangers are easy to clean with pressurized water, steam or chemicals, guaranteeing a long operating time. Calorplast shell-and-tube heat exchanger (see Fig. 3b) is intended to exchange heat between high-purity media. It can be used as heater, cooler, condenser or evaporator. The heat exchanger has a compact design and good thermal performance because it uses thin-walled tubes (outer tube diameter is about 5 mm). It has low fouling and can be easily cleaned with pressurized water and, depending on the material, steam.

Fig. 3 *Calorplast heat exchangers for aggressive environment: (a) immersion-type; (b) shell-and-tube type; (c) gas-to-liquid type and (d) plate type [7].*

Calorplast gas-to-liquid heat exchangers (see Fig. 3c) are used in heat recovery systems to utilize heat from aggressive exhaust air or gases in surface technology, chemical or the electronics industry, to cool or heat airflow with ground- or seawater, in very pure conditions or conditions with high hygienic requirements. In addition, they are applied as condensers in the chemical and pharmaceutical industries. These heat exchangers are easy to clean with pressurized water, steam or chemicals, guaranteeing a long operating time.

Calorplast plate heat exchangers (see Fig. 3d) are intended for heat transfer between low-viscosity liquids. They are used as heaters, coolers, condensers or evaporators in surface technology, the chemical industry, biogas generation, seawater aquariums, and in the semi-conductor and pharmaceutical industries. The main feature of this heat exchanger is that different alignment of plates can be realized depending on application.

Fig. 4 *Polytetra plastic heat exchangers: (a) Polytetraflon shell-and-tube type (b) Polytetraflon Mini type (c) Thermoron modular type (d) Polytetraflon Multi-surface type (e) Polytetraflon Suspendedtype [8].*

Different heat exchangers for the chemical industry are produced by Polytetra [8]. Plastics such as PP, PVDF, PTFE (Poly-tetra-fluoro-ethylene), PFA and ECTFE (Ethylene-chloro-tri-fluoro-ethylene) are used. Different designs and constructions are available: shell-and-tube, so called “suspended and plug-in”, “multiple-surface”, “modular” (see Fig. 4). Main feature of Polytetra heat exchangers is a compact design. Working conditions depends on material type and type of design.

Another group of applications includes pharmaceutical, biotechnology and food industries where ultra-pure and chemically neutral heat exchangers are needed. Ametek [9] produces shell-and-tube heat exchangers (see Fig. 5c) and immersion coils (see Fig. 5b) of high purity from PFA tubes. They are suitable for heating and cooling ultrapure water, acids and other corrosive chemicals. Ametek produces corrosive-resistant heat exchangers for the chemical industry also (see Fig. 5a). Take note that Ametek immersion coils are constructed based on very small FEP or PFA (Fluorinated ethylene propylene and perfluoroalkoxy-alkane are fluoropolymers similar to PTFE) tubes and have OHTC up to 680 W/m^2K.

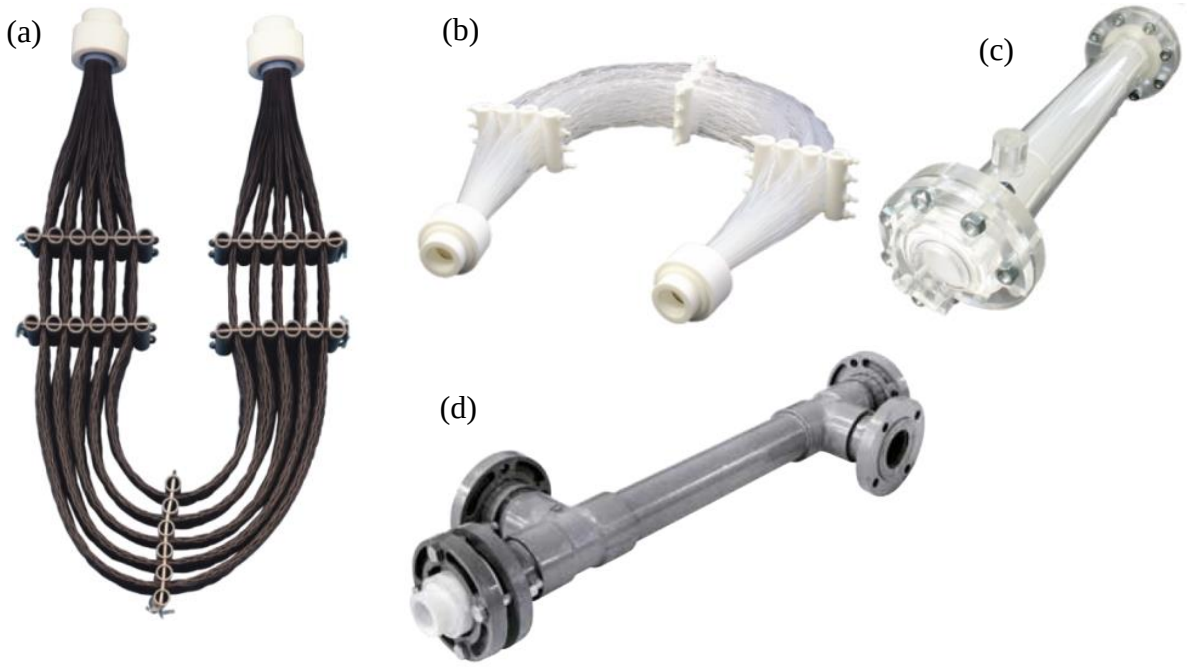

Fig. 5 *Ametek heat exchangers: (a) immersion-type Supercoil for aggressive liquids cooling (heating); (b) high-purity variant of Supercoil from PFA; (c) high-purity shell-and tube heat exchanger from PFA; (d) shell-and-tube heat exchanger made of FEP [9]*

Fig. 6 *Makatek heat exchanger: (a) inside flow pattern; (b) view of SP-500 model [10]*

Ametek's Teflon shell and tube (see Fig. 5d) heat exchangers are used for heating, cooling and condensing chemically aggressive process streams i.e. sulphuric, hydrofluoric, nitric, hydrochloric and other acids, caustic and other alkalis, halogenated compounds, salt solutions and organic compounds. Besides Teflon and PFA Ametek's heat exchangers also use tubes of PFA with graphite impregnation (PFA/G). The thermal conductivity of the impregnated PFA/G (0.378 W/m K) is twice that of pure PFA (0.193 W/m K), but costs of equal capacity heat exchangers are the same. Tubes are available in diameters of 9.5, 6.3, 4.4 and 3.2 mm and have a tube wall thickness of 10% of the diameter. The maximum working pressure given by the manufacturer is 6.5 bar at 60 ºC and 4.8 bar at 100 ºC. The heat exchangers shells are made of PP or CPVC (chlorinated polyvinyl chloride).

Makatek [11] produces liquid-to-liquid heat exchangers of polymeric spiral-wound plastic films (see Fig. 6). They are completely made of plastic material providing resistance to chemicals and corrosion. The plastics can even be chosen depending on their application so that they are chemically inert. The applied plastic film is thin so it provides high thermal performance (OHTC up to 1800 W/m^2K). Moreover, due to their wound-pattern structure, Makatec heat exchangers achieve a high surface area density and self-insulating effect (in many cases additional insulation is not needed).

Application of polymeric materials seems to be attractive also in transport industry because of dramatically low weight and flexibility. For example, as motor radiators, transmission oil coolers, hydraulic oil coolers, charge air coolers, oil coolers etc. Several types of liquid-to-gas heat exchangers have been built and demonstrated. Cesaroni [10] produces PolyCoil all-polymeric heat exchangers from PA (polyamide) for a variety of applications, ranging from vehicles (see Fig. 7a) to HVAC equipment (see Fig. 7b), thermal ice storage systems and evaporative fluid coolers.

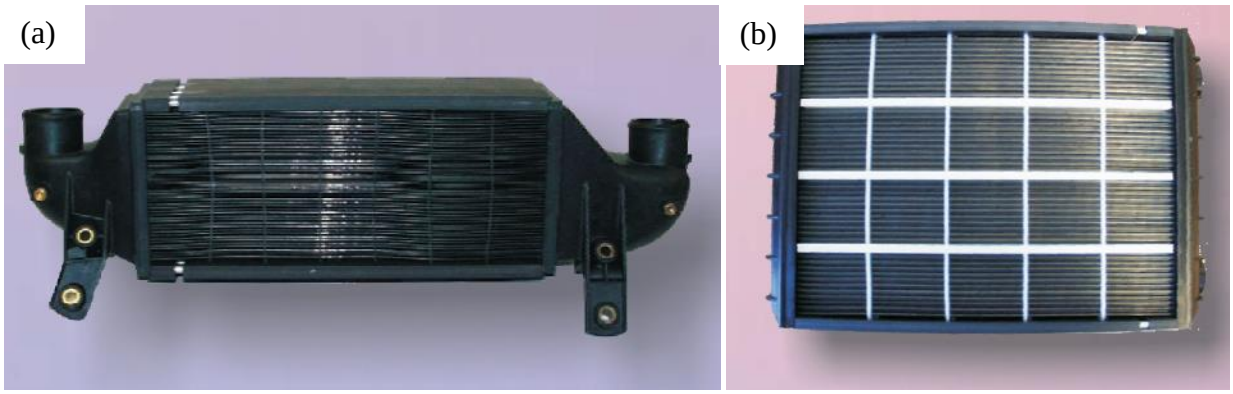

Fig. 7 *Cesarony heat exchangers from PA: (a) automotive gas-to-gas heat exchanger; (b) hotel fancoil [10]*

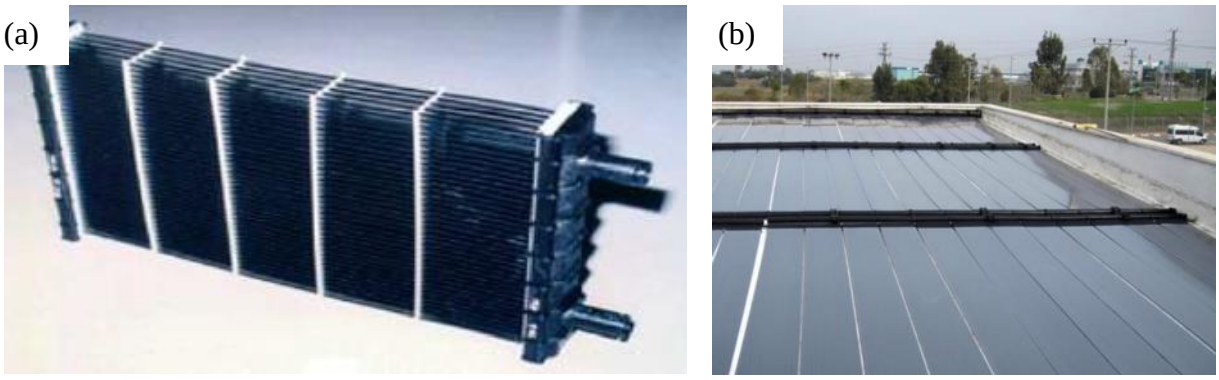

Fig. 8 *DuPont automotive liquid-to-gas heat exchanger [12] and (b) eco-Spark solar collectors connected in parallel [13]*

PolyCoil polymeric heat transfer systems are available in several styles and forms including a shell and tube style for liquid-to-liquid heat transfer applications and a flat panel array for liquid-to-gas applications. Gas-to-gas heat exchangers have been developed for several automotive applications.

A nylon (commercial name of PA) car radiator (see Fig. 8a) was produced and tested by DuPont [12]. For instance, a nylon car radiator conserves space and can be shaped in an engine compartment, which allows for greater design flexibility and significant weight saving. The unit comprises of thin-walled nylon tubing (3.7 mm outer diameter and 0.2 mm wall thickness). With 86 tubes, the heat transfer area is 0.42 m^2, 50% larger than the metal heat exchanger, whilst the heat transfer rate is 4700 W, 40% higher than its metal counterpart.

Magen eco-Energy [13] is specialized in the research, development and production of solar heating systems and plastic heat exchanger systems for swimming pools, domestic and commercial use, and for industrial and agricultural requirements. Certified compounded PP material with special ultraviolet inhibitor additives is used to ensure there is no deterioration over time due to the sun's radiation. Polymeric composition allows it to withstand swimming

pool chemicals, non-corrosive, no limescale build up, stabilized against the effects of ultraviolet radiation. One of the main products is eco-SPARK, an innovative solar collector for heating swimming pools and domestic hot water to medium temperatures (see Fig. 8b). Eco-SPARK is one seamless, leak-proof, integrally moulded thermoplastic panel. Each panel is encased in a partitioned polymeric glazing to create an internal greenhouse effect enhancing the solar collector performance. Square header assures tight fastening and mounting of the panel to any roof.

2.2 Laboratory-tested Plastic Heat Exchangers

Chen [14] investigated finned-tube heat exchangers made of two modified types of PP with high thermal conductivity (2.3 W/m K and 16.5 W/m K). It was found that the plastic finned-tube heat exchanger with thermal conductivity of 16.5 W/m K could achieve OHTC of 34 W/m^2 K. The results showed that there is a threshold value of material thermal conductivity. Below this value, improving of thermal conductivity can considerably improve the heat exchanger performance while over this value improving of thermal conductivity contributes very little to performance enhancement. For the finned-tube heat exchanger studied by Chen, when the plastic thermal conductivity can reach over 15 W/m K, it can achieve more than 95% of the titanium heat exchanger performance and 84% of the aluminium or copper heat exchanger performance with the same dimension.

Liu [15] studied the application of high temperature nylon and PEX (cross-linked polyethylene) to manufacture both shell-and-tube and immersed tube bundle heat exchangers for solar water heating. It was declared that polymer heat exchangers can provide thermal output equivalent to conventional copper heat exchangers at a lower cost. Preliminary analysis indicated that a nylon tube-in-shell heat exchanger is approximately 80% cheaper than a copper tube-in-shell heat exchanger. However, design and manufacturing method were not optimized and significant additional work is still needed.

Scheffler [16] described the method of impulse welding of thin HDPE and PP films on specially developed apparatuses to produce heat transfer elements. These elements can be used as low-cost heat transfer elements for energy efficient multi-effect distillation. Design, construction and testing of a simple falling saline film vapour compression desalinator (with vertically oriented air mattress-like multi-tube polyolefin film heat transfer elements) were briefly described.

Hornung [17] studied fluid flow and heat transfer performance of thermoplastic microcapillary films (MCFs). MCF is plastic film containing continuous arrays of microcapillaries (see Fig. 9a) that are extruded from thermoplastics where the capillaries within these films can be round or elliptical with diameters 30-500 μm. It was shown that the flow within the capillaries is laminar and pressure drop measurements is consistent with standard laminar flow predictions. A set of experiments involving single and two-flow systems were conducted to characterize the heat transfer performance of MCFs. The experimental heat transfer measurements were compared to finite-element model predictions for the MCF geometry and the modelling results were in good agreement with experiment. Thermal response of MCFs was additionally studied by Halmark [18]. Results showed that these devices are effective heat exchangers that can remove heat either from a heated surface or from a highly exothermic chemical reaction. Heat transfer coefficients based on internal volume have been typically 8-14 MW/m^3 K (400–800 W/m^2 K in terms of internal capillary area) when the MCF is in direct contact with the heated surface, or about 0.43 MW/m^3 K (about 21.5 W/m^2 K) for cases of natural convection. Plastic solar collector (see Fig. 9b) prepared based on MCFs was studied by Dorfling [19]. It was shown that performance of such a type of collector can be comparable to commercially available solar heat collectors.

Applicability of plastic compact heat exchangers for single-effect desalination systems was studied by E1-Dessouky [20]. Authors claim that PTFE evaporator and preheater have lower specific cost than of metal ones. However, use of PTFE polymer for construction of the shell-tube evaporators or plate preheaters necessitates reduction of the wall thickness because of the low plastic thermal conductivity. In this regard, use of spacers and other supporting structures is necessary to avoid collapse of the plastic material. Moreover, authors claim that there is lack of data about plastic heat exchanger in comparison with metal and it is necessary to support research for design, selection, and development of the plastic heat exchangers.

Zaheed [12] described an experimental investigation of the performance characteristics of a novel, cross-corrugated, polymer film, compact heat exchanger made of PEEK (poly-ether-ether-ketone). They used 100-μm, corrugated, PEEK films, which have a corrugation width of 2 mm and a corrugation height of 1 mm to prepare a square module; the dimensions of the sheets were 13.5×13.5 cm. The sheets were stacked together, each rotated at 90° with respect to the next sheet, creating the cross-corrugated matrix. One corrugated sheet and the sheets stacked in the matrix are illustrated in Fig. 10. Authors showed that these devices have a

potential as an alternative to conventional metallic units, due to the tremendous energy and cost savings. In addition, they are more compact, require less space, are lightweight and easy to maintain. It was shown that these devices weigh less than a quarter of the conventional metallic units, the pressure drop savings exceed 75% and 40% for the stainless-steel and aluminum units, respectively.

The use of cross-corrugated film heat exchanger for water vapor condensation was studied by Burns [22]. It was found that vapor condensation from a gas stream can be successfully realized in this heat exchanger. Visual analysis of the system has shown that condensation was in efficient drop-wise regime with OHTCs of 60-500 W/m^2 K.

Hazami [23] proposed low-cost capillary PP heat exchangers for conditioning of museum aquariums by 18 °C seawater. The tests showed that proposed system has a good thermal efficiency (up to 80%) and high values of *NTU*; values of OHTC were 10-170 W/m^2 K.

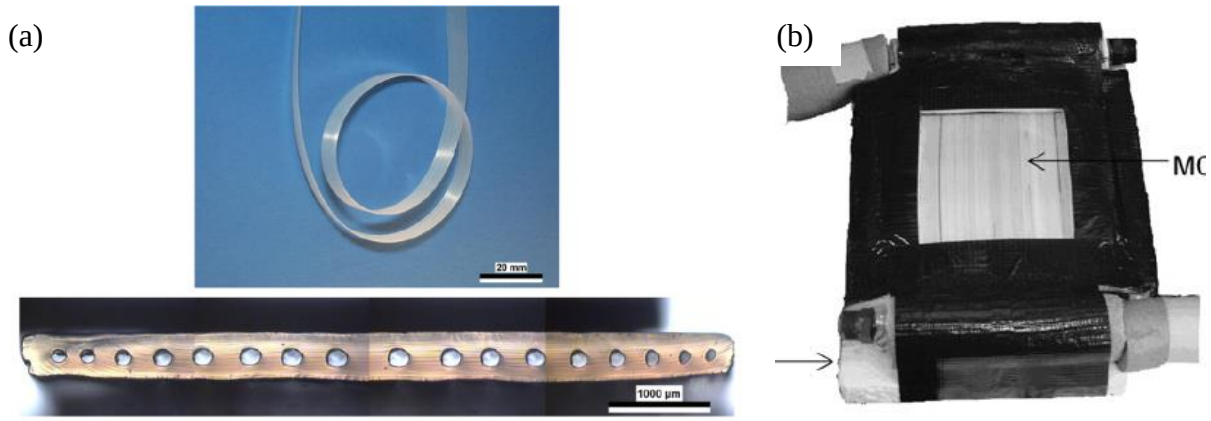

Fig. 9 *Plastic microcapillary film [17]; (b) Solar energy collector based on MCFs [19]*

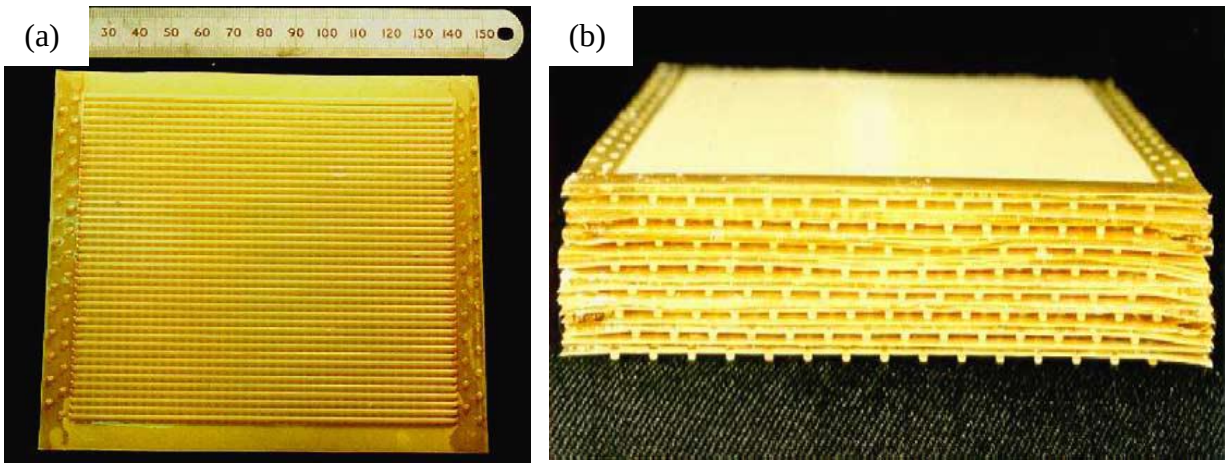

Fig. 10 *Cross-flow compact heat-exchanger: (a) cross-corrugated PEEK sheet and (b) heat exchanger matrix [21]*

3 POLYMERIC HOLLOW FIBER HEAT EXCHANGERS

3.1 Review of Published Papers on PHFHEs

PHFHEs for low-temperature applications were firstly proposed by Zarkadas [24]. Small devices containing a few hollow PP fibers with parallel flow were tested and showed good thermal performance. The OHTCs of these devices were 647-1314 W/m^2 K and 414-642 W/m^2 K for the water-water and ethanol-water systems, respectively. These are quite high values which are comparable to the values obtained in conventional metal shell-and-tube heat exchangers. It was shown that in several cases OHTC is limited by wall thermal resistance and is independent on flow conditions. The next advantage of these devices is a possibility to achieve large packing density (surface area to volume ratio). Despite tested devices having a packing density of 2-3 lower than similar commercially available membrane devices, authors showed that PHFHEs can transfer up to 1 order of magnitude more heat per unit volume than metal shell-and-tube heat exchangers. Moreover, despite small hydraulic diameter of fibers, PHFHEs can be operated with low pressure losses. Transient experiments proved a fast response of PHFHEs on change of flow rate. This feature is very beneficial in cases of application of PHFHE for temperature control. Authors assumed that if hollow fibers made out of better materials such as PTFE, PEEK, or HTN were used, then better properties of PHFHEs can be achieved. Extended information about experimental part of this work is presented the thesis of Christian [25].

Song [26] carried out a large experimental study of different PHFHEs with the emphasis on application for thermal desalination processes. Ten devices having different flow organization (see Fig. 11), type and number of the fibers, heat exchange area and packing density were investigated.

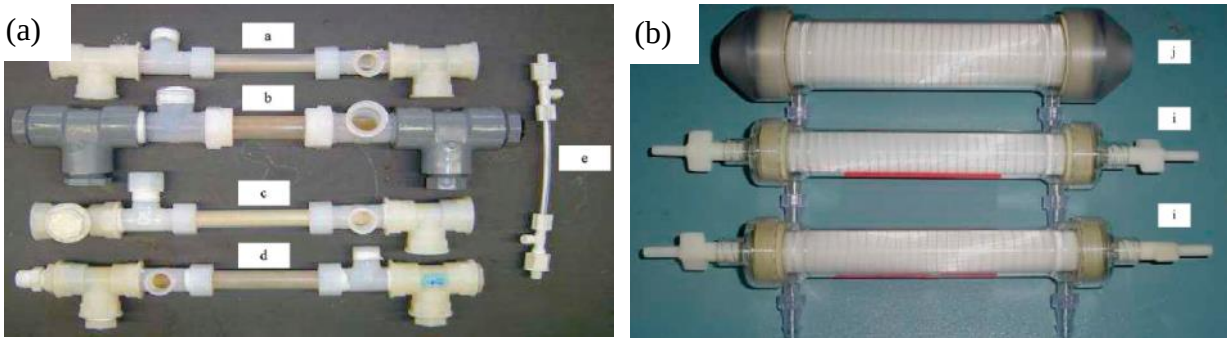

Fig. 11 *Polymeric hollow fiber heat exchangers: (a) laboratory-scale modules and (b) high packing density modules prepared by Membrana, Charlotte, NC [26**Chyba! Nenalezen zdroj odkazů.**].*

Three of these modules have large fiber amount (950-2750), heat transfer area (0.15-0.44 m^2) and packing density (up to 0.63). The heat transfer performance of these devices were studied for a hot brine (4% NaCl, 80-98 °C)-cold water (8-25 °C) system and for a steam (101-113 °C)-cold water (8-25 °C) system because these systems are typically encountered in thermal desalination plants. OHTC values about 2000 W/m^2K for brine-water systems and 1600-1800 W/m^2 K for steam-water system were achieved. Surface area per unit volume of tested devices was up to 4000 m^2/m^3 and their volumetric rate of heat transfer was very high. Moreover, authors concluded that compared to metallic heat exchangers used in desalination, PHFHEs weigh much less, do not suffer from corrosion, and are likely to be considerably cheaper. Like their counterparts in hollow fiber membrane contactor devices, they provide an opportunity for process intensification.

Qin [27] studied PHFHE constructed based on thermal-conductive PP hollow fibers. Heat-conducting PP was prepared by melt-mixing PP with graphite particles and maleated PP. Experimental results confirmed that the addition of graphite fairly improved the crystalline, thermal stability and conductivity of the PP and further improved the heat transfer efficiency of PP PHFHE. The OHTCs up to 1220 W/m^2 K were achieved, which is 5 times greater than that of pure PP-based PHFHEs, and the overall conductance per unit volume reached $1.1*10^6$ W/m^3 K which is 1.5 times higher than value of metal shell-and-tube heat exchangers.

Numerical simulation of water-to-water PHFHE using CFD (Computational Fluid Dynamics) software tool FLUENT was performed by Zhao [28]. It has been demonstrated that the rise of the tube- and shell-side velocities improves the OHTC but as the velocity increases to a certain value, the OHTC reaches plateau. Percent contribution of tube, shell and wall thermal resistance to the total resistance were 20%, 50% and 30%, respectively. Shell side and wall resistance are generally the dominant resistances. Moreover, influence of fiber packing density on the shell-side flow distribution and OHTC was analyzed. Authors concluded that the optimal value of packing fraction of hollow fibers is about 13-19%.

Liquid-to-liquid shell-and-tube PHFHE was studied by Yan [29]. Authors improved PHFHE described by Zhao [28] by introducing PP net to improve shell-side heat transfer. It has been observed that introducing of the net causes about a 40% increase of OHTC (650 W/m^2K to 920 W/m^2K). Additionally, CFD simulation of both examples was performed and results were compared with experimental data showing sufficient agreement.

Several aspects concerning large-scale PHFHEs were discussed by Raudensky [30]. Authors described fiber bundle consisting of 30,000 hollow fibers and specified the main difficulty: “each fiber must be active, i.e. each fiber must transfer heat”. Two approaches were proposed to fulfill this requirement. The first one is to use fiber overlength i.e. longer fibers than the distance between collecting pottings. The second approach is to use non-straight fibers of a special, “curly” shape. So-called fuzzy fractal analysis was proposed to study fiber curliness and distribution uniformity.

Bundles made of straight PP hollow fibers were studied as shell-and-tube heat exchangers by Partzsch [31] for water-to-water application. OHTCs of 80-680 W/m²K were achieved depending on flow rates. Authors stated that the bundles are suitable for thermal applications but additional research is required to improve their mechanical and thermal resistance.

Similar heat exchangers were studied by Gallik [32] for water-to-water (OHTCs up to 1900 W/m²K were observed) and water-to-air (OHTCs up to 50 W/m²K) application. Author tested different approaches how to distribute the fibers in the shell and intensify the shell-side heat transfer. It was found that the thermal performance of tested examples is significantly dependent on the shell-side configuration. Moreover, author proposed several possible applications for these devices, mainly considering corrosive and polluted environments.

Bundles made of twisted hollow fibers were experimentally studied by Weiß [33] for water-to-water application. The bundles were applied as immersed heat exchanger with cold water flowing through the bundles and hot water surrounding the bundle. Experiments confirmed that hollow fiber bundles can achieve high values of OHTC (up to 880 W/m^2K) and can transfer significant amount of heat in merit of their volume and weight (up to 22.7 kW for a 40x10x10 cm device weighting several hundred grams) making them competitive to commercial immersed heat exchangers.

Solar panel cooling system made of PP hollow fibers was studied by Schmidt [34]. This system integrated into the photovoltaic panel allows removing about 1 kW of heat, and reduces the module temperature from 90 °C to 50 °C. The mean efficiency increased about 50% and energy saved due to the cooling is significantly higher than the energy for pumping.

3.2 Properties of PHFHE Related to Polymeric Material

PHFHE is characterized by two main features: fibers are made of polymeric material; fiber diameter is small. These two features outline the advantages and drawbacks of PHFHE compared with conventional metal heat exchangers. Properties of polymers suitable for

manufacturing of hollow fibers are collected in the Tab. 1. The use of polymer material provides the following advantages:

- Low density of polymers allows making of lightweight constructions and reducing manufacturing, delivery and installation costs.
- Excellent chemical resistance provides application in chemically aggressive and high-corrosive environments.
- The smoothness of the polymer surface begets low friction on the wall and thereby pressure drops and good fouling characteristics. This feature causes small decrease of thermal performance during operation and simplify the maintenance.
- The hydrophobic surface of polymers promotes dropwise instead of filmwise condensation and consequently, higher HTCs. If needed, the surface properties can be modified to improve wettability.
- Polymers are easier to shape, form and machine than metals. The moulding and heat-sealing capabilities of thermoplastic polymers make it possible to fabricate complex shapes or large surface areas at low cost.
- Flexibility of polymers allows to create heat exchangers with changing shape.
- Polymers are non-toxic and chemically neutral so they can be used in the food industry and medicine
- Polymers can be blended with fillers, fibers, biocides and anti-stick agents to change mechanical, thermophysical or surface properties
- Polymers are environmentally friendly because they are suitable for recycling (totally recyclable in some cases). Moreover, the energy required to produce a unit mass of plastic is about two times lower than that of common metals
- Low price. Conventional polymers are cheaper than metals.

However, use of polymeric material is associated with several complications and drawbacks. Polymer's thermal conductivity is low, as usual 0.1- 0.4 W/m K which is 100-300 times lower than of metals. It considerably limits use of polymers for heat exchange equipment because of the thermal resistance of polymeric wall significantly decreases heat transfer. It is worth noting, that plastic's thermal conductivity can be increased by addition of thermal-conductive fillers. Polymers with improved thermal conductivity are already commercially available [35] and several studies on this issue are performed [36].

Conventional polymers have relatively lower mechanical strength and temperature resistance. The melting temperature of polymers is much lower than the same of metals and limits operation condition. Conventional polymers could be used for temperature below 90 °C; but so-called "engineering thermoplastics" and "high performance polymers" have better mechanical properties and temperature resistance. High thermal expansion of polymers creates some difficulties in design, but can be considered as a positive factor because it improves the resistance to fouling. Moreover, degradation of polymeric material, change in the properties under the influence of environmental factors such as heat, light, chemicals etc., should be observed.

Tab. 1 *Properties of polymeric materials suitable for extrusion*

Material	PP	PA	PC	PEEK	PVDF	PTFE	PPS	PE
Density, kg/m^3	932	103	120	1320	1780	2160	1700	950
Yield strength, MPa	31.3	42	55	102	42.5	27.5	96.3	
Elongation, %	158	6.6	19	30	65	362	4.47	
Young's modulus, GPa	1.44	2.4	20	4.48	1.8	0.496	1.63	1.39
Thermal conductivity, W/m K	0.18	0.22		0.262	0.184	0.27	2.44	0.42
Min. operating temp., °C	-30	-40	-40	-50	-52	-223		
Melting temperature, °C	163	267	189	335	165	327	285	120

3.3 Small Diameter of Hollow Fiber as a Key of High Thermal Performance

Feasibility of use of hollow fibers of a small diameter is the main question which should be answered. Nowadays miniaturization and decrease of hydraulic diameter of heat exchanger is world-wide tendency [3]. It is more pronounced for liquid-to-gas heat exchanges (majority of compact heat exchangers have compact surface on the gas side) but heat exchangers with compact surface on liquid side exist too. This tendency can be explained by the fact that diameter reduction increases compactness and the thermal performance of a heat exchanger. We will consider hollow fibers as tubes with outer diameter 0.4 – 2.0 mm.

3.3.1 Decrease of wall thermal resistance

As it was mentioned above polymer's thermal conductivity is low and thus wall thermal resistance significantly limits heat transfer. In case of heat transfer through the cylindrical wall, thermal resistance can be expressed as:

$$R_w = \frac{D_o}{2k} \ln\left(\frac{D_o}{D_i}\right) \quad (14)$$

It is evident that the value of wall thermal resistance can be decreased by the increase of wall material thermal conductivity, by reduction of outer diameter or diameter ratio (wall thickness):

$$R_w \downarrow = \frac{D_o \downarrow}{2k \uparrow} \ln\left(\frac{D_o}{D_i} \downarrow\right) \quad (15)$$

From the viewpoint of mechanical strength, it is not possible to decrease diameter ratio less than 10% for the majority of applications. However, the wall thermal resistance can be partially eliminated by a simple reduction of the tube diameter.

3.3.2 Influence of material thermal conductivity. Case studies

In this chapter, we will show how thermal conductivity influences heat transfer because it influences OHTC in different ways depending on application and conditions. For instance, finned-tube heat exchangers modified PP materials were studied in [14]. The results showed that there is a threshold value of material thermal conductivity, which divides the heat exchanger performance curve into two parts. Below this value, improving thermal conductivity can considerably improve the heat exchanger performance while over this value improving the thermal conductivity contributes very little to improve the heat exchanger performance. Despite PHFHEs having no fins, the similar behavior is typical for PHFHEs as well. We will consider two cases to show how thermal conductivity influences HTC.

Case study 1. Water-to-water shell-and-tube PHFHE with forced convection on both sides and liquid flowing cross-flow in the shell. OHTCs are calculated for the following conditions:

PP (0.17 W/m K)	modified PP with improved thermal conductivity (1.7 W/m K)
Inside/outside fiber diameter is 0.6/0.8 mm	
Flow conditions: inside water - inlet temperature 60 ºC, flow rate through each fiber is 0.5 l/hour (0.5 m/s), outside water - inlet temperature 10 ºC, flow rate – varied	

Results show (see Fig. 12) that thermal conductivity of material has a significant influence on resulting OHTC. PP with enhanced thermal conductivity (k = 1.7 W/m K) causes rise of OHTC approximately two times (from 1000 to 2200 W/m^2 K) comparing to basic PP material.

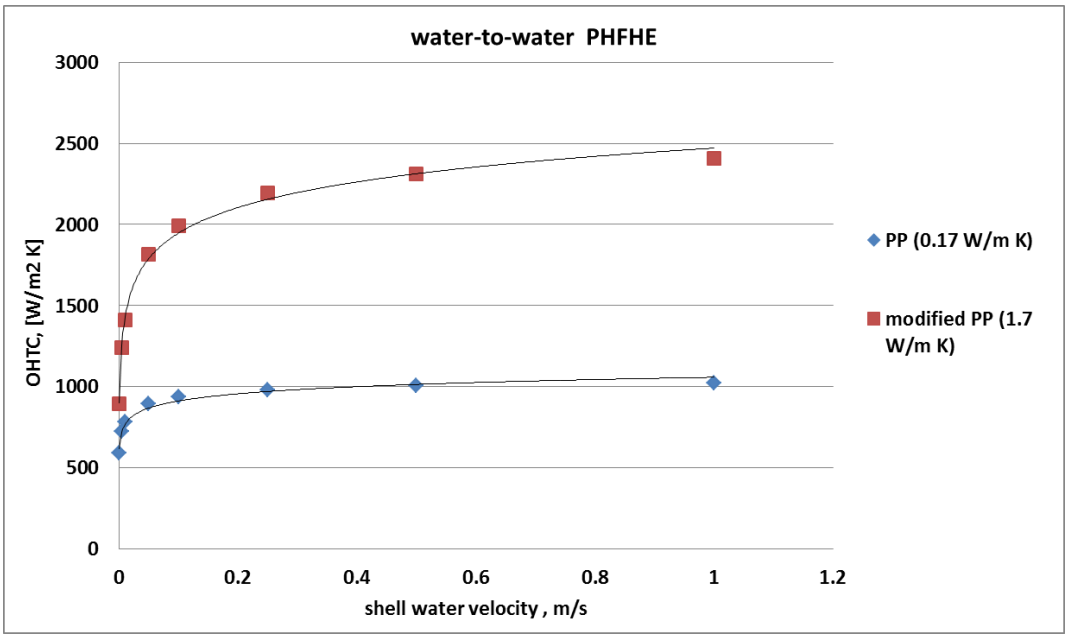

Fig. 12 *Overall HTC vs water velocity*

Case study 2. Water-to-air cross-flow PHFHE with forced convection on both sides and water flowing through the fibers and air flowing across the fibers.

PP (0.17 W/m K)	modified PP with improved thermal conductivity (1.7 W/m K)
Inside/outside fiber diameter is 0.6/0.8 mm	
Flow conditions: water flowing inside the fibers - inlet temperature 60 ºC, flow rate through each fiber is 0.5 l/hour (0.5 m/s) outside air - inlet temperature 10 ºC, flow rate/velocity – varied	

Results show (see Fig. 13) that the influence of thermal conductivity is significantly lower than in the case of water-to-water PHFHE (case-study 1). Thermal resistance on the air side eliminates the influence of the wall thermal resistance. The difference in OHTC caused by wall material is pronounced only for high air velocities. Mean difference between ordinary and modified PP is about 10 %.

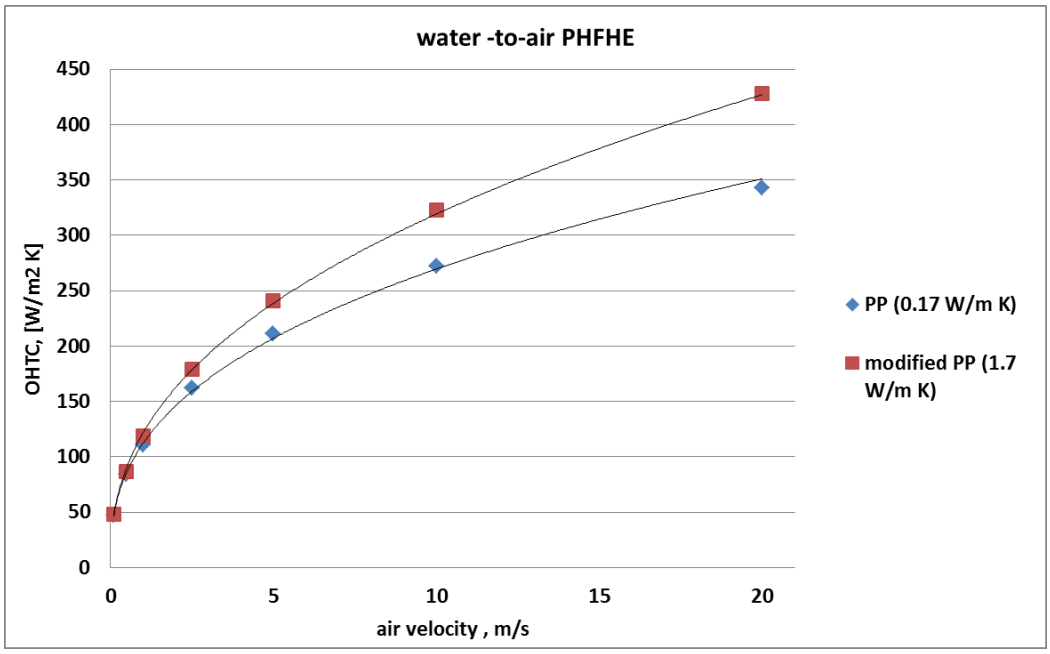

Fig. 13 *Overall HTC vs air velocity*

3.3.3 Influence of diameter on convective heat transfer

Fiber diameter has a strong influence not only on the heat transfer through the wall but on convective heat transfer too. Fig. 14 shows influence of fiber diameter on the convective HTC for the case of air flowing across a cylinder. Values of the HTC are calculated based on the Zukauskas equation [6] for different air velocities occurring in practice. It is shown that there is the critical tube diameter value (approximately 1 mm). Decrease of tube diameter below this value yields to a rapid increase of HTC. This tendency is valid for flow of another gases and liquids as well.

Fig. 15 shows the influence tube diameter on the convective HTC for water flowing inside the fiber. The change of the curves character corresponds to change of the flow regime from turbulent (right plateau on graph) to laminar (the left part). The Blausius equation was used to calculate the inside Nusselt for turbulent regime [6]; and the Hickman equation (Equation 28) is used for laminar regime [24]. Assumption of hydrodynamically fully developed flow was applied in both cases. The graph clearly shows that the HTC values of laminar flow (left side of the HTC curves) in small tubes (0.5-1 mm) are comparable with the HTC values of turbulent flow (zone where the HTC curves are almost horizontal) in ordinary channels (10 mm). In addition, HTCs do not depend on flow velocity in laminar regime so low liquid velocities can be employed to achieve a low pressure drop without the loss of thermal performance.

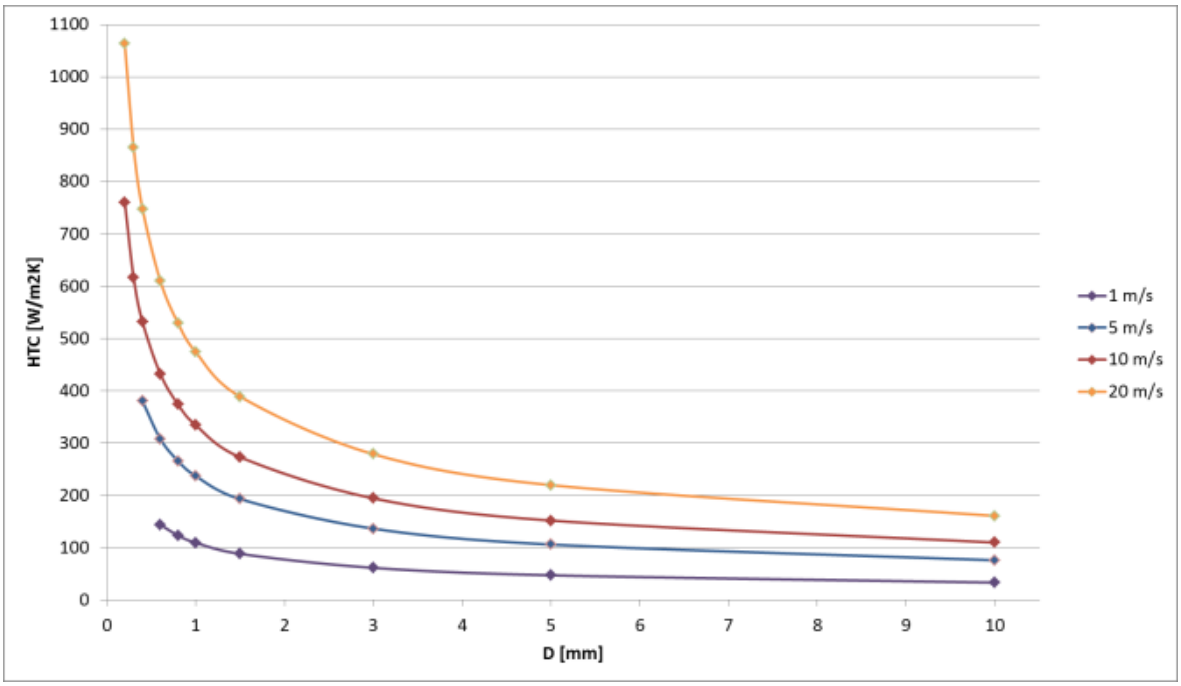

Fig. 14 *Outside HTC vs fiber diameter. External flow of air (20 °C) across a circular tube. HTCs are calculated for different diameters (0.1-10 mm) and air velocity (1-20 m/s).*

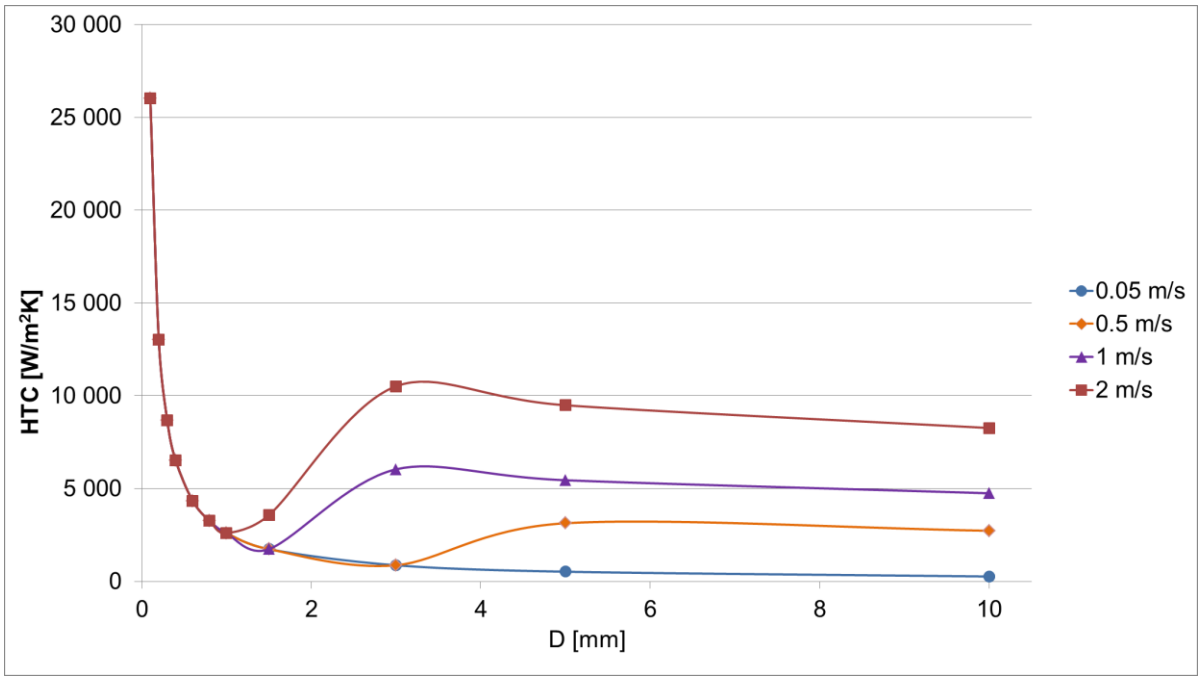

Fig. 15 *Inside HTC vs fiber diameter. Internal flow of water (20 °C) within a circular tube. HTC values for different diameters (0.1-10 mm) and velocity (0.05-2 m/s)*

3.3.4 Compactness

Another feature of PHFHEs is a possibility to achieve high compactness of design because of a large heat transfer area can be obtained in small volume. This can be explained by the fact that a surface area of an object can be estimated proportional to the square of its size; and its volume is proportional to the cube of its size. Thus, surface to volume ratio can be increased by a simple decrease of characteristic dimension.

Hollow fibers have a small diameter and they can be placed together in a high density. According to Song [26], the surface area density of hollow fibers can exceed 3000 m^2/m^3 and conductance per unit volume more than $3.5e10^6$. However, it means that many fibers should be connected together to create the heat transfer area. They must be uniformly distributed and supplied by liquids to achieve good thermal performance. Poor fiber distribution will cause bypassing of liquid and creates "dead zones" (without liquid flow) which decrease the effective heat transfer area.

Let's consider typical in-line and staggered patterns of tube bundles (see Fig. 16) and estimate compactness of the fiber bundles depending on diameter. These patterns are described by tube outer diameter D_o and width and depth pitches between tubes S_1 and S_2. The pitches between fibers can be varied in a wide range. We will consider $S_1 = 2D_o$ and $S_2 = 2D_o$ (the square pattern with $2D_o$ side) for in-line pattern; and $S_1 = 2D_o$ and $S_2 = \sqrt{3}D_o$ for staggered pattern (equilateral triangle pattern with $2D_o$ side). Fig. 17 shows that heat transfer surface made of hollow fibers with diameter 1 mm and lower can be considered as compact for both gas-side and liquid-side applications [3].

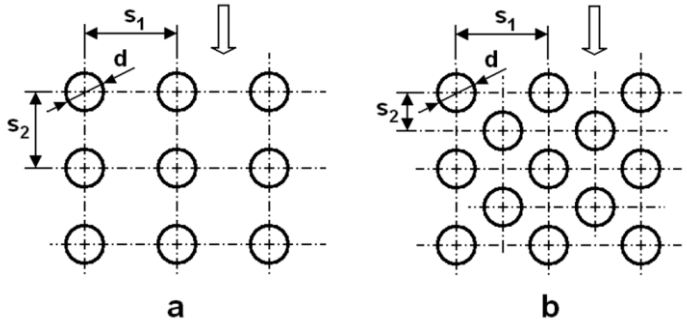

Fig. 16 *In-line (a) and staggered (b) tube bundle patterns*

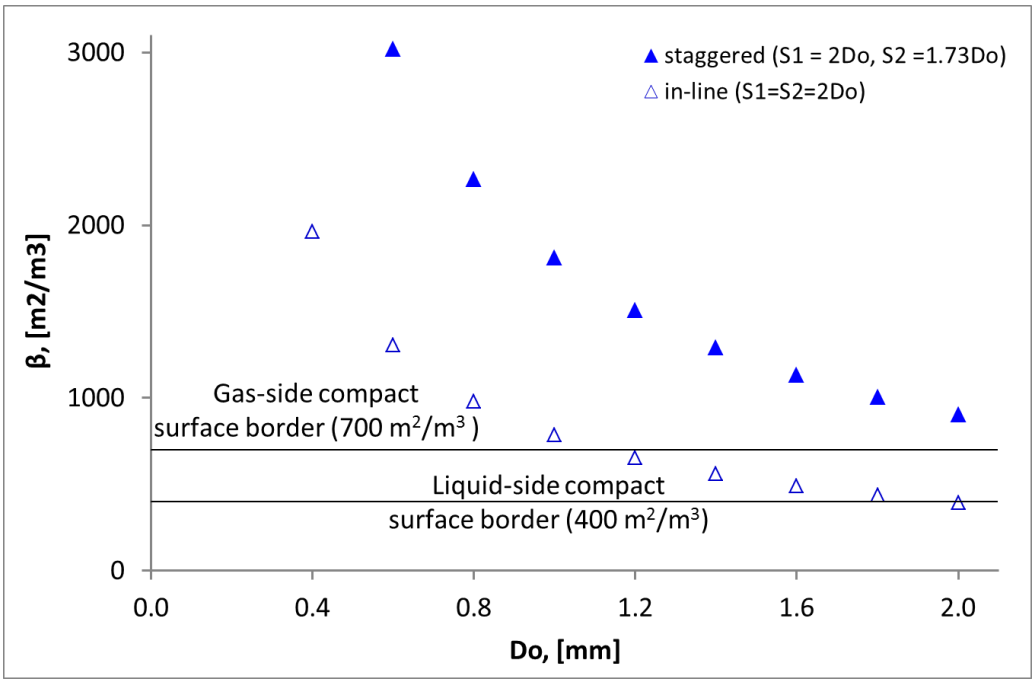

Fig. 17 *Surface area density vs diameter*

4 HEAT TRANSFER AND FLUID FLOW INSIDE OF FIBER

4.1 Theoretical Consideration

A polymeric hollow fiber is a tube of small diameter (smaller than 1 mm) and can be classified as a microchannel [36]. In the last several decades many theoretical and experimental investigations devoted to microscale heat transfer were performed. Many of them have stated a discrepancy between experimental results and conventional theory prediction. According to Yarin [38], there is no complete convincing explanation of the difference between experimental and theoretical results for laminar flow, and between experimental and semi-empirical results for turbulent flow.

In order to explain this behavior, many researchers argue that some new effects exist in microchannels, e.g., [39, 40]. Several authors have suggested new correlations in order to predict the friction factors and the convective heat transfer coefficients in micro-channels both in laminar and turbulent regimes. Unfortunately, the new correlations proposed to predict the Nusselt number in micro-channels disagree with one another and each correlation disagrees with the conventional prediction, as it was demonstrated by Owhaib [41].

That said, the phenomenon can be related to the discrepancy between the actual conditions of a given experiment and the theoretical or numerical solution obtained in the frame of conventional theory as shown by [36, 42]. It was observed that, in order to study the forced convection of liquids in a laminar regime, a common theoretical basis for macro- and micro-flows could be used; nevertheless, certain effects can be of differing importance for micro-systems when compared to macro-systems. These effects were called "scaling effects" and the following definition was used: “Scaling effects are those influences that can be neglected in the original scales but become important in different (larger or smaller) scales”.

It should be noted that the single-phase laminar flow of a liquid (not a gas) in a microchannel is considered here. In the case of gas flowing in a microchannel, the mean free path of molecules can be comparable to the diameter of the microchannel and the assumption of a continuum model (validity of Navier-Stock equation) can be broken down (for details, see [40]).

Based on the works of Herwig, Yarin and Morini [36, 38, 43] we can identify the following "scaling effects" for single-phase laminar flow in a microchannel:

- axial heat conduction in a liquid, in wall and combined axial conduction

- viscous dissipation
- variable property effects
- effect of the thermal entrance region
- wall roughness (non-uniform wall roughness distribution along the perimeter)

Next, we will discuss the influence of these "scaling effects" on convective heat transfer and fluid flow in detail with respect to heat transfer inside a hollow fiber.

4.1.1 Axial heat conduction in liquid.

Axial conduction in the fluid was studied in detail in [38]. The problem was discussed with assumptions of constant physical properties and negligible energy dissipation. It was supposed that the existence of axial heat conduction in the fluid increases the temperature difference between the wall and fluid and decreases the inner Nusselt number. A dimensionless parameter *M*, expressing the relationship between heat fluxes due to conduction and convection, was proposed to estimate the effect of axial heat conduction through fluid in a micro-channel. The critical value of parameter *M* subdivides the states at which the effect of axial conduction dominates ($M > M_{cr}$) or is negligible ($M < M_{cr}$). According to [45], $M_{cr} = 0.01$ can be applied and the following inequality (Equation 16) was proposed to estimate the length at which the axial conduction should be considered:

$$\frac{x}{r_i} Pe \leq 20 \qquad (16)$$

where $Pe = Re \cdot Pr$ is the Peclet number, x is the axial coordinate and r_i is the microchannel hydraulic radius. If we assume that hollow fibers have an inner diameter D_i = 0.5 mm, an outer diameter D_o = 0.6 mm, length 1 m and the material is PP, we obtain the critical value Pe_{cr} = 0.005. This value corresponds to the Reynolds number Re = 0.00075 if the Prandtl number Pr = 6.62 (Pr of 20 ºC water [46]). These extremely low values of Pe and Re cannot be considered as possible during the normal regime of operation of PHFHEs so we conclude that axial heat conduction in liquid is negligible for PHFHEs.

4.1.2 Axial heat conduction in wall.

Axial conduction in the wall of mini- and microchannels was investigated in detail in [46]. It was shown that conjugate heat transfer significantly influences the mean Nusselt number at low Reynolds numbers because conduction heat transfer along the wall is comparable to the convection heat transfer in this case. Numerical simulation [48] showed that the temperature

distribution along the microchannel is not linear if effects of conjugate heat transfer are predominant. The following criterion was proposed to estimate the significance of axial conduction in the walls:

$$M = \left(\frac{k_w}{k_f}\right)\left(\frac{D_o^2 - D_i^2}{D_i L}\right)\frac{1}{Pe} > 10^{-2} \quad (17)$$

where k_w, k_f – are thermal conductivities of wall and fluid; D_o, D_i, L is outer, inner diameters and length of microchannel. This inequality was recommended as well in [43] and [48].

The critical value Pe_{cr} = 0.0065 was obtained by using Equation 17 and the previously described fiber dimensions. The thermal conductivity of isotactic PP k_w = 0.18 W/m K was used as wall conductivity [6] and thermal conductivity of 20 ºC water was used as fluid k_f = 0.606 W/m K. As previously mentioned, such a low value of *Pe* cannot occur in PHFHEs under their operating conditions, so we can conclude that axial wall conduction is negligible.

4.1.3 Combined axial heat conduction.

The combined axial conduction problem was discussed in [38] based on the work of Petukhov [45]. The following estimation criterion was proposed:

$$M = \frac{\Lambda}{4\chi^+} \quad (18)$$

$$\Lambda = \left(k_w/k_f\right)(D_o/D_i)^2 \quad (19)$$

$$\chi^+ = (Pe \cdot x)/2D_i \quad (20)$$

where Λ is a factor corresponding to the geometry and properties of the wall and fluid and χ^+ is a dimensionless distance in the axial coordinate. The critical value M_{cr} = 0.01 can be used in the same manner to determine critical *Pe*. The critical value of *Pe* = 0.0107 was obtained for the same conditions as in the previous cases so we conclude that the combined axial heat conduction is negligible for PHFHEs.

4.1.4 Viscous dissipation.

Under some conditions, the heat released due to viscous dissipation leads to a drastic change of flow and the temperature field: in particular, it leads to flow instability, transition to turbulence, oscillatory motions, etc. [38]. Detailed discussion of this effect can be found in [38, 43, 50]. According to [43], the viscous dissipation effects in adiabatic micro-channels cannot be neglected if the following condition is satisfied:

$$4\frac{Ec}{Re}[fReL^*] \geq 1 \quad (21)$$

where $Ec = u^2/(2c_p\Delta\theta_{ref})$ is the Eckert number, $L^* = L/D_i$ is a dimensionless micro-channel length and $\Delta\theta_{ref}$ is a reference temperature rise. Note that the combination of *f* and *Re* is *Po* (the Poiseuille number). *Po* equal to 64 can be used in the case of developed laminar flow in circular channels and Equation 21 can be rewritten in the following form:

$$\frac{128\,\mathrm{Re}\cdot\nu^2\cdot\mathrm{L}}{\mathrm{C_p}\cdot\Delta\theta_{\mathrm{ref}}\cdot\mathrm{D_i^3}} \geq 1 \qquad (22)$$

For example, water dynamic viscosity decreases by about 20–25% per 10 K; for this reason, the authors [43] proposed to use $\Delta\theta_{ref}$ equal to 1 K. Thus, the critical value of Re_{cr} = 4420 was obtained for our geometry and 20 ºC water (ν = 9.61·10^{-7} m^2/s, c_p = 4183 J/kg K) [46]. This value corresponds to turbulent flow and can occur only with high velocities which are not reasonable to use in PHFHEs. We can conclude that that viscous dissipation is mostly insignificant in the case of water flowing in fiber but should be carefully considered for the flow of high-viscosity fluids.

4.1.5 Variable property effect.

According to [38] only a few solutions of the laminar flow forced convection problem and experimental investigations are available in the literature with some variations of the associated thermophysical properties. For example, no experimental study is available to clarify the effect of the Prandtl number on the heat transfer in micro-channels but some authors studied the effect of thermophysical property variations with temperature. A hollow fiber is a long microchannel and large temperature gradients can occur along its length, causing large property gradients. Thus, liquid properties should be carefully considered to avoid associated errors.

Liquid properties can be considered constant or variable depending on effects which are important at microscale. Different effects have a different impact on heat transfer at microscale: some of them can be neglected and some cannot. For example, natural convection plays a small role because the values assumed by the Grashof number are very small (*Gr* is dependent on the third power of the characteristic length) [38]. Small density variations have no significant influence on other effects and liquid density can be considered constant.

Thermal capacity and thermal conductivity strongly influence heat transfer but the change of these properties with temperature is not very pronounced. For example, water heat capacity

change is less than 1% for temperature change from 20 ºC to 60 ºC [46]. The associated change of thermal conductivity is less than 8%. Thus, these liquid properties can be assumed constant except in some special cases.

On the other hand, liquid's viscosity has very strong dependence on temperature and viscous forces play an important role at microscale. For example, water viscosity changes more than twice for a temperature change from 20 ºC to 60 ºC (such temperature gradient can easily occur in PHFHE). This example shows that the variation of the fluid viscosity cannot be neglected in the analysis of micro-flows. Thus, we consider that for engineering calculation all fluid properties could be considered as constant except of the viscosity.

4.1.6 Thermal entrance region effect.

The thermal entrance region is a microchannel inlet section where the liquid temperature profile develops. It is associated with higher temperature gradients between the wall and fluid and higher Nusselt numbers compared to the thermally fully developed region. The thermal entrance region length can be estimated by the Graetz number:

$$Gz = \frac{D_i}{L} RePr \tag{23}$$

According to [48], a thermally fully developed profile is achieved when $Gz < 10$. This value can be used to estimate the length of thermal entrance region. For our fiber geometry (D_i = 0.5 mm) and 20 ºC water flowing inside with a velocity 0.1 m/s thermal entrance region length is about 16 mm. As usual, the fiber length of PHFHEs is significantly longer, hundreds of millimeters, and the thermal entrance region is just a small portion of the whole fiber length. Therefore, we can conclude that the influence of thermal entrance region is mostly negligible for majority of PHFHEs and should be considered only for short fibers.

4.1.7 Influence of wall roughness.

The role of surface roughness on fluid flow and heat transfer in micro-channels has been emphasized by several authors. According to [50], tubes can be considered smooth or rough depending on roughness size. The authors proposed the following equation to estimate the boundary that subdivides the flow in smooth and rough channels:

$$\frac{k_s}{r_i} = \frac{5}{1.41 Re^{1/2}} \tag{24}$$

where k_s – height of roughness, r_i – microchannel radius. This equation correlates well with [38], which noted that for $Re \sim 2000$, the relative roughness (roughness of pipe divided

by internal diameter) that corresponds to the boundary between the smooth and rough channels is about 0.08. The authors also noted that for small diameters tubes (*Di* < 0.6 mm), a relative roughness larger than 0.003 can increase the heat transfer up to 25–30% in the range of *Re* = 1000-2000.

Our studies of available hollow fibers showed that their internal surface is very smooth and has an absolute roughness less than 1 μm (see for example Fig. 18). For 500 μm inner-diameter hollow fibers it gives a value of relative roughness less than 0.002, so the hollow fiber can be considered to be a hydrodynamically smooth tube. We suppose that such a low roughness does not influence fluid flow and heat transfer.

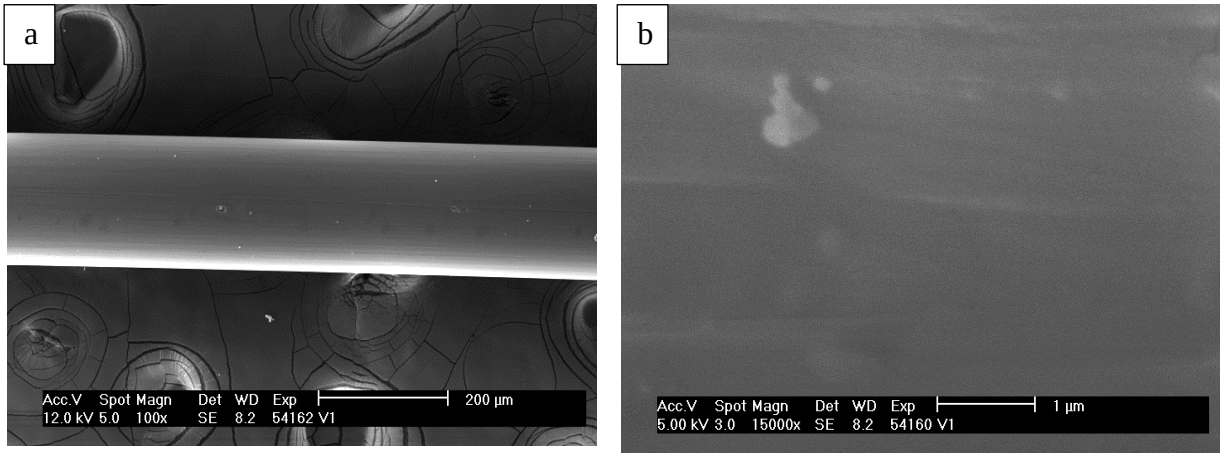

Fig. 18 *Images of PP hollow fiber surface made by electronic microscopy: (a) the outer fiber surface x100 magnification; (b) the outer fiber surface x15000 magnification. The surface is smooth, without any pores or defects; the absolute roughness is evidently less than 1 μm.*

4.2 Pressure Drop Calculation

4.2.1 Pressure drop calculation based on conventional Poiseuille number

As it was mentioned above, hollow fibers can be considered as smooth microchannels and conventional Poiseuille number *Po* = 64 can be used to calculate pressure drop. However, variable liquid viscosity along fiber length should be considered. Thus, pressure drop (along the fiber, due to the viscous friction, excluding pressure drops of fiber inlet/outlet) can be expressed as:

$$\Delta p_{it} = \frac{128 \cdot \mu_{av} \cdot l \cdot Q_{f,t}}{\pi \cdot D_i^4 \cdot N} \quad (25)$$

where $Q_{f,t}$ is a volumetric flow rate through the fiber, l is fiber length, D_i is internal diameter, N is number of fibers and μ_{av} is average value of viscosity along the fiber.

Firstly, hydrodynamic response of hollow fibers was studied by Zarkadas [25]. Authors found that there is discrepancy between experimentally obtained results and conventional theory. They observed that experimental data are correlated with slope of the curve of -0.88 ($f = 64 * Re^{-0.88}$) compared to the theoretical prediction of -1 ($f = 64 * Re^{-1}$) for Hagen-Poiseuille flow, revealing that higher friction factors were obtained in the PP fibers. The friction coefficients obtained were higher than theoretical predictions by 1-41% and increased as Reynolds number became larger. Authors explain this shift from conventional behavior of laminar flow by influence of surface roughness, which can be often neglected for laminar low in conventional tubes. There were explained that the roughness of a few microns in a microchannel corresponds to high relative roughness values. This can lead to larger frictional losses and more flow disturbances and cause for an early transition from laminar to turbulent flow. Such explanation correlates, for example, with conclusions of Mala and Guo [51, 52]. However, authors [52] noted that a few studies have considered the effect of roughness on laminar flow since Nikuradse [53] and Moody [54] concluded that the roughness effect on the laminar flow characteristics could be ignored if relative wall roughness is less than 5%.

Very similar conclusions about fiber roughness were done by Gallik [32]. Author experimentally studied hydraulic response of "transparent" (fiber with smooth, non-deformed surface) and "porous" (fibers deformed by stretching, with cracks and pores) PP hollow fibers and concluded that "porous" hollow fibers have higher friction pressure drops due to the surface roughness. Despite the author considered Equation 25 as appropriate, there were no comparisons between experimental data and the theoretical prediction by the Equation 25 was performed. Nevertheless, the provided experimental data shows strong proportionality of the pressure drops to the volume flow rate typical for conventional laminar flow behavior.

It is important to mention that there was a period of intensive development of microscale fluid flow and heat transfer during 2000's. Many experimental work was performed providing better understanding in the discussed subject. The reliable data was collected and discussed in a comprehensive paper by Hetsroni [50]. The following main conclusions were done by authors:

- The behavior of the flow in micro-channels, at least down to 50 μm diameter, shows no differences with macro-scale flow. For smooth and rough micro-channels with relative roughness $0.32\% \leq k_s \leq 7\%$ the transition from laminar to turbulent flow occur between $1800 \leq Re_{cr} \leq 2200$.

- For single-phase fluid flow in smooth micro-channels of hydraulic diameter from 15 to 4010 μm, in the range of Reynolds number $Re < Re_{cr}$ the Poiseuille number, *Po* is independent on the Reynolds number, *Re*.
- Majority of experimental data shows that the friction factor is inversely proportional to the Reynolds number i.e. $f = \frac{const}{Re}$
- The comparison of experimental results to those obtained by conventional theory is correct when the experimental conditions were consistent with the theoretical ones. The experimental results corresponding to these requirements agree quite well with the theory.

Considering hollow fibers, we can conclude that hollow fibers should be considered as smooth tubes or tubes with very low relative roughness (less than 1%). We expect that conventional *Po* = 64 should be applied and Equation 25 can be used for pressure drop calculation for such conditions.

For real heat exchanger, we should consider not only the pressure drop along the fiber due to viscous friction but also local pressure drops of the inlet and the outlet of the fiber, in manifolds etc. These pressure drops can be determined using conventional approaches; however several of our experimental studies and calculations [55] showed that they are relatively low comparing to pressure drops in along the fiber (1-2% of total pressure drops).

4.2.2 Experiments on pressure drop of hollow fiber bundles

Let's consider the results of joint experimental work performed in close cooperation with the Faculty of Mechanical and Process Engineering of Augsburg University of Applied Sciences (for details see [33, 55]). The study (see [33]) was intended to define the thermal performance and pressure drop characteristics of bundles of polymeric hollow fibers. Three hollow fiber bundles were prepared for tests. Bundles (see Fig. 19a, b, c) were built from PP fibers whose ends were collected and potted together by epoxy resin (see Fig. 19d). Tab. 2 shows the parameters of the tested PHFHE bundles. The subjective assessment of the distribution of the fibers (poor, moderate or good) is based on the comparison of eight different bundles. The distribution is described as good, if the fibers are not concentrated in several areas but homogenously dispersed in the whole volume.

Fig. 19 *Tested hollow fiber bundles and quarter of the cross section of bundle no. 1.*

Tab. 2 *Parameters of tested bundles*

parameter	no. 1	no. 2	no. 3
distribution of fibers	good	moderate	good
bundle volume [m^3]	0.0043	0.0036	0.0068
bundle packing density/porosity, [%]	2.9 / 97.1	4.2 / 95.8	1.1 / 98.9
inner diameter of fibers [mm]	0.61	0.63	0.37
outer diameter of fibers [mm]	0.81	0.81	0.54
number of active fibers	332	397	811
length of fibers [mm]	744	745	885
outer heat transfer surface [m^2]	0.62	0.75	1.21

For all experiments values of tube Reynolds numbers were in the 181-1313 range thus all experiments were conducted with tube-side flow in laminar regime. Fig. 20 reveals results of the pressure drop dependency Δp on volumetric flow rate V_t. As expected, bundles' pressure drop increases proportionally with an increasing flow rate which corresponds to the behavior of developed laminar flow. The bundle no. 3 has the highest pressure drop due to fiber smaller diameter. Bundles no. 2 has a slightly lower pressure drop than bundle no. 3 because it has approximately 20 % more fibers and other parameters that are the same.

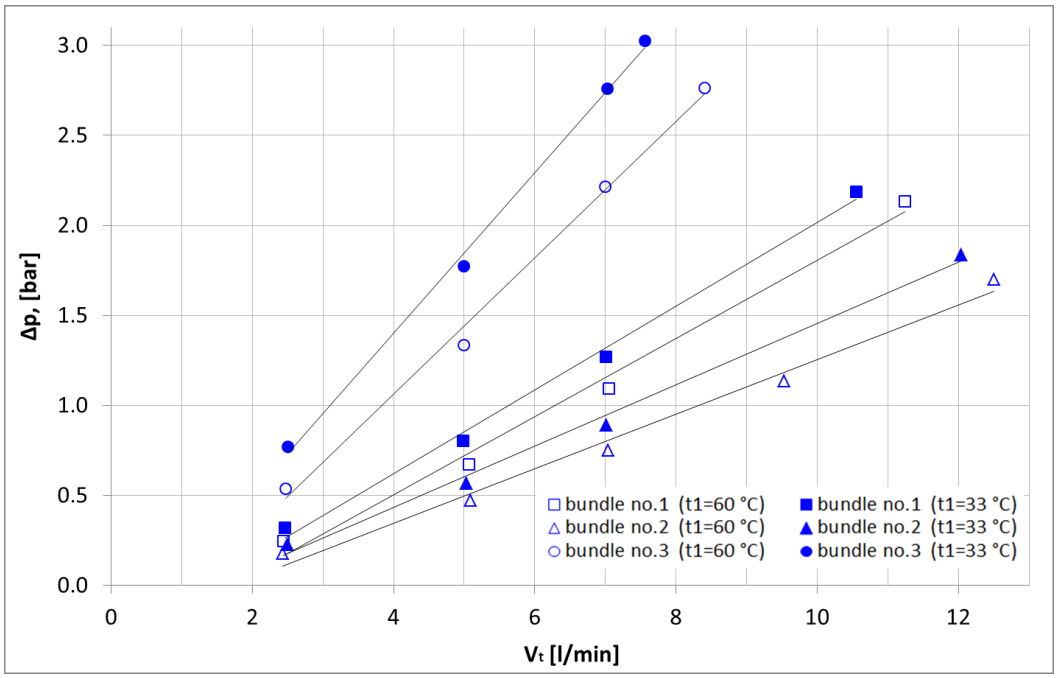

Fig. 20 *Pressure drops vs flow rate graph. Experimental results [55]*

In addition, there is an obvious influence of temperature regime on pressure drops. Higher reservoir temperature t_1 causes lower tube-side pressure drop of bundles. This effect is the most pronounced for the bundle no. 3 which has the highest pressure drop (about 25% difference). This effect can be explained by two reasons. Firstly, water viscosity is dependent on water temperature so the experimental results were influenced by change of mean temperature of fiber water. Take bundle no. 1 for example, if the reservoir temperature was T_1 = 60 °C the mean temperature of fiber water was in range of 24.9-34.9 °C and viscosity was 0.72-0.89 kg/(m s). For the reservoir temperature T_1 = 33 °C, the mean temperature of fiber water was 18.2-21.8 °C and viscosity was 0.96-0.105 kg/(m s). Thus, even change of the reservoir temperature causes change of the pressure drop of about 20%. Secondly, the fiber diameter is influenced by temperature and pressure. Higher temperatures (experiments with reservoir temperature T_1 = 60 °C) causes fiber diameter increase because of material thermal expansion and mechanical deformation by inner pressure. It should be noted that PP decreases its stiffness with increasing temperature. It should be noted that PP decreases its stiffness with increasing temperature. For example, PP Young's modulus decreases approximately four times (from 1.61 GPa to 0.44 GPa) with the rise of temperature from 21.5 °C to 75 °C [56]. Yield strength decreases approximately twice (from 35 MPa to 36 MPa) for the same conditions. Thus, the combination of these two factors causes lower pressure drops for

experiments in hotter surrounding water. Thus, the combination of these two factors causes lower pressure drops for experiments in hotter surrounding water.

At this point, experimental results will be examined against the theory presented earlier. Fig. 21 shows comparison of experimental results with theoretical prediction by Equation 25. Correlation about ±10 % was observed for the majority of experiments (9 of 13). However, worse correlation was observed for 4 tests in the low range of flow rates. It should be mentioned that pressure drops are very sensible on fiber diameter (see Equation 25) thus even small error in diameter causes high discrepancy.

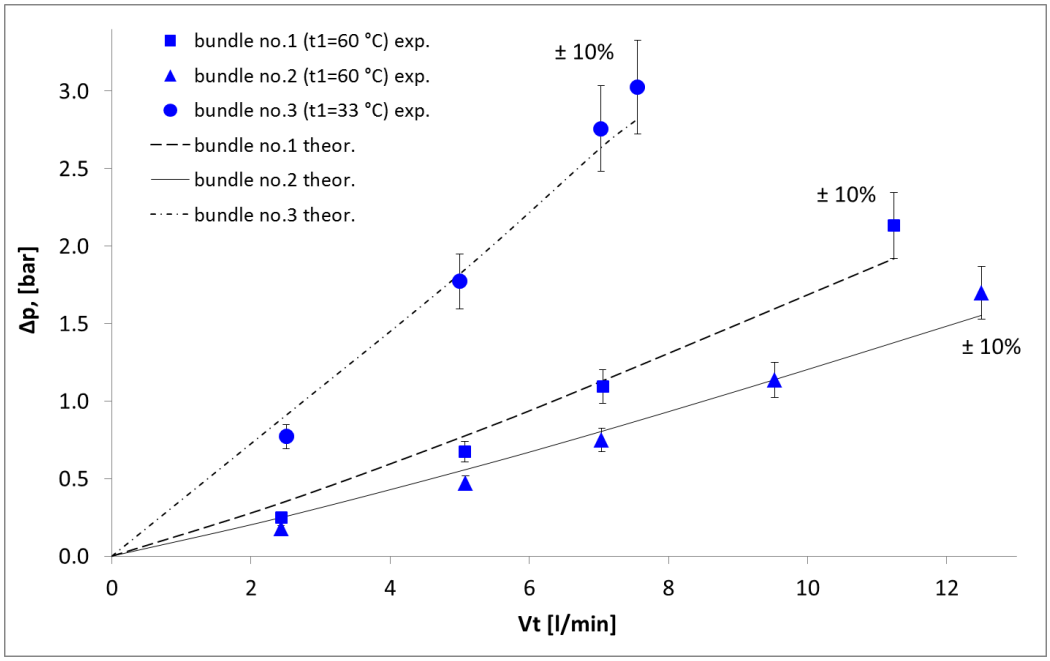

Fig. 21 *Pressure drops vs flow rate graph. Comparison of experimental results and theoretical prediction by Equation 25. [55]*

4.2.3 Influence of diameter measurement precision

Proper defining of hollow fiber is drastically important for correct use of Equation 25 because influence of diameter is very strong (diameter is in the fourth degree). This statement agreed with chapter 3.7 «Effect of Measurement Accuracy» of [38] providing the following equation for uncertainty definition:

$$\frac{\delta(fRe)}{fRe} = \left\{\left(\frac{\delta(\Delta P)}{\Delta P}\right)^2 + \left(\frac{4(\delta D_h)}{D_h}\right)^2 + \left(\frac{\delta(L)}{L}\right)^2 + \left(\frac{\delta(m)}{m}\right)^2\right\}^{1/2} \quad (26)$$

where f, Re, m, ΔP, d_h, L are the friction factor, the Reynolds number, mass flow rate, pressure drop, hydraulic diameter and channel length, respectively.

Polymeric hollow fibers are produced by extrusion process and one kilometer or even several kilometers of fiber can be used to produce one heat exchanger. Characteristics of the extrusion process strongly influence the resulting parameters of hollow fiber. Thin wall of the fiber should be used to achieve a high thermal performance. Manufacturing of thin-wall hollow fiber includes its elongation after extrusion from the extruder head and cooling of the fiber. It is very difficult to produce hollow fiber with a very precise diameter due to elongation step of the extrusion process. Different factors affect this step and causes oscillation of diameter of fiber. HeatLab uses special equipment to measure outer diameter of fiber before it is wounded on the final spool. Fig. 22 shows interface of software used for recording and analyzing fiber parameters. There is evident that hollow fiber has several points with diameters significantly different from required mean outer diameter of 0.8 mm (for example the peak between the second and the third kilometer, see Fig. 22). This fiber on the spool is marked as defective and is not used.

Fig. 23 shows graph of diameter of 18 kilometers of fiber measured along its length. This fiber is considered as good because there are no diameter defects, but only standard fluctuations of diameter. It can be used to manufacture heat exchangers.

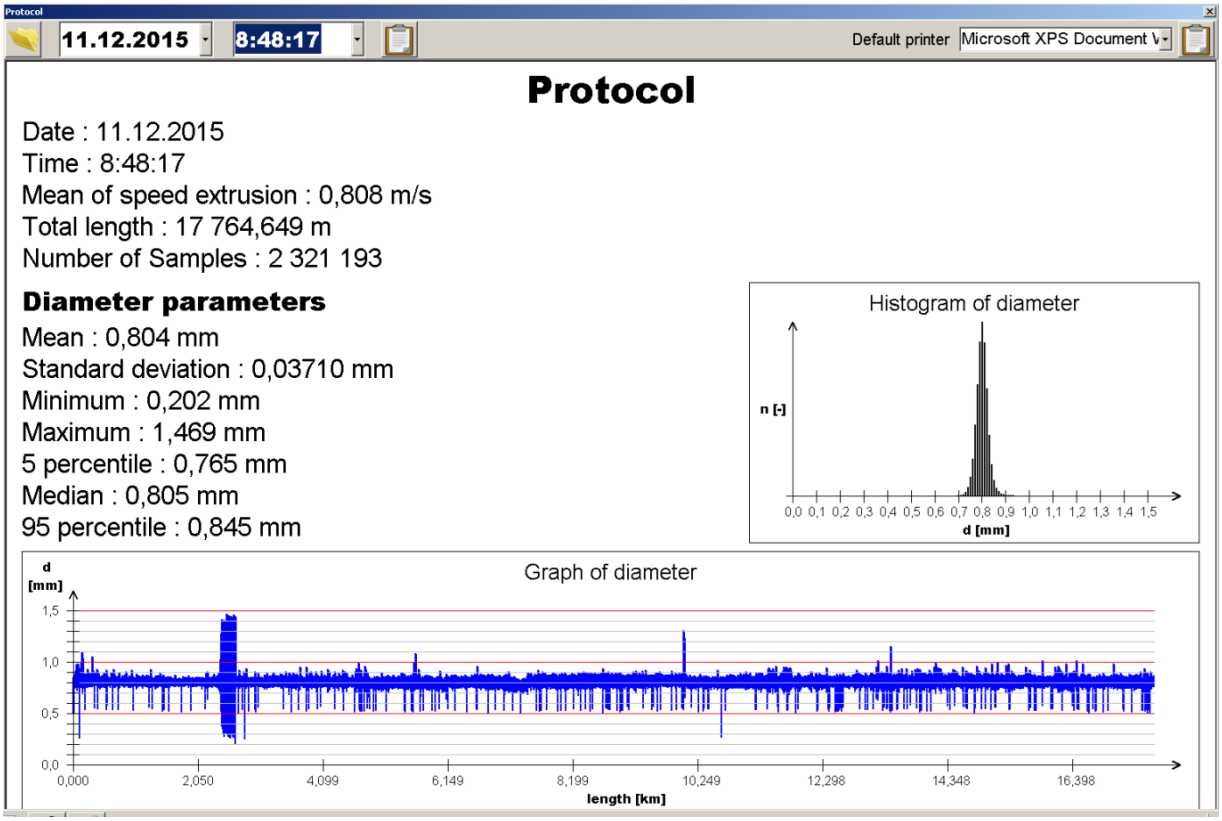

Fig. 22 *User interface of the software for measurement of parameters of extruded fiber.*

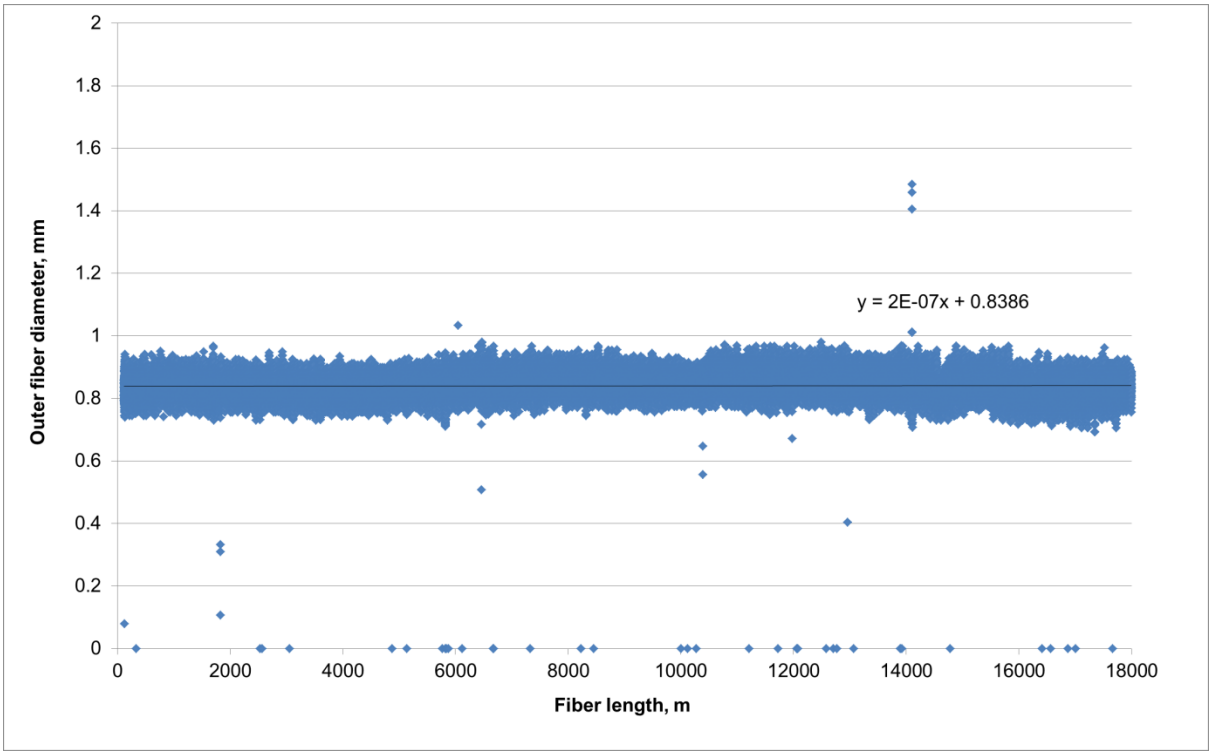

Fig. 23 *Fiber diameter measured for 18 kilometers of fiber. 16 measurements were done per 1 meter of fiber, thus the diameter was determined more than 300,000 times along fiber length).*

Let's consider a proper way how to define the diameter of the fiber for calculation of pressure drop. We propose the following equation to define the fiber diameter:

$$D_4 = \sqrt[4]{\frac{\sum_{i=1}^{n} D^4}{n}} \qquad (27)$$

where n – is number of diameter measurements.

We defined diameter of first 1 kilometer of fiber (the same data as shown in Fig. 23) as arithmetic average and by Equation 27. Diameter defined as arithmetic average is D_{av} = 0.8393 (corresponds to plateau value 0.8386 shown in Fig. 23) mm and D_4 = 0.8240 mm. The error in the pressure drop calculation due to the use of arithmetic average of diameter instead of D_4 will be 7.7%! The error will be even higher for hollow fiber with higher diameter oscillation (fiber produced from other materials, with a smaller diameter etc.). Thus, it can be strongly recommended use of Equation 27 to define the diameter for pressure drop calculation.

4.3 Prediction of the Nusselt Number

Two different methods of determining the temperature profile inside a polymeric hollow fiber heat exchanger were analyzed in [24]. These methods are a simplified correlation suggested by Hickman and a rigorous solution of the extended Graetz problem by Hsu. Hsu's method of the extended Graetz problem is the most complete because it is solved for the thermal developing region, taking in account the axial heat conduction within the fluid. As in the case of the classical Graetz problem, this analysis is based on the assumptions of constant physical properties and incompressible fluid flow with negligible viscous dissipation. It was shown that experimental results correlate well with data predicted by Hsu's approach. On the other hand, this approach is complex and requires many calculations, making its usage inconvenient.

Hickman's approach [24] gives a solution for incompressible fluid flowing through a circular tube (maintained at constant temperature), with constant physical properties, a fully developed laminar velocity profile and a thermally developing temperature profile. The T3 convective boundary condition is utilized; this assumes that the outside wall temperature of the circular duct is axially constant and that the heat flux is linearly proportional to the temperature difference between the outside wall temperature and the inside wall temperature, which can vary axially as well as peripherally. The following equation was proposed to determine the asymptotic Nusselt number:

$$\mathrm{Nu}_{\mathrm{T3}} = \frac{(48/11)+\mathrm{Nu}_{\mathrm{w}}}{1+(59/220)\mathrm{Nu}_{\mathrm{w}}} \tag{28}$$

Equation 28 yields Nu_{T3} values which fall between 3.66 and 4.36. The lower limit of this Nusselt number range is the asymptotic Nusselt number corresponding to the constant wall temperature boundary condition ($Nu_w = \infty$) and the upper limit is the limiting Nusselt number corresponding to the constant heat flux boundary condition ($Nu_w = 0$) [24]. This simplified solution doesn't take into account the influence of a developing flow region, and underestimates heat transfer for short ducts but is sufficient for long fibers ($L/D_i > 200$).

The next relationship was proposed [47] to calculate the internal mean Nusselt number of the channel with thermal developing region based on asymptotic Nusselt numbers calculated by Hickman's approach and incremental heat transfer numbers calculated by Hsu's approach:

$$Nu_{T3} = \frac{\left(\frac{48}{11}\right)+Nu_w}{1+\left(\frac{59}{220}\right)Nu_w} + \left\{0.05 - \frac{0.065}{[1+exp(0.46\cdot Nu_w+2.47)]}\cdot(4Gz/\pi)\right\} \tag{29}$$

Equation 29 predicts inner Nusselt number within a precision of -1.5 and 3.4% of those obtained by the Hsu analytical solution for $Gz \leq 26$ [47]. This equation can be applied easily and does not need any sophisticated software for calculations. Author considers that it can be used effectively for PHFHE with short fibers observing the possibility of scaling effects.

According to Yarin [38] the experimental study of the heat transfer in micro-channels is problematic because of their small size. It makes a direct recording of temperatures in the fluid and the wall very difficult. Investigation of heat transfer inside the hollow fibers experimentally is even more difficult because it is mostly impossible to create uniform and well-defined boundary conditions on the inner surface of hollow fibers. It was shown [38] that use of the wrong boundary conditions can cause misleading results of HTCs in microchannels.

Equation 28 and 29 are based on analytical solution of Hickman [24] for boundary conditions of the third type on the fiber outer surface. They can be used to derive inside HTC from the experimentally obtained OHTCs and to predict inside HTCs if outside HTCs are known. However, these equations were not proven by experiments throughout the entire range of the inside boundary conditions. In all published papers about PHFHEs (see Chapter 3.1) and in our studies, experimental conditions did not allow estimating inside HTC independently (without use of equations 28 and 29). However, it should be noted that Equation 28 includes solutions for boundary conditions of constant heat flux (Nu = 4.34) and constant temperature (Nu = 3.66) on the inner surface. These solutions are proven experimentally for ordinary microchannels [38], and thus Equation 28 is partially approved.

5 HEAT TRANSFER AND FLUID FLOW ACROSS BUNCHES OF FIBERS

5.1 Theoretical Consideration

Heat exchangers are manufactured mainly from a large amount of identical discrete elements. For example, in shell-and-tube heat exchanger, fluid flow in a shell is organized across the system of cylindrical tubes. This kind of flow can be characterized as an external flow because boundary layers around cylinders develop freely, without constraints created by adjacent surfaces. Thus, there is a flow region outside the boundary layer in which velocity and temperature gradients are negligible. The primary objective is to define suitable correlations for the pressure drop and HTCs of cross-flow heat exchangers.

The geometrical configuration of fibers in heat exchangers (tube pitches) varies. In some cases, fibers are placed in large distances (pitch to outer diameter ratio > 3) and, possibly, do not influence each other. It is possible to consider such a displacement of fibers as bunch of separated tubes and use equation for a cylinder in a flow. Fluid flow of non-ideal fluid (viscous) across separated cylinder is characterized by the boundary layer which starts to form on the front part of the tube, then continues along the cylinder periphery and splits from the cylinder surface in the rear part. The Churchill and Bernstein relation was proposed [46] to calculate the Nusselt number across a separate cylinder for the entire range of the Reynolds numbers and Peclet numbers $Pe = Re\,Pr > 0.2$):

$$Nu = 0.3 + \frac{0.62 Re^{1/2} Pr^{1/3}}{\left[1+(0.4/Pr)^{2/3}\right]^{1/4}} \left[1 + \left(\frac{Re}{282.000}\right)^{5/8}\right]^{4/5} \quad (30)$$

Authors [6] caution that empirical equation should not be considered as “sacrosanct” because it is reasonable over a certain range of conditions and accuracy better than 20% should not be expected.

If the pitches between fibers are smaller (pitch to outer diameter ratio < 3) then the system should be considered as the bunch of fibers. A forced convection problem across a separate tube and bank of tubes has been studied in depth by various authors. The heat-transfer characteristics of staggered and in-line tube banks were studied by Grimson [46], and the results can be represented in the form of Equation 31. The values of the constant *C* and the exponent *m* depend on the geometric parameters used to describe the tube-bundle arrangement. The Reynolds number is based on the maximum velocity occurring in the tube bank; that is, the velocity through the minimum-flow area.

$$Nu = C\ Re^{m}\ Pr^{1/3} \quad (31)$$

5.2 Experimental section

5.2.1 Tested heat exchangers

Several examples of liquid-to-gas cross-flow heat exchangers were prepared from PP hollow fiber fabric and microtubes (one module was made of stainless steel tubes) in the HeatLab to study heat transfer on fiber bunches (see Fig. 24). Tab. 3 represents parameters of ready modules: number of tubes/fibers N, fiber length L, outer and inner diameters (D_o and D_i), tube pitches in width and depth (b_1 and b_2), overall heat transfer area based on outer surface (A_o) and frontal flow area (A_f).

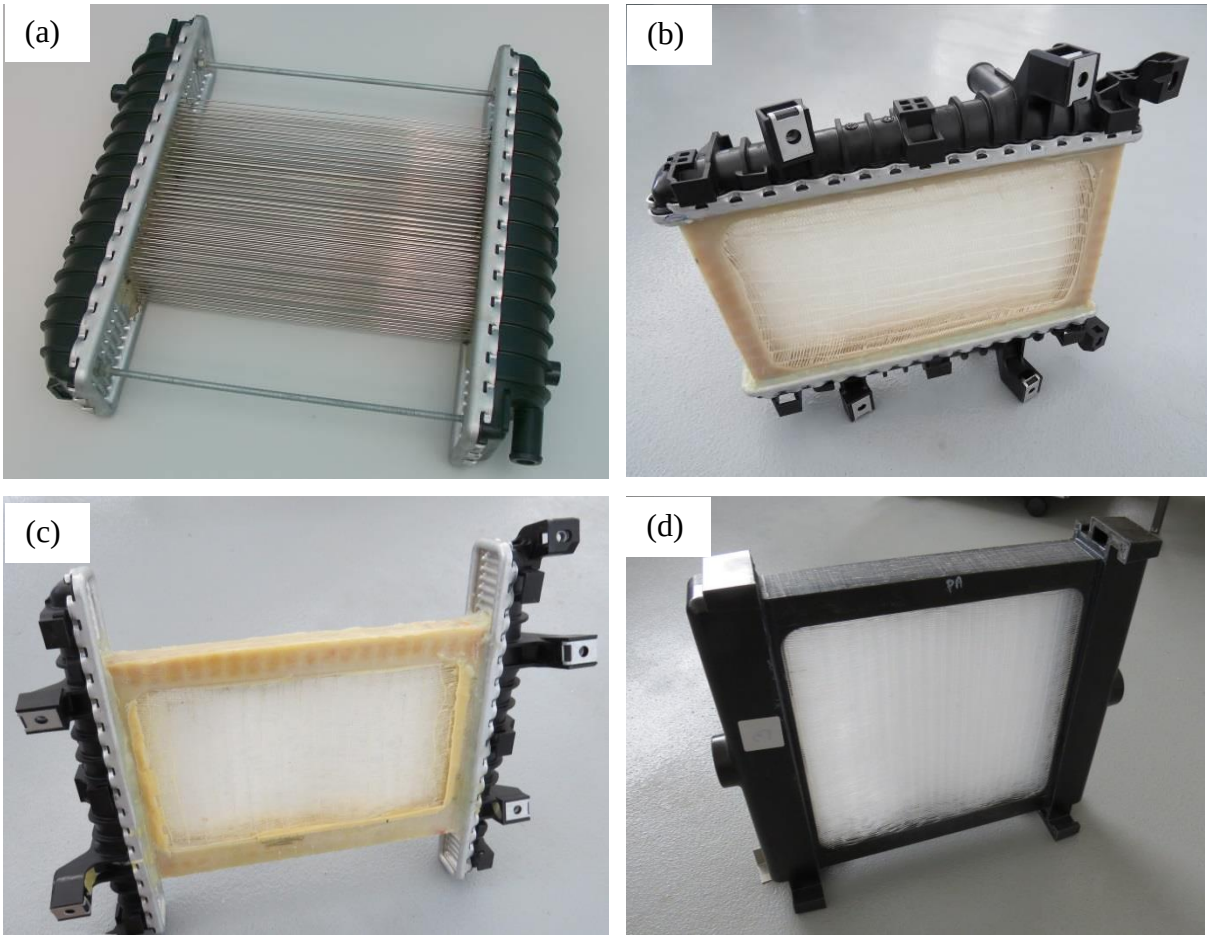

Fig. 24 *Tested heat exchangers: (a) heat exchanger made of stainless steel tubes (module S1) (b, c) heat exchangers based on hollow fiber fabric (modules P1 and P2) (d) heat exchangers based on hollow fiber fabric made by pilot-operated link (modules P3 and P4)*

Tab. 3 *Geometrical characteristics of tested modules (S1, P1, P2, P3 and P4)*

module	N	L (mm)	D_o (mm)	D_i (mm)	b_1 (mm)	b_2 (mm)	A_o (m^2)	A_f (m^2)
S1	200	185	1	0.75	7	5.8	0.12	0.025
P1	728	135	0.7	0.60	2.3	3	0.22	0.032
P2	560	260	0.55	0.45	1.7	3	0.25	0.032
P3	1960	250	0.6	0.48	1.8	2	0.92	0.060
P4	1904	220	0.8	0.64	1.8	2	1.05	0.053

5.2.2 Experimental setup and experimental conditions

Thermal performance tests were performed in a certified calorimeter room (modules S1, P1, P2, P3 and P4) designed for measuring automotive radiator performance (see equipment scheme on Fig. 25). An ethyleneglycol-water solution (50% by volume) was used as a hot medium circulated in the tube side of modules (hot coolant circuit) and air flowed around the fibers as a cooling media. The inlet and outlet temperatures and volume flow rates of the two streams were observed in real time (frequency measurement of 1 Hz) and were recorded during steady-state regime tests. Air temperatures were measured using a set of PT 100 temperature sensors placed in regular intervals upstream (8 sensors) and downstream (19 sensors) of cross-section of the heat exchanger, which gave an approximation of air temperature fields. Inlet and outlet temperatures of EG solution were measured using five PT 100 sensors. Volumetric flow rates of EG solution and air were measured using calorimeter flow meters (two flow meters on the EG side and three inserts for different ranges of air flowmeter). Then the recorded data was recalculated automatically to the mass flow rates using the calorimeter software with respect to the thermal properties of liquids.

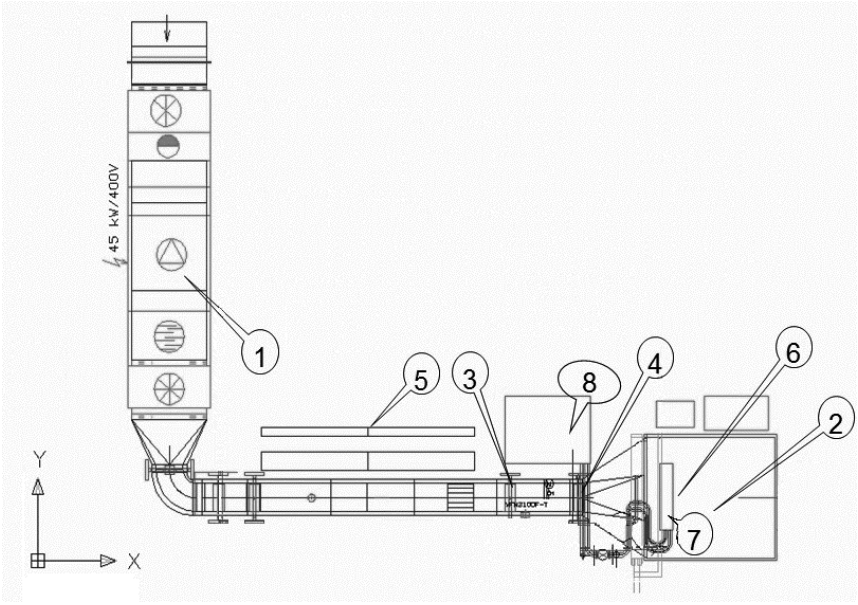

Fig. 25 *Calorimetric room scheme of automotive company used for measurements with high air flow rates (1 - air fan controlling air velocity through the heat exchanger cross-section; 2 - the calorimetric room space; 3 and 4 - electrical heater and refrigerant cooler to control air inlet temperature; 5- three inserts of air flowmeter (ranges 300-2200 kg/hour, 1800-7000 kg/hour and 6000-25000 kg/hour); 6- air temperature sensors; 7- tested heat exchanger; 8- hot coolant circuit).*

Additionally, modules P3 and P4 were tested in the calorimetric chamber of HeatLab (see Fig. 26, Fig. 27 and Fig. 28). The reason for these experiments was to define thermal performance of the modules P3 and P4 with low air velocity (it was not possible in calorimeter of automotive company). This calorimeter room allows to measure thermal performance of heating equipment up to 4 kW. The flow rate and inlet/outlet temperature of water through the HEX is set up and measured by integrated equipment of calorimeter. Air side tunnel was built to supply heat exchangers by air and measure air temperatures and flow rate. The air flow was created by centrifugal ventilator, regulated by shutter and uniformly distributed across channel by perforated net. The air velocity was tentatively measured by anemometer and the air temperature was measured in 9 points (three on inlet and six on outlet) by PT100 temperature sensors (1/3 DIN precision) connected to data acquisition system. Moreover, liquid differential manometer was used to collect data about pressure drops. Pressure drops were defined as difference of static pressure before and after tested modules.

Fig. 26 *HeatLab calorimetric chamber for heating/cooling equipment testing*

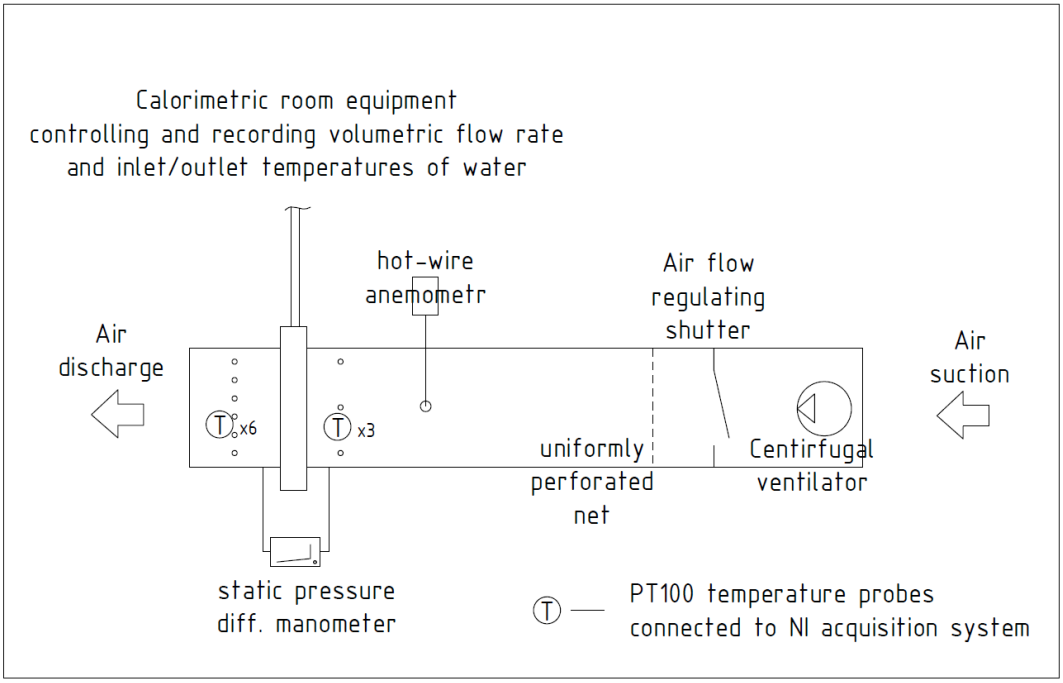

Fig. 27 *Experimental setup installed in the calorimetric chamber of HeatLab. It was used for experiments with low flow rates of air.*

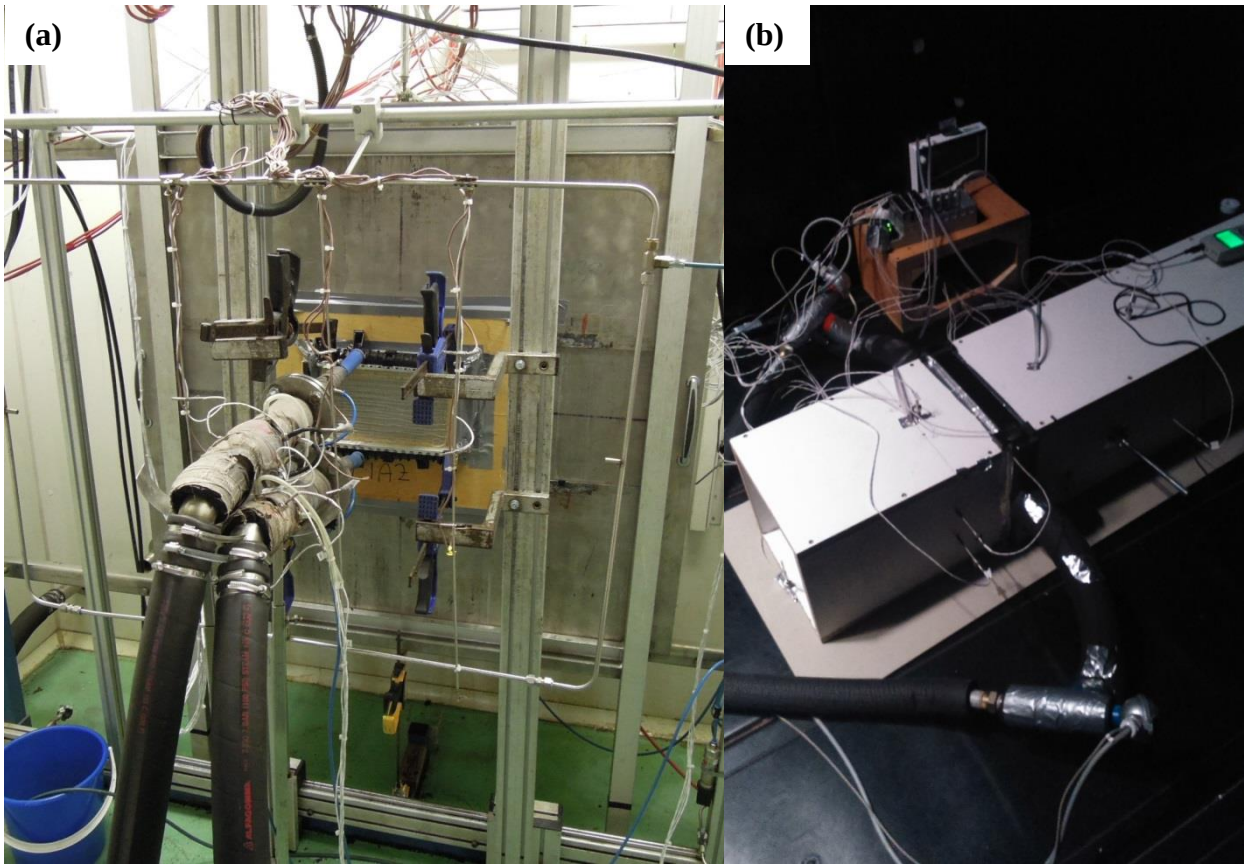

Fig. 28 *(a) Module P1 installed in automotive company calorimeter room and (b) module P3 tested in calorimeter room of NETME Centre.*

5.2.3 Reduction data

Reduction data were performed as proposed by Zarkadas [24]. Effective mean temperature difference averaged over the total heat exchange area was determined using logarithmic mean temperature difference (*LMTD*) and appropriate *LMTD* correction factor *F*. A correction factor was calculated according to Jeter [57]. Air-flow was considered as completely mixed and flow in tubes was considered as completely unmixed. Additionally, the iterative procedure proposed by Zarkadas [24] was used to determine both the tube- and air-side heat-transfer coefficients based on experimentally obtained OHTCs. In all calculations, properties were evaluated at the average temperature between the inlet and outlet. The wall thermal conductivity needed for the calculations was taken to be equal to 0.18 W/m K for isotactic PP and 12 W/m K for stainless steel [56].

5.2.4 Experimental results for modules S1, P1 and P2

Tab. 4 provides the range of results obtained for the 21 heat-transfer experiments performed. It contains the tube- and air-side Reynolds numbers, the heat-transfer rates, the OHTCs based on the outside fiber area, the heat exchanger effectiveness and the number of transfer units (*NTU*). Tab. 4 shows that the heat-transfer rate in heat exchangers with small non-finned tubes can reach high values, up to 2200 W for a device that is about 15x25x5 cm in size and several hundred grams in weight. The obtained OHTCs (up to 590 W/m^{2}K) are reasonably high compared to finned-tube metal heat exchangers. In the literature [6], design values of 25-55 W/m^{2}K are noted for water-air systems in finned-tube heat exchangers. These values include a total dirt factor which needs to be incorporated in the coefficients given in Tab. 4. However, the incorporation of the same fouling factor for polymer surfaces is questionable because limited experimental data for polymeric hollow fiber fouling are available. However, based on the extremely high values of OHTCs, it can be assumed that PHFHEs have high thermal performance. Tab. 4 shows that the values of the heat-exchanger effectiveness and the *NTU* were relatively low, up to 0.51 and 0.6, respectively. The thermal effectiveness is a function of the relative heat capacity rates of both streams and the general requirement for a high thermal effectiveness is the achievement of a high *NTU*. Low *NTU* values were caused by the small heat transfer area of the tested heat exchangers, despite the high OHTC values.

Tab. 4 *Thermal Performance of Heat Exchangers*

module	number of runs	Re_t	Re_{air}	Q (W)	U (W/m^{2}K)	ε	NTU
S1	4	620-650	390-1290	1300-2260	270-480	0.12-0.16	0.10-0.13
P1	12	70-240	180-930	960-2050	300-530	0.17-0.41	0.17-0.47
P2	5	125-135	150-740	1530-2190	400-590	0.38-0.51	0.44-0.60

Tab. 5 provides the range of tube- and air-side coefficients obtained for all modules tested. It is evident that the tube-side coefficients are very high and air-side coefficients are significantly lower. Tab. 5 also shows the percent contribution of each resistance to the total resistance. The results presented reveal that for aqueous systems the tube-side resistance would be the smallest of the three and that little improvement in the overall heat-transfer performance should be anticipated by increasing the tube-side Re number. Additionally, it

clearly seen that air-side thermal resistance is dominant and limits the overall heat transfer coefficient for all cases. The influence of wall thermal resistance was slightly higher for hollow fibers than for steel tubes but was not a significant factor. It can be concluded that the low thermal conductivity of PP not an obstacle for use of hollow fibers for gas-to-liquid heat transfer. The contribution of wall thermal resistance is small for both fibers and stainless tubes, but it is more pronounced for fibers because of the low thermal conductivity of PP. Moreover, both tube and air-side convective coefficients rise with decreasing diameters of the tube (fiber). For example, module P3, which has the smallest diameter (D_i = 0.45 mm ID), showed 25% higher h_t than steel tubes (D_i = 0.8 mm).

Tab. 5 *Tube- and air-side HTCs*

module	h_t (W/m^{2}K)	h_o (W/m^{2}K)	R_t/R_{ov} (%)	R_w/R_{ov} (%)	R_o/R_{ov} (%)
S1	2950-2980	320-670	7-13	6-11	76-87
P1	3160-3520	390-850	8-13	13-22	64-79
P2	4100-4140	390-940	6-12	13-25	63-80

Next, experimental results will be examined against the theory presented earlier. Fig. 29 shows a graph of the outer (air-side) HTC versus air Reynolds number for module S1. A large discrepancy exists between the experimental data and the theoretical prediction by the Churchill and Bernstein model. This model gives significantly underestimated results for the whole range of Reynolds numbers. We should note that this module has enough large pitches between steel tubes; the ratio of pitch to outer diameter b_1/D_o = 7 and b_2/D_o = 5.8. On the other hand, the prediction by the Grimson model is close to experimentally obtained data. Fig. 30 shows comparisons of theoretically obtained and experimental data for PP fiber modules P1 and P2. Data have the same tendency: values theoretically predicted by the Churchill and Bernstein equation differ significantly from experimental data (underestimated). Nevertheless, agreement between the theoretical prediction by the Grimson model and experimental data is significantly better. Results are underestimated for low *Re* and slightly overestimated for high *Re*.

The standard deviation of experimentally obtained data from the theoretical prediction by Grimson equation was 4% for module S1, 11% for module P1, and 8% for module P2. Thus, prediction by the Grimson equation shows good agreement with experimental data and can be recommended for calculation of heat transfer across banks of fibers. Furthermore, it should be

mentioned that the tested heat exchangers have relatively low fiber packing density and heat transfer areas. Production of fabric with lower pitch between fibers can significantly increase the heat transfer rate from the point of view of compactness.

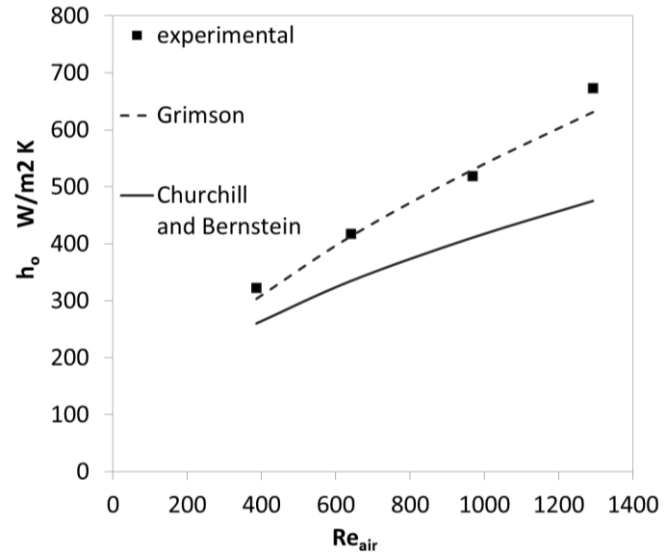

Fig. 29 *Outer heat transfer coefficients versus air Reynolds number of module S1*

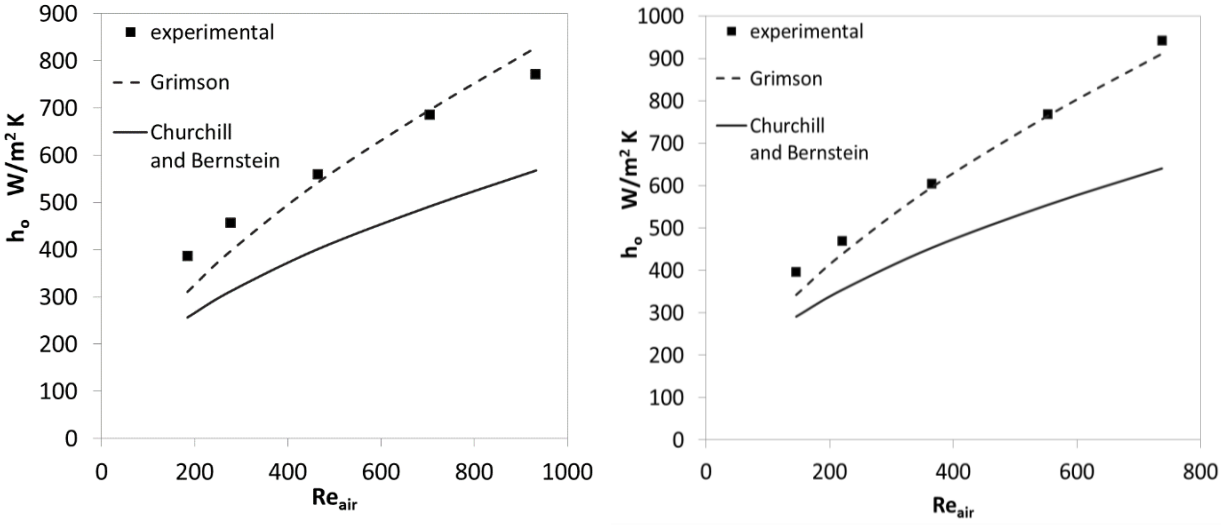

Fig. 30 *Outer heat transfer coefficient versus Reynolds number of modules P1 and P2*

5.2.5 Experimental results for modules P3 and P4

As it was mentioned above, modules P3 and P4 were tested in a wide range of air-velocities in calorimeter of automotive company and NETME Centre calorimeter. They have significantly higher values of compactness. For module P3, the ratio of width fiber pitch b_1 = 1.8 mm and depth pith b_2 = 2 mm; and, for module P4, b_1 = 1.6 mm and b_2 = 2 mm. Thus, the ratio $b_1/D_o \approx 2$ and $b_2/D_o \approx 2.5$ for both modules. Fig. 31, Fig. 32 and Fig. 33 shows the

results of experimentally obtained pressure drops, heat transfer rates and OHTC of these modules.

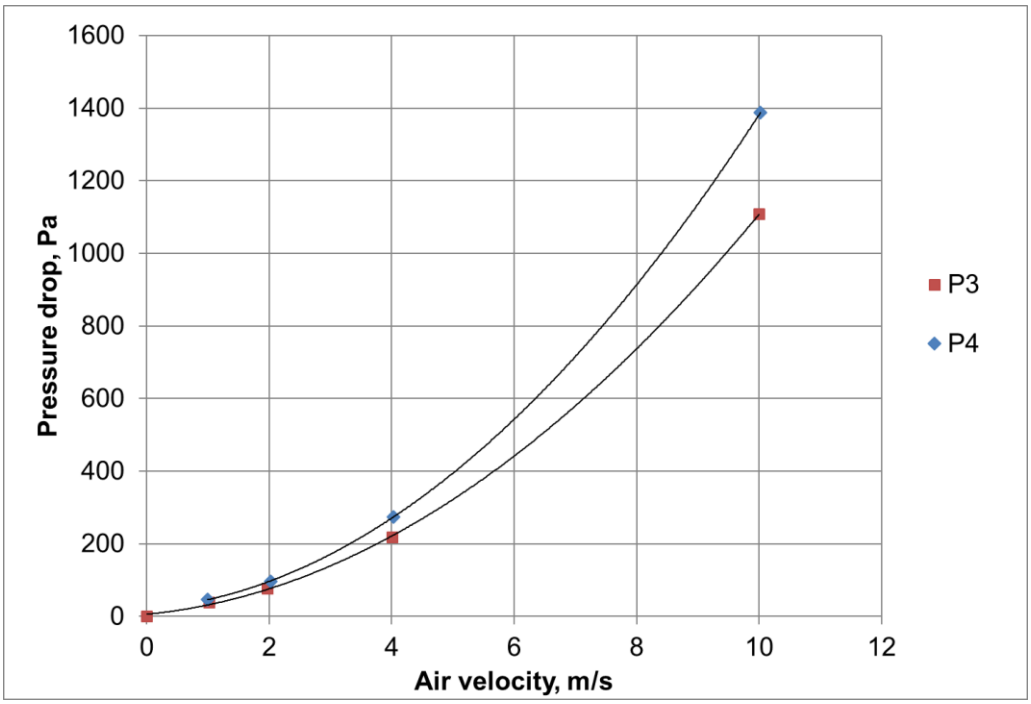

Fig. 31 *Air pressure drop vs air velocity in cross-section (flow rate is 220-2200 m^3/h).*

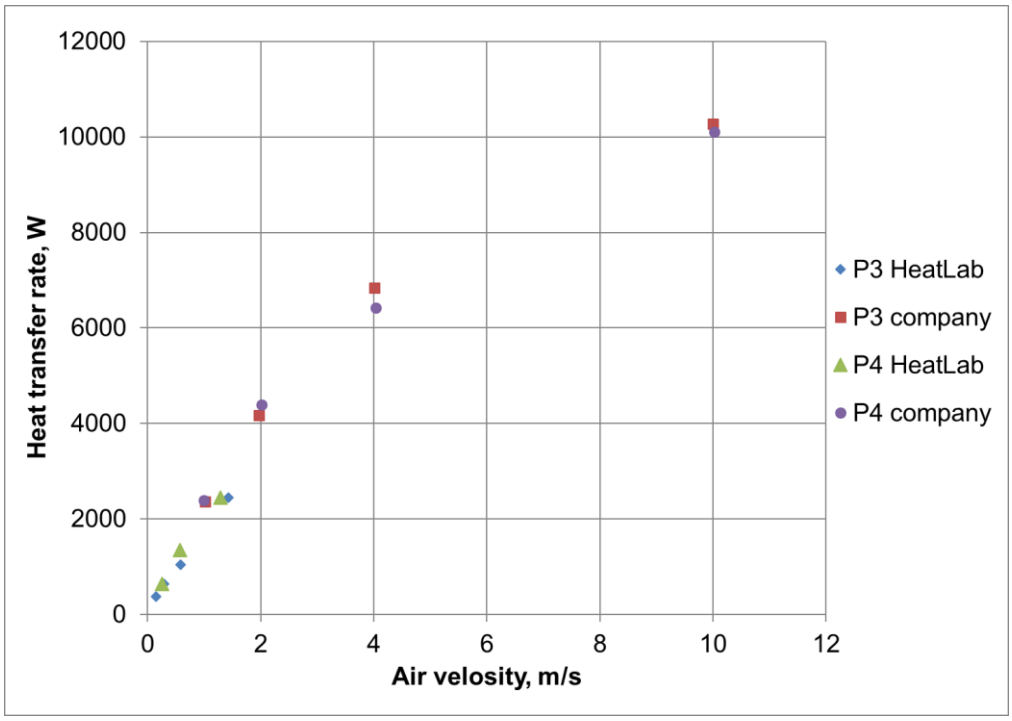

Fig. 32 *Heat transfer rate vs air velocity. There is mostly linear dependence of heat transfer rate on air velocity for low velocities (up to 2 m/s) measured in HeatLab. This fact is caused by the large NTU numbers (heat exchanger is too large for such small air quantities).*

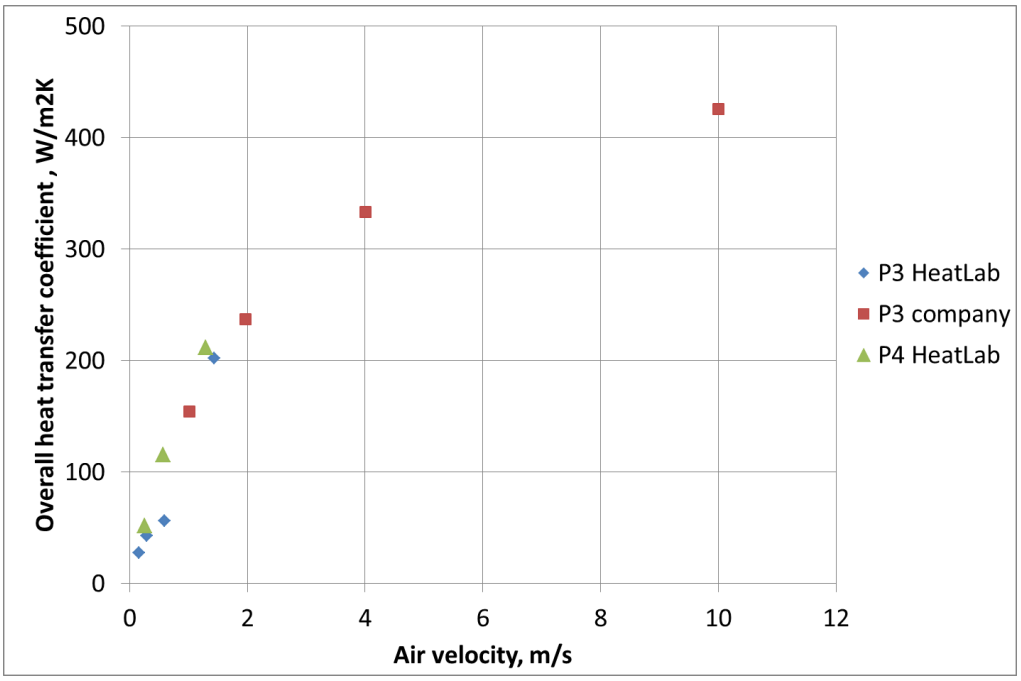

Fig. 33 *OHTC vs air velocity. There is a trend showing that PHFHEs achieve high OHTC values starting from relatively low values of air velocity (1 m/s).*

5.3 Comparison of PHFHEs and Conventional Finned-Tube Heat Exchangers

Heat transfer surfaces of modules P3 and P4 were invented to be used as liquid-to-gas heat transfer surfaces in different systems. For example, they can be used to replace existing car radiator heat transfer surfaces. Fig. 34 shows the heat transfer surface of currently widely used heat transfer surface of car radiators. It is made of aluminum flat tubes with aluminum fins soldered to their surface. This design can be considered as very modern and high-efficient; in fact, this technology is very close to being most effective existing solution of liquid-to-gas heat transfer surface. Thus, we assume that if hollow fiber surface will be competitive to such a structure – it will be thermally competitive to the majority of another existing metal liquid-to-gas heat transfer surfaces. Tab. 6 presents detailed information about the car radiator and module P3. We used experimentally obtained results of pressure drops (see Fig. 31) and OHTCs (Fig. 32) of module P3 to calculate surface-to-air HTC. To estimate parameters of aluminum core of conventional radiators we used thermal performance data of low temperature radiator VPATBH 8005 AA (automotive part of Audi Q7). Fig. 35 presents graphs of pressure drops and air-side HTCs h_o of both heat exchanger cores depending on air velocity. We can conclude that the core made out of hollow fibers is very competitive from the point of view of heat transfer. The pressure drops are slightly higher for fiber core but we

expect that this drawback can be eliminated by additional optimization of fiber distribution and decomposition.

Tab. 6 Comparison of parameters of aluminium radiator and module P3

Low temperature radiator LTR VPATBH 8005 AA made of aluminium alloy. Core size is 290x292x25 mm, 1x5 mm fins on 1.5x25 mm flat tubes, 1.9 m^2 surface.	Module P3, total fiber number is 1960 (14 layers 140 each), outer/inner fiber diameter is 0.6/0.48 mm, length 250mm. Core size is 250x250x40 mm, 0.92 m^2 surface.
Weight of empty core (without coolant and headers), full core weight and weight ratio:	
933 g, 1502 g, 100%	101 g, 396 g, 26%

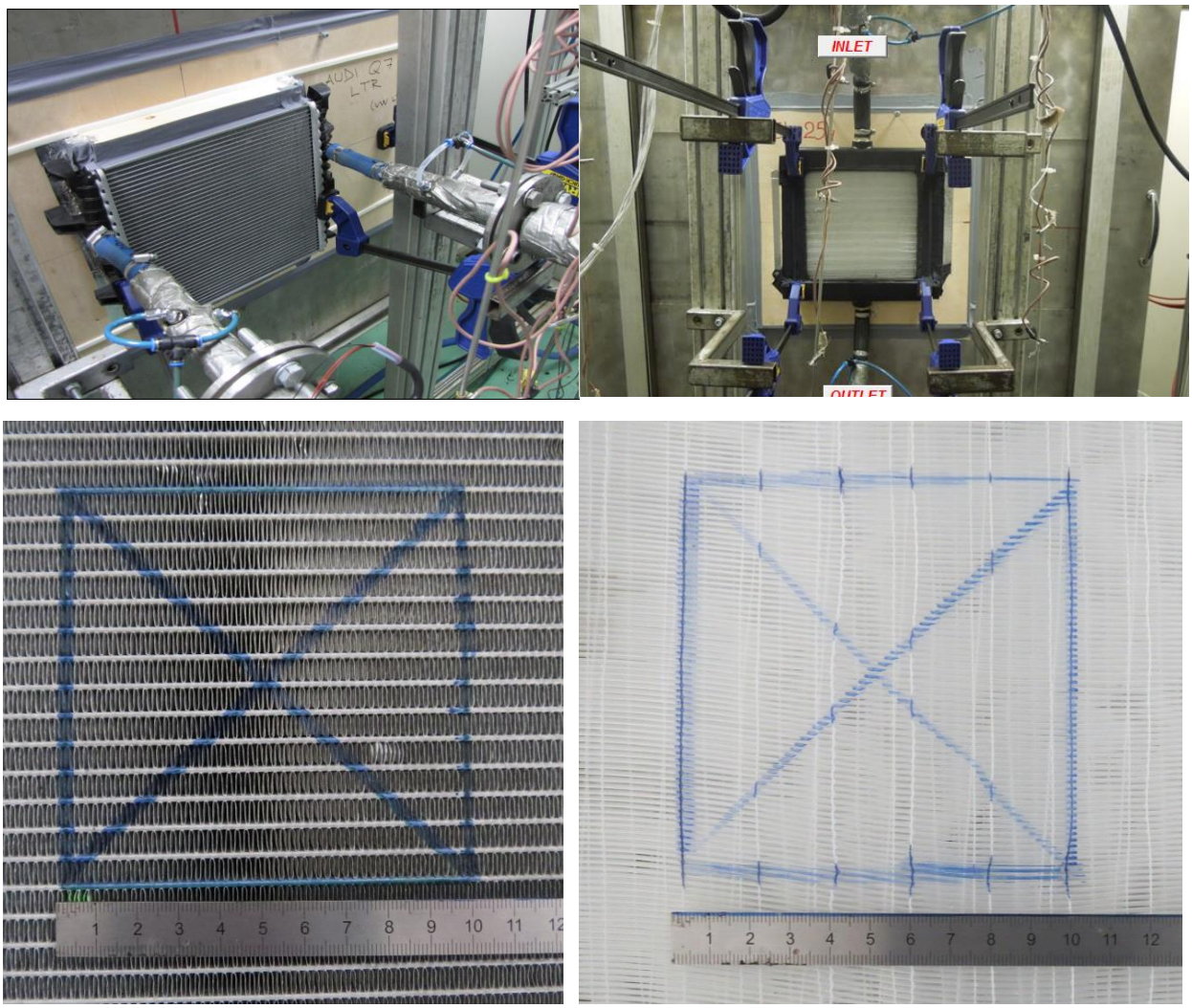

Fig. 34 *Comparison of heat exchange core of conventional aluminum car radiator and the fiber core of module P3.*

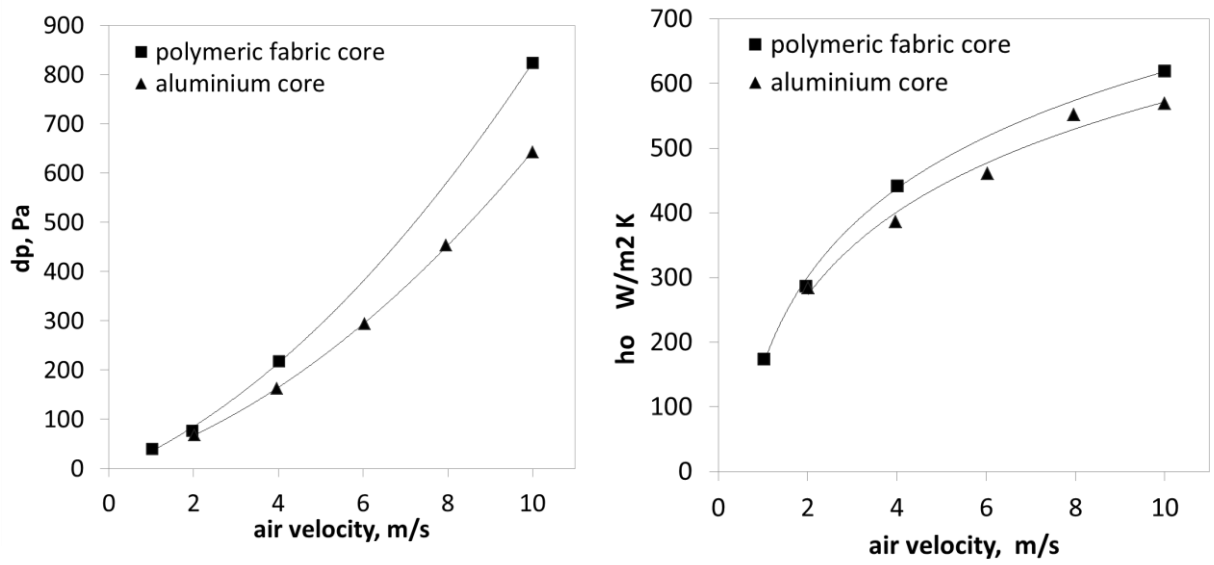

Fig. 35 *Pressure drops and surface-to-air HTC vs air velocity for aluminium core of car radiator and core made on fiber fabric (module P3).*

6 FOULING OF POLYMERIC HOLLOW FIBER SURFACES

The accumulation of unwanted deposits on the heat exchanger surface is referred to as fouling process [58]. The presence of these deposits creates a resistance to heat transfer and reduces the efficiency of the particular heat exchanger. Considering possible applications of PHFHEs two types of fouling were studied. The first one is particulate fouling by titanium oxide ($TiO_{2)}$ in photocatalytic reactor and the second is fouling by wastewater.

6.1 Experimental Study of Particulate Fouling by TiO_2 particles

The photocatalytic degradation of organic pollutants is based on the ability of TiO_2 particles to perform oxidation and reduction on their surfaces. This process is used to treat different types of polluted water. The basic precondition is that TiO_2 particles have the adequate crystallographic form and they must be activated by suitable ultraviolet (UV) radiation. However, it is a well-known fact that the efficiency of UV radiators is relatively low and therefore a significant fraction of the total electricity input is transferred not into UV radiation but into heat. The heat generation is so intensive that coolers are required to prevent the water from boiling. The heat exchangers are used either in the separation or degradation sections. Fouling is an integral part of the work of these heat exchangers. It depends on the wastewater type that has to be cleaned but anyway it is associated with particulate fouling of heat exchanger by TiO_2 particles.

The nature of particulate fouling is described in detail by Grandgeorge [59]. Particle accumulation on surfaces from liquid suspension flow can be considered to be a continuous process. Particles are transferred from the suspension bulk at the concentration c_b to the wall surface and then adhere to it. The deposition flux Φ_d can be expressed as:

$$\Phi_d = k_d c_b \tag{32}$$

$$\frac{1}{k_d} = \frac{1}{k_m} + \frac{1}{k_a} \tag{33}$$

where k_d, k_m and k_a are, respectively, the overall deposition coefficient, the mass transfer coefficient and the adhesion coefficient. According to the respective values of k_m and k_a, the global process is limited by the mass transfer or by the adhesion.

During particle deposition, the deposit thickness generally reaches a constant asymptotic value R_f^* [59]. On the one hand, it is possible that a continuous removal process occurs during the deposition process. On the other hand, the asymptotic behavior can be explained if the deposition flux decreases with the deposit thickness. If the deposit thermal conductivity and

density are constant, time evolution of the fouling thermal resistance can be expressed through asymptotic value R_f^* and fouling process time constant t_c as [59]:

$$R_f(t) = R_f^*\left(1 - e^{-t/t_c}\right) \quad (34)$$

Value of R_f^* shows the maximum level of fouling and its influence on heat transfer and t_c indicates the rate of its development. Both parameters are influenced by parameters of flow such as foulant concentration, particle size distribution, pH (measure of the activity of the hydrogen ion) and liquid velocity.

The heat exchanger from the PP hollow fibers was prepared to cool TiO_2 suspension and tested under fouling conditions. It is a low weight, low cost and corrosion resistant heat exchange system. It is expected that this heat exchanger has a high thermal performance as well as a high fouling resistance and defouling ability. Moreover, polymeric fibers have a smooth surface whose properties substantially differ from conventional metals. This feature can provide lower fouling based on a decrease of adhesion coefficient k_a. Furthermore, polymer fibers is flexible enough to move in a flow. In accordance with Wicaksana [60] bubbling is commonly used to control the fouling of submerged hollow fiber membranes. In the same manner, injecting of pressurized air can be used to increase liquid velocity causing the movement of fibers and deposit removal.

6.1.1 Experimental Setup

The heat transfer bundle (see Fig. 36) was built from PP fibers whose ends were collected in plastic screwed pipe fittings. Used fibers were twisted with different curvatures (50-100 mm) to ensure equal distribution of these fibers in volume. To produce this curvature the fibers were wound around 50 mm outer diameter steel tubes. Tubes with fibers were heated up to 120 °C for 5 minutes and then they were cooled naturally to stabilize this twisted shape. Epoxy resin was used to fill the space between fibers in the fittings. The ends of the fittings were milled and heated by hot air (about 120 °C) to remove burrs and open all ends of fibers. In addition, the bundle was pressurized by water up to 4 bar gauge pressure to ensure an absence of leakages in fittings and fibers. All damaged fibers (which showed leakages during the test) were eliminated. Moreover, colored water (with a small addition of ink) was used to determine fibers through which water can flow. The total amount of functional fibers in the bundle was 262 and effective immersed length was 1300 mm. It should be mentioned that extruded polymeric fiber has relatively high oscillation of both diameters along the length.

The relative difference of outer diameter measured in two places can exceed 5%. Inner and outer fiber diameters (0.461 and 0.523 mm respectively) were statistically obtained by studying light-microscope photos of milled cross-sections of the fittings as a mean values. Thus, the total heat transfer area based on the inner fiber surface was 0.493 m^2.

The experimental setup is a liquid/liquid heat transfer system. It mainly includes a tested heat exchange element, a hot foulant circuit, cooling water circuit and pressurized air injection system. The experimental setup scheme is shown in Fig. 36. The heat transfer bundle was placed into a transparent plexiglas tube (100 mm inner diameter) which was the shell of the heat exchanger. The shell was under atmospheric pressure and hot foulant fluid circulated through the shell naturally (circulating pump lifted the slurry up and then it flowed down through the shell). The fouling fluid was a suspension of TiO_2 in tap water (with concentration 1-5 g/l). Suspension particle size distribution was measured by laser difraction method by Malver Mastersize 2000 granulometer. 90% (by mass) of TiO_2 particles have size of 1-10 μm. The level of the liquid in the shell was adjusted by siphon piping and the shell flow rate was controlled by a three-way valve installed upstream. The slurry returned from the shell was re-heated in a bath having three heaters with a total capacity of 6 kW to temperature around 28-30 °C.

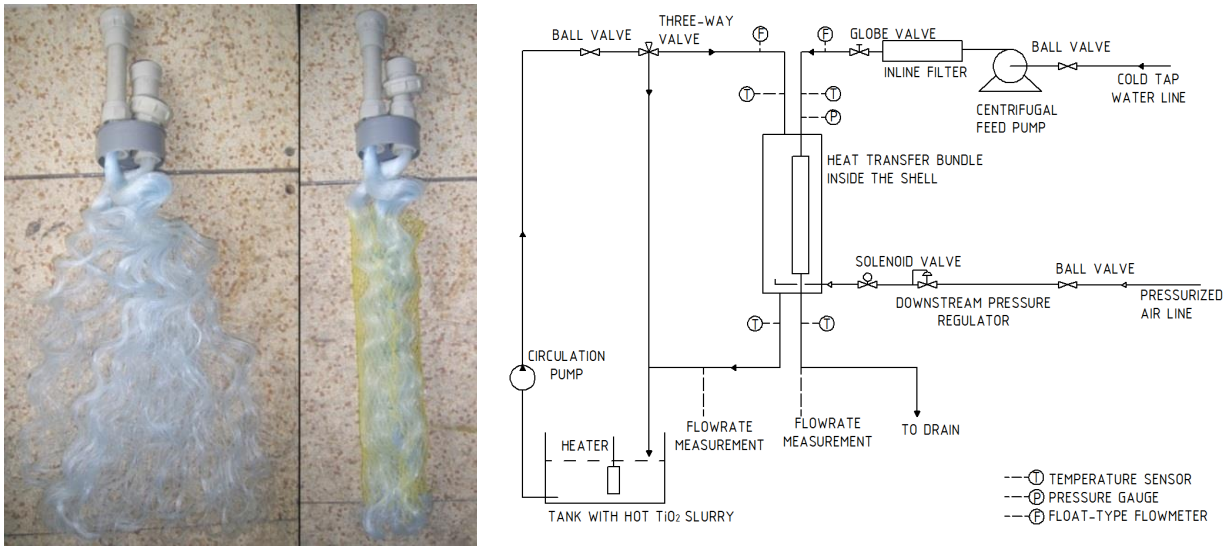

Fig. 36 *Hollow fiber heat transfer bundle (at the left) and experimental setup scheme*

The cold tap water was used as a cooling medium. It was pumped through the fiber bundle by means of a centrifugal pump. The flow rate of cooling water was adjusted by means of a valve but the temperature was not controlled and was 8-10 °C. An inline filter (50 μm particle

size) was installed upstream from the fiber bundle to protect lumen path of fibers from fouling.

The shell and tube (lumen path of fiber) flow rates were measured by float-type flowmeters calibrated for water and checked at the two ends by measuring the time required to collect a certain volume of liquid. Inlet and exit temperatures of both streams were measured with an accuracy of ± 0.1 °C by PT100 resistance sensors with 3-wire connections. They were recorded with frequency 0.1 Hz by datalogger throughout the measurements.

The source of pressurized air was connected to the bottom side of the shell to inject air bubbles inside the shell and remove the collected particulate deposit. It consisted of a downstream pressure regulator to control the injection pressure and solenoid valve to control time of injecting.

6.1.2 Fouling Test Procedure

Experiments consisted of three sets. The goal of the first part was to determine values of asymptotic fouling resistance R_f^* relative to the foulant velocity. The heat transfer bundle was removed and mechanically cleaned between measurements for different velocity. Firstly, stationary regime tests were performed on pure water to obtain reference values of HTC dependence on velocity. The tube flow rate was maintained constant (0.1 kg/s) and the shell flow rate was varied (0.025 – 0.4 kg/s). Secondly, the same set of measurements was performed for fouled conditions.

The goal of the second part was to study the rate of deposit growth (fouling process time constant t_c) and the influence of TiO_2 suspension concentration on it. Flow conditions of both (tube and shell) liquids were maintained constant for all runs (tube flow rate was 0.1 kg/s and shell flow rate 0.25 kg/s). A typical experiment started with pure water flowing through the experimental section. After the stationary regime was achieved, pre-diluted concentrated TiO_2 slurry was added to the heat bath and fouling started. Outlet temperature change was observed in-real time and used to determine the changing HTC.

When the HTC had decreased significantly a cleaning procedure was used to remove the deposit. The cleaning process was the same for all runs. It consisted of 5 one-second air injection pulses with a two-second pause between pulses. The injection pressure was set-up to 2 bars by a downstream pressure regulator. The injection air volume was limited by the open cross-section of solenoid valve seat and was approximately 20 l (at atmospheric pressure) for the whole set of defouling.

6.1.3 Evaluation of Experimental Data

Thermophysical properties of the suspension were estimated as properties of pure water because of low TiO_2 concentration of suspension. Experimentally observed inlet and outlet temperatures for the shell-side and tube-side liquids were used to determine the density, viscosity and thermal conductivity of the liquids using the following correlations [26]. The averages of the inlet and outlet of the tube-side and shell-side liquid temperatures T_{av} were substituted in the following correlations. For density, kg/m^3

$$\rho = 10^{-5}T_{av}^3 - 6 \cdot 10^{-3}T_{av}^2 - 3 \cdot 10^{-3}T_{av} + 1003 \quad (35)$$

dynamic viscosity, kg/(m s)

$$\mu = (-0.4607\, ln\, T_{av} + 2.3669)/1000 \quad (36)$$

thermal conductivity, W/(m K)

$$k = (-0.0097T_{av}^2 - 2.1662T_{av} + 559.2)/1000 \quad (37)$$

Constant value of water specific heat C_p = 4180 J/(kg K) was used for the whole temperature range of test.

The diameter-based shell-side Reynolds number Re_{sh} was calculated based on the shell interstitial velocity u_{sh} and equivalent hydraulic diameter D_h:

$$Re_{sh} = \rho u_{sh} D_h/\mu = \left((Q_{f,sh}/A_{sh})\rho D_h\right)/\mu \quad (38)$$

$$A_{sh} = \pi D_{sh}^2/4 - \left(\frac{1300}{500} \cdot \pi N D_o^2/4\right) \quad (39)$$

where $Q_{f,t}$ is tube volume flow rate, A_{sh} is shell free cross-section, D_{sh} is internal shell diameter, D_o is outer fiber diameter and D_h is equivalent hydraulic diameter calculated as:

$$D_h = 4A_{sh}/P = Q_{f,sh}/\left(\pi D_{sh}^2/4 + \left(\frac{1300}{500} \cdot \pi N D_o^2/4\right)\right) \quad (40)$$

where P is wetted perimeter consisted of internal shell surface and external fiber surface. It was assumed that the occupied cross-section and wetted perimeter for 1300 mm twisted fiber bundle can be calculated as 500 mm straight fiber multiplied by 1300/500 ratio.

Fouling causes a decrease of overall HTC and can be expressed as fouling thermal resistance R_f [58]. It is given by

$$R_f = \frac{1}{U_f} - \frac{1}{U_0} \quad (41)$$

where U_f and U_o are heat transfer coefficients for clean and fouled conditions. In the stationary test set we fitted experimentally observed HTC values by the curve $U = f(Re_{sh})$ and found resulting fouling resistance. Moreover we used Hickman's approach [24] to

determine and compare inside, outside, wall and fouling deposit thermal resistances. For more details about reduction data sequence see [61].

The overall heat transfer coefficient is assumed constant and is calculated:

$$U = Q/\int_{A_i}\left(T_{sh,b} - T_{t,b}\right)dA_i \quad (42)$$

where $(T_{sh,b} - T_{t,b})$ is mean difference of bulk temperatures of shell and tube water. Effective mean temperature difference averaged over the total heat exchange area was determined by using *LMTD* and appropriate *LMTD* correction factor *F*. Thus, the OHTC was calculated based on inside fiber surface area as

$$U = Q/(\Delta T_{lm} \cdot F \cdot A_i) \quad (43)$$

where *LMTD* was determined as

$$\Delta T_{lm} = \frac{(T_{sh,in} - T_{t,out}) - (T_{sh,out} - T_{t,in})}{ln((T_{sh,in} - T_{t,out})/(T_{sh,out} - T_{t,in}))} \quad (44)$$

and correction factor was obtained from ChemSOF LMTD Correction Factor Charts [62] and checked by diagrams for one-shell heat exchanger with a one tube path [6]. The *Q* value for the tube-side stream is used since the latter does not present any heat losses to the surroundings.

On the other hand, the OHTC can be expressed as a combination of convection, wall and fouling thermal resistances:

$$U = 1/(\frac{1}{h_i} + \frac{D_i}{k} ln \frac{D_o}{D_i} + R_f + \frac{D_i}{h_o D_o}) \quad (45)$$

where h_i and h_o are convective HTCs, R_f are fouling thermal resistance $(D_i/k)(ln\,(D_o/D_i))$ is thermal resistance of wall. We modified and used this expression to fit experimental obtained HTC data.

We used Hickman's formula [24] to evaluate the asymptotic Nusselt number for laminar flow inside hollow fiber (see chapter for details 4.3). It will be shown later that the inside HTC values, which were derived from experimental results by mean of Hickman's formula, are in good agreement with the assumption of constant inside HTC.

Additionally, we calculated Gr/Re^2 complex to estimated influence of natural convection in the shell because shell-side velocities were very low. It was obtained that the natural convection contribution is negligible even for the smallest Reynolds numbers and shell-side convection was considered as forced. Shell-side HTC can be expressed through Nusselt number by the following common equation:

$$h_0 = Nu\frac{k}{D_o} = C\ Re_{sh}^m Pr^{1/3}\frac{k}{D_o} \quad (46)$$

where *Pr* is Prandtl number which can be considered as function of temperature and assumed as constant (temperature differences were small). *C* and *m* are constants which depend on geometrical configuration of flow around fibers. All parameters in Equation 46 were maintained constant during experiments except of Reynolds number. Thus substituting h_o values to Equation 45 gives us following function:

$$U = f(Re_{sh}) = \frac{1}{C_2 + (1/C_1 Re_{sh}^m)} \quad (47)$$

where $1/C_1\, Re_{sh}^m$ is shell convection thermal resistance and C_2 is lumped resistance consisting of all other components including fouling resistance. We calculated parameters C_1, C_2 and *m* and fitted appropriate curves in Origin 9 software. As first step, parameters C_1 and *m* were varied for the fixed value of C_2 ($C_2 = 0$). As second step, values of C_1 and *m* were fixed and parameter C_2 were obtained.

6.1.4 Results and discussion

Firstly, it should be mentioned that obtained values of overall HTC are relatively high for both clean (up to 2100 W/m^2 K) and dirty (up to 1750 W/m^2 K) conditions. Tab. 7 compares the OHTC values of different hollow fiber heat exchangers with a regular water-to-water heat exchange system. It can be concluded that the system used has high, competitive HTC values.

Tab. 7 *OHTCs of polymeric hollow fiber heat exchangers*

Heat exchanger type	*U*, W/m^2 K
Water-to-water [a]	850-1700
PP [b]	1310
HEPP3 [c]	2080
HEPEEK2 [c]	1930
Membrana 041938 [c]	1100
PES [c]	2100
PP-based hollow fiber M4 [d]	1230
PP, clean [e]	400-2100

[a] regular water-to-water heat exchanger [6]; [b] Zarkadas and Sirkar [24]; [c] Song et. al. [25]; [d] Qin et. al. [27]; [e] present study

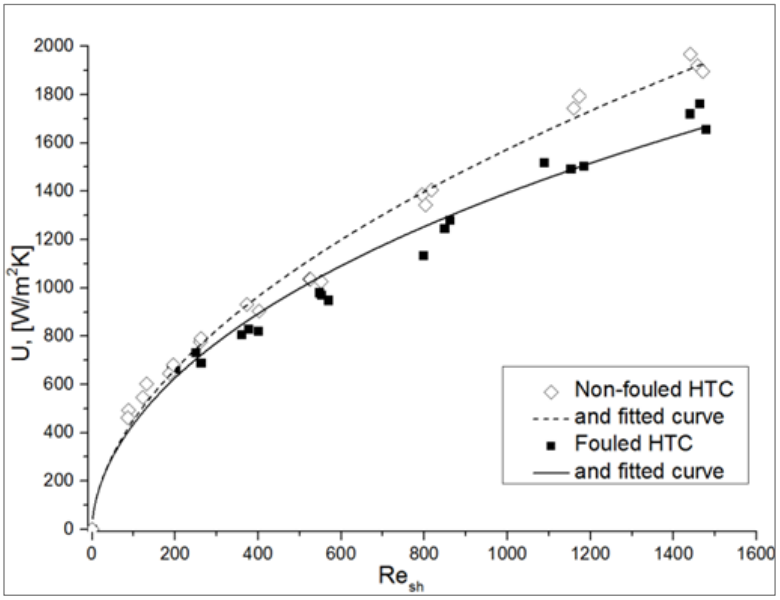

Fig. 37 *Overall heat transfer coefficient versus shell-side Reynolds number for clean and fouled (c_b = 1 g/l) conditions.*

Fig. 37 shows variation of OHTC for clean and fouled surfaces with a change of the shell Reynolds number. It is obvious that HTC has a strong dependence on the shell Reynolds number. It means that shell-side thermal resistance is dominant. We assumed fouling resistance independent on shell velocity and experimental results have been correlated by using Equation 47. For clean HTC: C_1 = 35.21, C_2 = 3.34*10^{-5} and m = 0.558 and for fouled condition HTC: C_1 = 35.21, C_2 = 1.15*10^{-4} and m = 0.558. Asymptotic value of fouling resistance R_f^* of 8.2*10^{-5} m^2 K/W was obtained in this way.

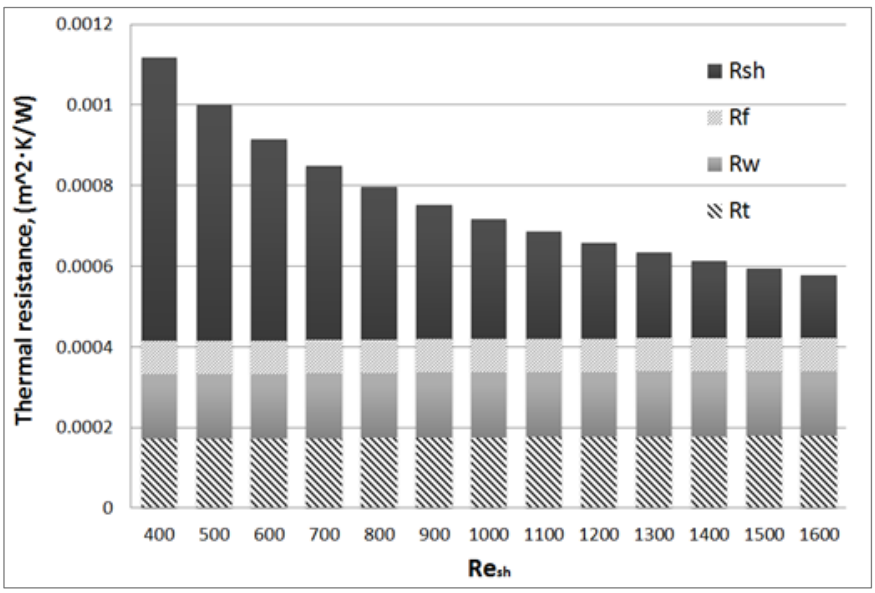

Fig. 38 *Contribution of shell R_{sh} and tube R_t convective, wall R_w and fouling R_f thermal resistances to overall thermal resistance versus shell-side Reynolds number*

It was used in combination with Hickman's approach to determine the contribution of separate thermal resistances to the overall one (see Fig. 38). It is clearly shown that deposit layer resistance is relatively low in comparison with the resistance of wall, tube convection resistance and especially shell convection resistance. In fact, it has no significant influence on heat transfer for Reynolds numbers lower than 600. Grandegeorge [59] claims values of TiO_2 particulate fouling R_f^* up to $5.5*10^{-4}$ (m^2 K)/W for liquid flowing with a velocity 0.2 m/s inside channel of plate heat exchanger. Extrapolation of this result on lower velocities used in the present study (0.007-0.045 m/s) shows that R_f^* obtained here is order of magnitude smaller.

On the other hand, the assumption of fouling resistance independent on shell velocity is not strict because dependence on liquid velocity is very important and R_f^* depends on liquid velocity as u^{-2} [59]. We correlated the HTC test results by second-order polynomials and used Equation 41 to determine R_f^* dependence on velocity (see Fig. 39). These values were fitted by the following function:

$$R_f^* = (1.075 * 10^{-7})/u^2 \quad (48)$$

It can be seen that the inclination of the curve changes at the critical velocity value of around 0.1 m/s. Asymptotic value of fouling resistance R_f^* has a strong dependence on the velocity and sharply increases below this value. This R_f^* behavior is in good agreement with the results obtained by Grandegeorge [59]. Unfortunately our results cover a narrow range of velocities (range of Re = 800-1600 in Fig. 37) and this is not enough to characterize R_f^* behavior. In general, we can characterize the fouling level of tested heat exchanger as low.

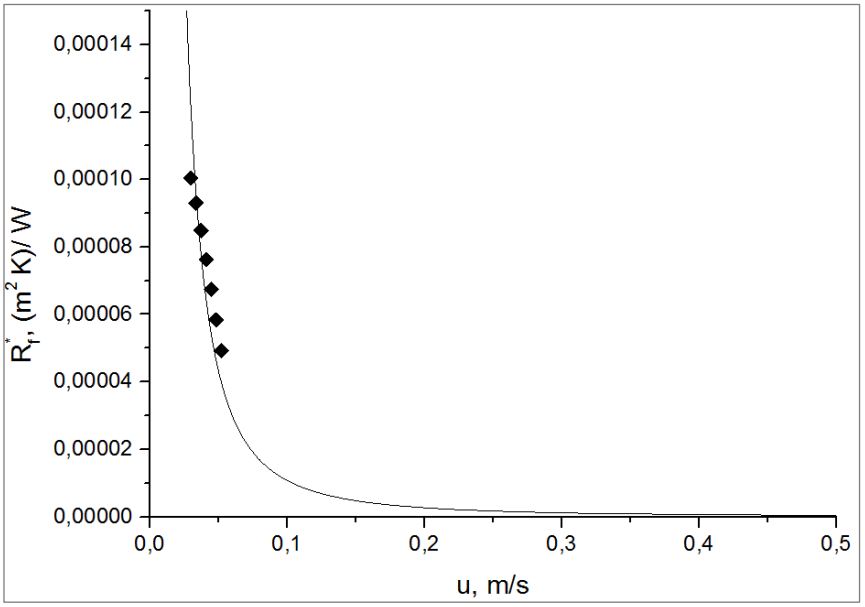

Fig. 39 *Asymprotic fouling resistance versus shell-side liquid velocity*

During fouling evolution tests, we were watching as TiO_2 particles were accumulating in the shell. It was seen that fiber surface collects a deposit irregularly which was caused by non-uniform velocity field and random fiber distribution inside the shell. In some places, the surface of fibers was relatively clean whereas deposit was seen in other places. The most significant fouling agglomerations were observed in locations where fibers were touching each other. Fig. 40 shows fouling evolution for two concentrations: 1 g/l and 5 g/l.

We used Equation 34 to correlate experimental results and obtained the following equation. For 1 g/l concentration foulant:

$$R_{f1}(t) = 1.34 * 10^{-4}\left(1 - e^{-t/142}\right) \quad (49)$$

and for 5 g/l concentration foulant:

$$R_{f2}(t) = 1.34 * 10^{-4}\left(1 - e^{-t/53}\right) \quad (50)$$

In both cases, fouling develops rapidly and achieves asymptotic values in just a few hours. It can be associated with very low liquid velocities in the shell and, as it was mentioned before, low level of maximum fouling value R_f^*. The previous study [59] showed that liquid velocity strongly influences deposition coefficient k_d value which sharply increases with a decrease of velocity below 0.1 m/s. Fig. 40 shows that concentration of foulant c_b has influence on the rate of deposit development (deposition coefficient k_d) but has no influence on its maximum value R_f^*.

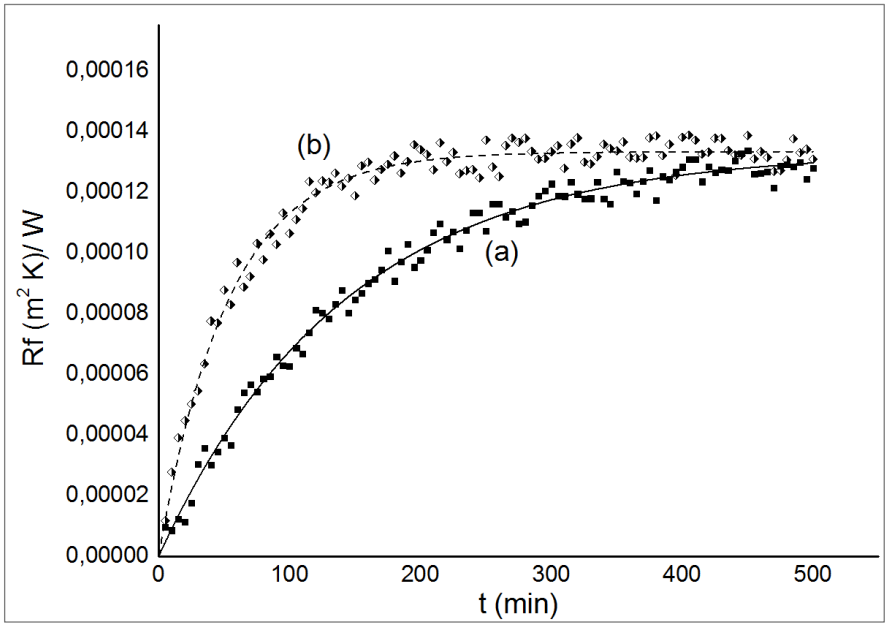

Fig. 40 *Fouling evolution in time (u = 0.04 m/s): (a) TiO_2 bulk concentration c_{b1} = 1 g/l; (b) c_{b2} = 5 g/l.*

We used air bubbling as the defouling procedure to clean the fiber surface from the deposit. It was observed through a transparent shell that fibers were moving and particles were being removed from the fiber surface during the cleaning. It is worth noting that defouling was not absolutely complete. Bubbles destroyed particle agglomerates and removed the main mass of deposit particles but some particles remained. The graph on Fig. 41 shows the typical OHTC behavior during defouling. The plateau on the left part of the graph corresponds to maximum fouling state (U = 1480 W/m^2 K). It is around 75% of the initial clean value (U_0 = 2020 W/m^2 K). Steep HTC rises at 13:50 and 14:50 corresponds to air injecting. It should be noted that HTC sharp peaks are associated with an abrupt rise of liquid velocity during defouling. On average HTC grows to 1800-1900 W/m^2 K (90% of initial value). The evolution of the deposit after defouling is character to clean surface fouling but starts from a higher level and goes faster than fouling of the initially clean (or mechanically cleaned) surface. This fact is also documented by Grandegeorge [59] which quotes that a surface cleaned by change of liquid velocity collects deposit faster than an initially clean surface. We also expect that defouling efficiency should decrease during long-term operation.

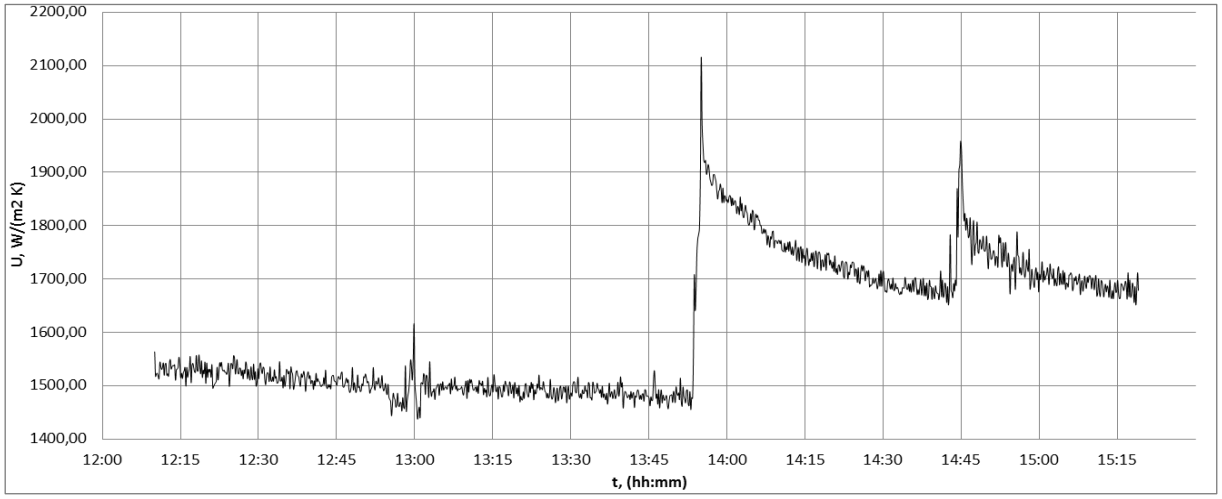

Fig. 41 *HTC change during defouling procedure (u = 0.04 m/s, c_b = 5 g/l)*

6.2 Experimental Study of Fouling of Hollow Fiber Bundles by Wastewater

Wastewater (sewage) is a source of energy that can be used for heating buildings and tap water with heat pumps. The technology is simple and proven. According to Schmidt [63], over 500 wastewater heat pumps are in operation world-wide. However, heat exchangers installed in sewage channels are negatively affected by fouling. Fouling in sewage is complex and consists of two basic types: particulate fouling and bio-fouling. Particulate fouling is the growth of deposits on a surface associated with the adhesion of solid particles. Bio-fouling is the growth of a layer of microorganisms (bacteria, algae and fungi) or macro-organisms (mussels, barnacles, hydroids) [58]. Crystallization and corrosion is considered insignificant and non-affecting.

The growth of deposits on heat exchange surfaces creates additional resistance to heat transfer and decreases the efficiency of the system. Fouling is considered to be a major disadvantage and a challenge for wastewater heat pump applications [64]. Several articles about wastewater applications of plastic heat exchangers have been published and they show that plastic heat exchangers are more advantageous than metal for such conditions [65]. A comparison of several plastics showed that PTFE is a very good choice due to its mechanical properties, chemical stability and low adhesion [66]. Nevertheless, cheaper materials such as PP are suitable also. A low-cost and lightweight heat exchanger from PP hollow fibers was prepared and tested under fouling conditions in wastewater. Such devices can be used for in-building heat recuperation. Our previous study showed that small-diameter PP fibers have a superior OHTCs [61] as well as smooth surface, chemical inertness and low adhesion [56].

6.2.1 Wastewater specification

Three types of wastewater were studied: wastewater from gym showers, from a commercial laundry (which mainly washed work clothing) and from an experimental laundry (which only washed dormitory bed linen). The following wastewater parameters were chosen as relevant (see Tab. 8):

- The chemical oxygen demand (COD) test is commonly used to indirectly measure the amount of organic compounds in water. Most applications of COD determine the amount of organic pollutants found in surface water or wastewater, making COD a useful measure of water quality. It is expressed in milligrams per liter (mg/l), which indicates the mass of oxygen consumed per liter of solution.
- The biochemical oxygen demand (BOD) is the amount of dissolved oxygen needed by aerobic biological organisms in a body of water to break down organic material present in a given water sample at a certain temperature over a specific time period. This is not a precise quantitative test, although it is widely used as an indication of the organic quality of water. The BOD value was expressed in milligrams of oxygen consumed per liter of sample during 5 days of incubation at 20 °C and is often used as a robust surrogate of the degree of organic pollution of water.
- pH is a measure of the acidity of an aqueous solution.
- Electrical conductivity (specific conductance) measures a material's ability to conduct electricity.
- Turbidity is the cloudiness or haziness of a fluid caused by individual particles (total suspended or dissolved solids) that are generally invisible to the naked eye. Turbidity is measured with a nephelometer and expressed in Nephelometric Turbidity Units (NTU).
- P_{ov} and N_{ov} are the overall amounts of dissolved phosphorus and nitrogen, respectively. Nitrogen and phosphorus in the water cause algae to grow faster.
- Escherichia coli (E. coli) are anaerobic, rod-shaped bacteria that are commonly found in the lower intestine of warm-blooded organisms.
- Coliform bacteria are a commonly used bacterial indicator of the sanitary quality of water. While coliforms themselves are not normally causes of serious illness, they are easy to culture and their presence is used to indicate that other pathogenic organisms of fecal origin may be present.

Tab. 8 *Properties of tested wastewaters*

Parameter	Unit	Shower wastewater	Laundry wastewater 1	Laundry wastewater 2
Wastewater origin		Gym showers	Commercial laundry	Washing machine; only washing steps using hot water were used, and one step of washing was with chlorine
COD	mg/l	248	242	189
BOD	mg/l	51.1	136	62.6
pH	-	8.1	7.9	7.8
Electrical conductivity	µS/cm	897	781	810
Turbidity	NTU	36	29	22
P_{ov}	mg/l	1.1	1.1	1.1
N_{ov}	mg/l	0.28	4.4	3.5
E. coli	KTJ/100 ml	0	68	32
Coliform bacteria	KTJ/100 ml	50	299	145

6.2.2 Hollow fiber bundles and experimental setups

Bundles made of PP hollow fibers were produced for tests in HeatLab. Fibers were collected together and potted with epoxy resin; the pottings were milled to open entrances inside all fibers. Fibers were twisted with different curvatures (50-100 mm) to improve their volume distribution. This is a very important feature because straight fibers connected together create a very compact bundle with fibers touching each other, therefore a large area of fibers cannot be in contact with the surrounding liquid and thus transfer a small amount of heat. The bundle was pressurized by water up to 4 bar gauge pressure to ensure an absence of leakages. Moreover, colored water (with a small addition of ink) was used to check permeability through the fibers. Inner and outer fiber diameters were statistically obtained by studying stereomicroscope photos of milled cross-sections of the fittings as a mean value. Tab. 9 shows the parameters of the tested PHFHE bundles.

Tab. 9 *Parameters of tested fiber bundles*

	bundle no. 1	bundle no. 2	bundle no. 3	bundle no. 4
Fiber number	470	470	430	550
Outer/inner fiber diameter, mm	0.7/0.55	0.7/0.55	0.8/0.65	0.55/0.45
Fiber total/effective length, mm	1100/640	900/650	900/700	900/700
Heat transfer area (outer), m^2	0.67	0.67	0.76	0.67

The first setup (see Fig. 42) was intended to study fouling with forced convection on the bundle surface. The fiber bundle was placed into a transparent Plexiglas shell (100 inner diameter) to create a heat transfer section like shell-and-tube heat exchanger. Wastewater and cooling circuits were connected by the test section, creating the experimental setup. The hot wastewater flowing through the shell was cooled by tap water flowing through the lumen path of the bundle. The shell is under atmospheric pressure and the wastewater flows though it aided by gravity, and then a circulating pump (Calpeda NCE EL) lifts the wastewater up and it flows down through the shell. The level in the shell is adjusted by siphon piping and the shell flow rate is controlled by a three-way valve installed upstream. This flow regime is similar to the flow in unpressurized sewage systems. The wastewater returned from the shell is reheated in a tank with a 6 kW heater to 30 °C. The wastewater flow rate is measured with a float-type Parker LoFlow 802414 flowmeter (3-22 l/min range). The cold tap water is pumped through the fiber bundle by a centrifugal pump (Pumpa PKM80-1). The flow rate of tap water is adjusted by means of a globe valve and measured by a Parker LoFlow 802413 flowmeter (2-10 l/min range). The flowmeters were calibrated by measuring the time required to collect a certain volume of liquid. The tap water temperature was not controlled and was in the range of 10-12 °C depending on flow rate. An inline filter (50 μm size) was installed upstream from the fiber bundle to protect the lumen path of fibers from fouling. All temperatures were measured using PT100 (1/3 DIN Class B precision) sensors and recorded by an Omega Daqpro-5300 datalogger with an accuracy of ± 0.1 °C and frequency of 0.1 Hz.

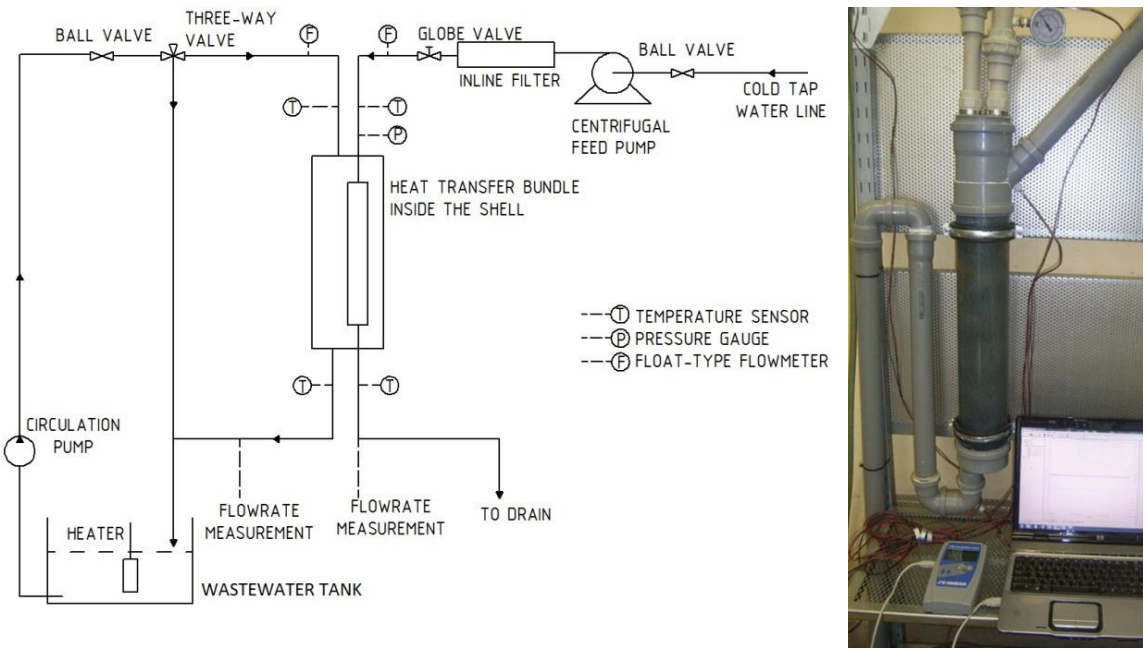

Fig. 42 *Experimental set-up diagram (right) and view of test section.*

The second setup (see Fig. 43) was built to study fouling with natural convection on the bundle surface. Bundles were placed in the 2 m^3 PP accumulation tank and were equipped with inlet/outlet temperature sensors, a flow meter, a filter and regulating valves. The tank was connected to a wastewater supply from a washing machine (Primus FX 240) through the intermediate tank with a pump. Several temperature sensors were placed in the tank to estimate the bulk temperature of the wastewater.

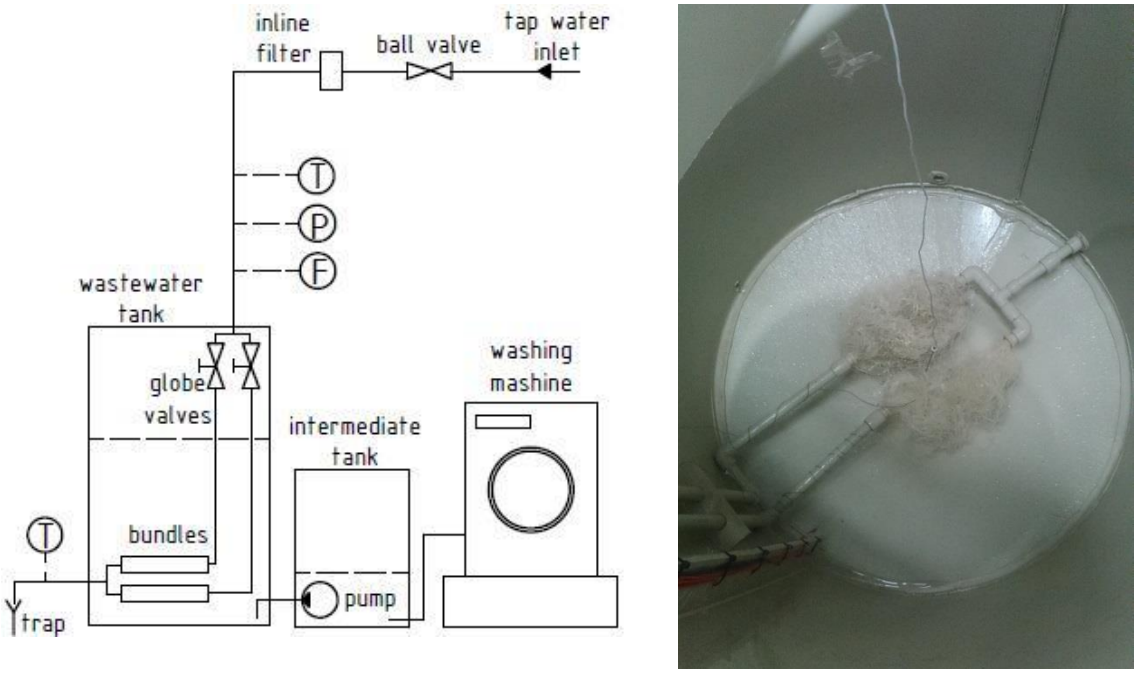

Fig. 43 *Experimental set-up diagram (right) and view of bundles placed in the bottom of the wastewater accumulation tank.*

6.2.3 Test procedures and reduction of data

Experimental conditions for all tested bundles are shown in Tab. 10. The table includes the inlet temperature and flow rate of tap water T_1 and m_{12}, the inlet temperature and flow rate of wastewater (for setup 1) T_3 and m_{34} and temperature of wastewater in the tank T_5 (for setup 2). All experiments started with a new, clean bundle and OHTCs were defined with pure water. Then, tests with wastewater were conducted. Wastewater circulated in the fouling circuit (or in the tank) during the entire experiment. Tap water was pumped through the bundles only during measurements of OHTC once per several days to estimate fouling evolution. At the end of each experiment, the fouled heat transfer bundle was removed and inspected for the presence of deposits.

Tab. 10 *Review of conditions for wastewater fouling experiments*

Bundle	Wastewater type	Setup	Test conditions
no.1	Shower wastewater	1	14-day experiment, wastewater was changed once per week T_1 = 12 ˚C, T_3 = 30 ˚C, m_{12} = 0.12 kg/s, m_{34} = 0.26 kg/s
no.2	Laundry wastewater 1		35-day experiment, wastewater was changed once per week T_1 = 10 ˚C, T_3 = 30 ˚C, m_{12} = 0.13 kg/s, m_{34} = 0.27 kg/s
no.3	Laundry wastewater 2	2	94-day experiment, wastewater was changed once per week T_1 = 13 ˚C, T_5 = 42 ˚C, m_{12} = 0.13 and 0.067 kg/s
no.4			94-day experiment, wastewater was changed once per week T_1 = 13 ˚C, T_5 = 42 ˚C, m_{12} = 0.067 kg/s

The fouling process was monitored by measuring the reduction of the overall heat transfer coefficient (OHTC), which can be expressed as:

$$U = Q/(\Delta T_{lm} \cdot A_o) \tag{51}$$

where q is the exchanger heat transfer rate (W), A_o is the heat transfer surface area based on outer bundle surface (m^2) and ΔT_{lm} – is the logarithmic mean temperature difference (K). Fouling causes reduction of OHTC and can be expressed as fouling thermal resistance R_f [58]. It is given by

$$R_f = \frac{1}{U_f} - \frac{1}{U_0} \tag{52}$$

where U_f and U_0 are heat transfer coefficients for clean and fouled conditions.
During fouling, the deposit thickness generally reaches a constant asymptotic value R_{fa} [58]. If the fouling layer thermal conductivity and density are constant, the time evolution of the fouling thermal resistance can be expressed through the asymptotic value R_{fa} and fouling process time constant t_c as:

$$R_f(t) = R_{fa}\left(1 - e^{-t/t_c}\right) \tag{53}$$

6.2.4 Results and discussion. Fouling during forced convection (setup 1)

At the beginning of the experiment, a clean heat transfer coefficient was defined with pure water. For bundle no. 1, the OHTC obtained with pure water (1640 W/m^2 K) was higher than that obtained with shower wastewater (1430 W/m^2 K). The same behavior was observed for bundle no. 2; the OHTC of pure water was 2020 W/m^2K while the OHTC of laundry wastewater was 1750 W/m^2 K. This difference can be explained by the deviation of thermophysical properties of wastewaters from pure water and by changing the flow regime. It should also be noted that shower and laundry wastewaters have detergent residues and

produce foam and bubbles when moving in an unpressurized volume. In fact, the shell-side flow (setup 1) consisted of a water-foam mixture. It seems reasonable that such a mixture has a lower thermal conductivity, leading to a decrease of heat transfer.

Tab. 11 presents representative heat-transfer data covering the entire range of experiments. It includes the day of the experiment, mass flow rates of cooling water and wastewater (m_{12}, m_{34}), inlet and outlet temperatures of both streams (T_1, T_2, T_3, T_4), the heat transfer rate Q (calculated based on cooling water data), the log-mean temperature difference LMTD, OHTC U_{ov} and fouling thermal resistance R_f.

For shower wastewater, during two weeks no significant reduction of OHTC was observed (HTC values were similar to reference value). The small oscillation of HTC is related to the oscillation of flow rate and temperatures during measurements. Few solid particles were observed on the fiber surface at the end of the experiment. The bio-fouling presence was small, so what fouling did occur was particulate fouling. The low rate of biological growth is confirmed by the bacteria level and BOD of shower wastewater. Adhesion forces between particles and the fiber surface were not strong, so deposits could be removed relatively easily.

Fouling by laundry wastewater was much more intense than with shower wastewater. The heat exchange bundle was removed from the shell at the end of experiment (see Fig. 44). It had collected a great deal of viscous and sticky deposits consisting of biofilm and solid particles. The presence of bio-fouling was also confirmed by wastewater analysis: a high BOD and bacteria level.

Tab. 11 *Review of experimental results for bundles no.1 and no.2*

bundle	day	m_{12} kg/s	T_1 ˚C	T_2 ˚C	m_{34} kg/s	T_3 ˚C	T_4 ˚C	Q W	ΔT_{lm} ˚C	U_{ov} W/m^{2}K	R_f (m^{2}K)/W
no. 1	1	0.12	12.2	25.8	0.26	30.6	25.6	6880	8.4	1430	0
	2	0.12	12.0	24.3	0.25	28.4	24.2	6160	7.4	1440	-6.2E-06
	8	0.12	12.3	24.9	0.26	29.6	24.5	6300	7.9	1390	17.8E-06
	13	0.12	11.5	24.2	0.26	28.4	24.1	6410	7.7	1460	-14.2E-06
no. 2	1	0.13	11.3	23.3	0.27	27.3	21.4	6630	6.6	1750	0
	2	0.13	11.0	22.7	0.27	27.3	22.6	6480	7.6	1490	0.00010
	7	0.13	10.7	22.1	0.27	26.9	22.6	6130	7.8	1250	0.00023
	12	0.13	10.7	21.7	0.27	29.3	25.4	6090	10.8	980	0.00045
	19	0.13	10.4	21.7	0.27	30.0	26.6	6260	11.8	920	0.00052
	35	0.13	10.1	22.5	0.27	31.8	27.6	6450	13.0	860	0.00059

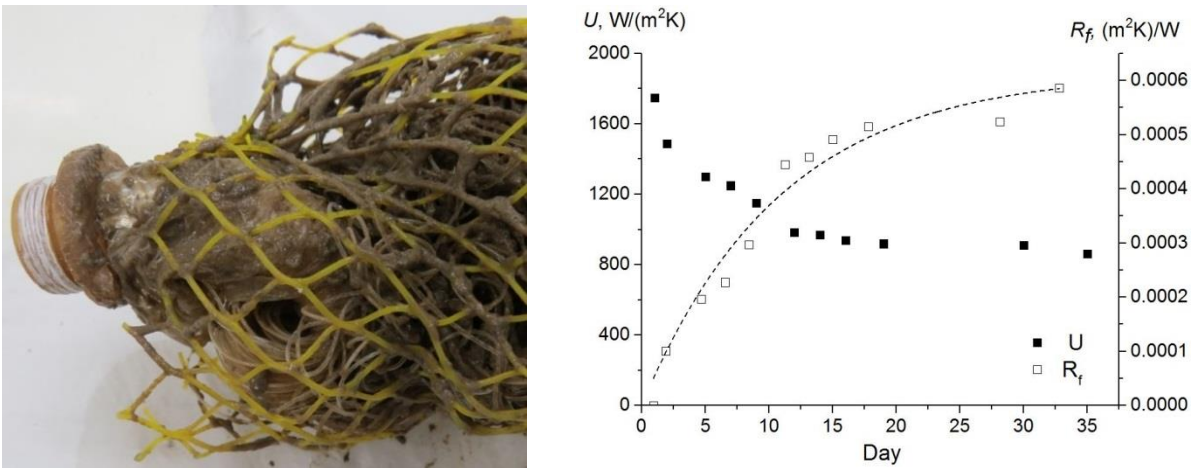

Fig. 44 *Heat exchange bundle no. 2 after 35-day experiment with laundry wastewater no. 2 (left) and fouling evolution in time: OHTC (black squares) and fouling thermal resistance (white squares).*

The OHTC decreased approximately twice during the 35-day experiment. The values of fouling thermal resistance were, by Equation 52 based on OHTC, fitted according to Equation 53. The asymptotic resistance R_{fa} = 0.00062 and time constant t_c = 12 were achieved, so Equation 53 can be used as $R_f(t) = 0.00062\left(1 - e^{-t/12}\right)$. Fig. 44 shows the evolution of OHTC and fouling thermal resistance. It can be concluded that fouling achieved approximately an asymptotic (maximum) value during the 35 days. The value of asymptotic fouling resistance R_{fa} is about 5 times higher that R_{fa} found by Chen [66]. This difference can be explained by different experimental conditions, including wastewater properties, type of heat transfer surface, and flow velocity.

6.2.5 Results and discussion. Fouling during natural convection (setup 2)

For bundle no. 3 and no. 4, the OHTCs obtained with pure water were 245 W/m^2 K and 260 W/m^2 K, respectively. There no significant differences between these values and OHTs obtained with wastewater on clean bundles were observed (236 W/m^2 K and 271 W/m^2 K respectively). Thus, in contrast to forced convection in the shell-and-tube section, no differences between pure water and wastewater were found for natural convection. A probable explanation is that there was no foam and bubbles from wastewater no.2 during natural convection.

In Tab. 12, the representative heat-transfer data for bundles no. 3 and no. 4 are presented. All values are as described before and T_5 is the temperature of wastewater in the accumulation tank. Fig. 45 shows bundles at the end of the experiment and a graph of the

fouling evolution. After the 94-day experiment only a few solid particles were observed on the surface of the bundles. It seems reasonable that bio-fouling did not occur due to the presence of chlorine used for washing bed linen. Small amounts of particles do not influence heat transfer much and no significant reduction of OHTC was observed (see Fig. 45).

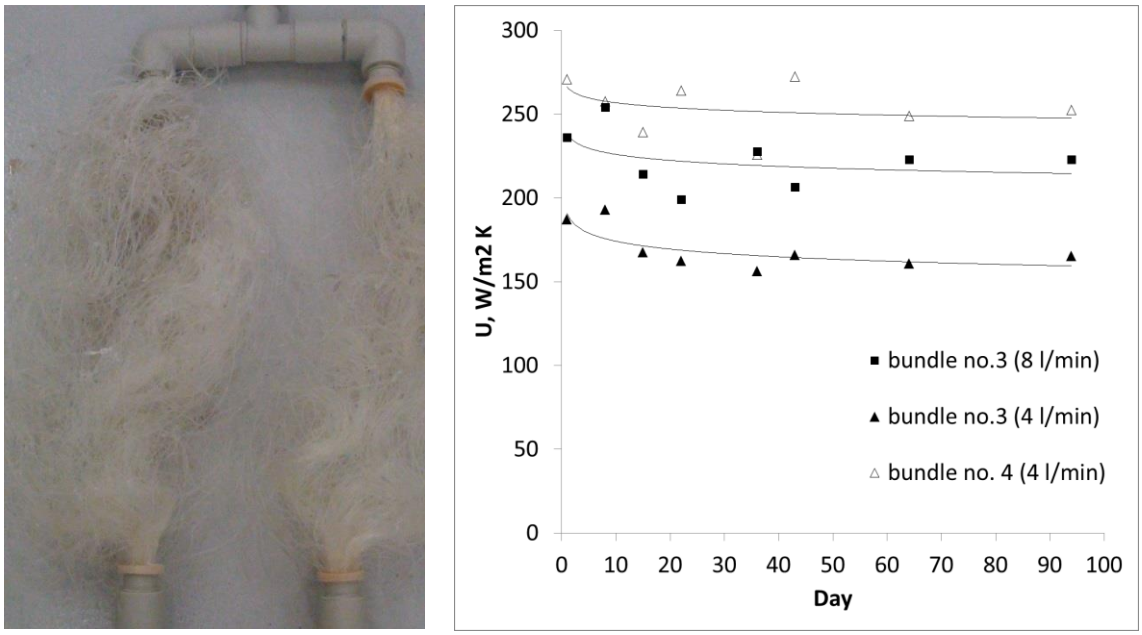

Fig. 45 *Heat exchange bundles no. 3 and no. 4 after 94-day experiment with laundry wastewater no. 2. and graph of fouling evolution in time.*

Tab. 12 *Review of experimental results for bundles no.3 and no.4*

bundle	day	m_{12} kg/s	T_1 ˚C	T_2 ˚C	T_5 ˚C	Q W	LMTD ˚C	U_{ov} W/m^2 K
3	1	0.130	11.2	20.4	43.5	5130	28.7	236
		0.067	11.5	23.8	43.0	3510	24.8	187
	8	0.130	11.5	21.0	42.8	5300	27.6	254
		0.067	11.9	25.3	43.0	3730	23.6	193
	36	0.130	11.9	19.7	42.6	4570	28.9	228
		0.067	12.1	22.8	41.0	3120	24.3	156
	64	0.130	13.3	21.3	41.1	4460	26.5	223
		0.067	14.4	23.7	40.3	2590	23.4	161
4	1	0.067	11.2	26.5	42.5	4000	23.7	271
	8	0.067	12.1	26.5	42.7	3970	23.4	258
	36	0.067	12.4	26.2	41.2	3840	21.9	264
	64	0.067	13.2	25.8	40.7	3510	21.2	249

CONCLUSION

The main object of interest of this thesis is polymeric hollow fiber heat exchangers (PHFHEs), a new type of devices which are made out of small diameter polymeric tubes. These devices were introduced in 2004 and were the object of interest of several studies. It was shown that the devices have a high thermal performance despite that they are made out of thermally non-conductive plastics; they are light, compact and chemically resistant. Despite some theoretical background proposed in previous papers, available information is insufficient and many issues required additionally studied. This thesis developed additional knowledge about PHFHEs.

The first part of this thesis provides basic information about heat exchanger and their classification. Special attention is paid to the characteristics of compact heat exchangers because the majority of PHFHEs should be considered as compact. Different characteristics of heat exchangers (including thermal performance criteria) are briefly discussed in the chapter. The main conclusion is that the cost of the whole heat transfer process should be considered as the most important parameter for the majority of applications. Other parameters (such a weight, dimensions or reliability) should be considered as additional, but may be more important than the price in certain conditions.

The second part of thesis deals with the current state of the art concerning application of plastic heat exchangers. Analysis of commercially available devices shows that applications are limited by several niches. More than 90% of installations are related to the radiant heating systems, chemical industry, or automotive and aerospace. This can be explained by the fact that metal heat exchangers have a long history and well-designed manufacturing technologies and, thus the companies do not want to depart from well-established practices. Plastic heat exchangers are used only in those conditions, where their advantages significantly predominate or where the use of non-plastic heat exchangers is not impossible. On the other hand, plastic heat exchangers are devices of increasing interest. Number of scientific publications, variety of commercially available designs and manufacturing companies constantly increase.

The third chapter is devoted to the review of published results and basic analysis of PHFHEs. Study of the available literature shows that at least three Master theses, one PhD thesis and about 20 scientific articles concerning PHFHEs were published since 2004. Furthermore, special attention is paid to justify using of hollow fibers. It was shown that small

diameter is a key point allowing to create heat exchanger with superior characteristics. The main findings are as follows:

- Small diameter reduces thermal resistance of polymer wall to the appropriate level and allows the fiber to withstand high internal pressure
- Due to small hydraulic diameter of a fiber, the heat transfer coefficients are high on both, the inside and the outside fiber surfaces
- Use of small diameter fiber is basic property provides high rate of compactness.

The fourth part provides deep theoretical background concerning fluid flow and heat transfer inside of a hollow fiber. Hollow fiber is considered as microchannel and appropriate theory from previous studies of microchannel is applied. Special attention is paid to the discussion about so-called "scaling effects", effects that are not significant in conventional tubes but are playing an important role in microchannels. The main conclusion is that the conventional microchannel theory is almost suitable to describe fluid flow and heat transfer inside a hollow fiber. However, several special points should be considered to prevent misleading results. The main finding of the chapter are as follows:

- Firstly, special attention should be paid to careful determination of fibers diameter. Equation 26 is recommended as appropriate for the hollow fiber with variable diameter.
- Thermally dependent thermophysical properties of liquid are strongly recommended for precise calculations. The most important is the use of the appropriate viscosity model.
- Influence of fiber surface roughness on fluid flow and heat transfer is mostly negligible. Our studies of polypropylene fiber surface showed that its roughness is low, typically lower than 0.002 and, thus, fibers such fibers should be considered as hydrodynamically smooth tubes.
- Influence of another microchannel scaling effects (axial heat conduction, thermal entrance region and viscous dissipation) has minor influence on heat transfer and fluid flow and can be neglected in majority of conditions.
- Equations 25, 28 and 29 are suitable for calculation of pressure drops and the inside Nusselt number. Equation 25 is verified by experimental results an appropriate correlation was found. Equation 28 is recommended for long hollow fibers (majority of cases) and Equation 29 is recommended for short fibers when

influence of thermal entrance region is more significant. Equations 28 and 29 were not verified by experimentally because it is not possible for PHFHEs (see detailed explanation in the Chapter 4.3).

- Author thinks that fluid flow and heat transfer inside of the fibers is well-known now and does not require any additional studies.

The fifth chapter is devoted to study of heat transfer across bunches of hollow fibers. This type of heat transfer surfaces can be used as a core of liquid-to-gas cross-flow heat exchangers. Several modules of PHFHEs were manufactured and studied experimentally. The main findings are the following:

- Heat exchange surface made of fibers has high thermal performance and appropriate pressure drops. It is competitive to heat transfer surface of contemporary compact aluminium heat exchanger (car radiator). Thus, from the thermal performance point of view, it can compete to the majority of conventional finned tube metal surfaces.
- The Churchill and Bernstein equation (for single cylinder) is not appropriate even for fiber structure with high pitches because it underestimates heat transfer.
- Grimson approach showed well agreement with experimental results and, thus it is recommended to predict heat transfer coefficients on fiber bunches.
- However, there is a large variety of different structures made of fibers. Some of them are significantly different from the structures studied in this thesis, therefore there is enough points which can be studied in the frame of fluid flow and heat transfer on fiber bunches.

The sixth chapter discusses the problem of fouling on the bundles of polymeric hollow fibers. It was found that such bundles have high values of overall heat transfer coefficient (up to 2100 W/m^2K) but, they are influenced by fouling in different ways. Two types of fouling (particulate fouling and biofouling) were experimentally studied.

- Concerning particulate fouling by titanium oxide particles, we can conclude that such kind of the fouling is not a significant problem. The low adhesion of the plastic surface can be sufficient precaution to prevent this kind of fouling. Maximum observed fouling resistance was up to $15*10^{-5}$ $(m^2K)/W$ and caused maximum reduction of overall heat transfer coefficient of 20% approximately. Moreover, it was shown that particulate deposit can be relatively easily removed

from the fiber surface by air bubbling (increase of fluid velocity). The defouling procedure was evaluated as adequately efficient because the bubbles destroyed the particle agglomerates and removed the main mass of deposit.

- Study of the fouling by wastewater showed that it strongly depends on the type of wastewater. Experiments with shower wastewater and with chlorinated laundry wastewater showed, that fouling is low because microorganisms growth do not occur, and fouling is associated with the accumulation of solid particles only (particulate fouling). In such case there is no large decrease of thermal performance even during a long-term operation. For instance, there was no significant decrease of overall heat transfer coefficient was observed in this case during 95-day experiment. However, fouling is much more intense when it is associated with both particulate fouling and bio-fouling. In this case, smooth and low-adhesive surface of plastic is not sufficient precaution to prevent high rate of fouling. For instance, when intense biofouling occurred, the thermal performance can decrease twice in approximately one month.

NOMENCLATURE

Latin symbols	unit	description
A	m^2	heat transfer area
A_c	m^2	flow area
A_s	m^2	surface area
C	W/K	heat capacity rate
CUV	W/m^3K	conductance per unit volume
c_b	kg/m^3	mass particle concentration
c_p	J/(kg K)	heat capacity
D	m	diameter
d_h	m	hydraulic diameter
F	-	LMTD correction factor
f		Darcy friction factor
h	W/m^2K	heat transfer coefficient
k	W/(m K)	thermal conductivity
k_a	m/s	adhesion coefficient
k_d	m/s	overall deposition coefficient
k_m	m/s	mass transfer coe¦cient
k_s	m	height of roughness
L	m	length
L^*	-	dimensionless length
ΔT_{lm}	K	logarithmic mean temperature difference
$\dot{m}$	kg/s	mass flow rate
N	-	number of tubes (fibers)
NTU	-	number of transfer units
M	-	dimensionless parameter defining of axial conduction
P	m	wetted perimeter
Q	W	heat transfer rate
Q_f	m^3/s	volumetric flow rate
r	m	radius
R	$(m^2 K)/W$	thermal resistance
t	s	time
t_c	s	fouling process time constant
T	ºC	temperature
ΔT	K	temperature difference
u	m/s	fluid velocity
U	W/m^2K	overall heat transfer coefficient
V	m^3	volume
V_s	m^3	vetted volume
x	m	axial coordinate

Greek symbols	unit	description
β	m^2/m^3	surface area density
ε	-	heat exchanger efficiency
$\Delta\theta_{ref}$	-	reference temperature rise
Λ	-	geometry factor
μ	kg/(m s)	dynamic viscosity
ν	m^2/s	kinematic viscosity
σ	-	porosity
ρ	kg/m^3	density
χ^+	-	dimensionless axial coordinate
Φ_d	kg/(s m^2)	deposition flux

Dimensionless numbers		description
Ec	$Ec = u^2/(2c_p\Delta\theta_{ref})$	Eckert number
Gz	$Gz = \frac{D_i}{L}RePr$	Graetz number
Gr	$Gr = \frac{g\,\beta(T_s - T_\infty)L^3}{\nu^2}$	Grashof number
Nu	$Nu = hD/k$	Nusselt number
Pe	$Pe = RePr$	Peclet number
Po	$Po = fRe$	Poiseuille number
Pr	$Pr = c_p\mu/k$	Prandtl number
Re	$Re = uD/\nu$	Reynolds number

Indices	description
a	absolute
av	average
b	bulk
i	inlet/inner
c	cold/cross-section
cr	critical
f	fluid/frontal/fouling
h	hot, hydraulic
lm	logarithmic
min	minimum
max	maximum
o	outlet/outer
ov	overall
ref	reference
s	surface
sh	shell
t	tube
T3	convection boundary condition (the third type)
w	wall

LIST OF FIGURES

LIST OF TABLES

REFERENCES

1. KAKAÇ, S. *Heat exchangers: selection, rating, and thermal design*. 3rd ed. Boca Raton: CRC Press, c2012. ISBN 978-1-4398-4990-3.
2. DIGIOVANNI, MARK A., RALPH L. WEBB. Uncertainty in Effectiveness-NTU Calculations for Crossflow Heat Exchangers. *Heat Transfer Engineering*. 1989, **10**(3), 61-70. DOI: 10.1080/01457638908939709. ISSN 0145-7632. Available from: http://www.tandfonline.com/doi/abs/10.1080/01457638908939709
3. HESSELGREAVES, J.E. *Compact heat exchangers: selection, design and operation*. 1st ed. Amsterdam: Pergamon, 2001. ISBN 00-804-2839-8.
4. KUPPAN, T. *Heat exchanger design handbook*. Second edition. ISBN 978-143-9842-126.
5. SHAH, R.K., *Compact Heat Exchanger Surface Selection, Optimisation and Computer-aided Design*, in Low Reynolds number Flow Heat Exchanger, ed. Kakac et al. Hemisphere, New York. (1983)
6. HOLMAN J. P. *Heat Transfer*. McGraw Hill Higher Education.
7. CALORPLAST HEAT EXCHANGERS. Available from: <http://www.calorplast-waermetechnik.de/category/products/?lang=en>
8. POLYTETRA HEAT EXCHANGERS. Available from: <http://www.polytetra.de/en/products.html>
9. AMETEK HEAT EXCHANGERS. Available from: <http://www.ametekfpp.com/Shell-and-Tube-Heat-Exchangers/index.aspx>
10. CESARONI HEAT EXCHANGERS. Available from: <http://www.cesaroni.net/polymericheat.php>
11. MAKATEK HEAT EXCHANGERS. Available from: <http://apparate.makatec.eu/en>
12. ZAHEED L., JACHUCK R.J.J., Review of polymer compact heat exchangers,with special emphasis on a polymer film unit. *Fuel and Energy Abstracts*. 2006, **47**(1), 43-. DOI: 10.1016/S0140-6701(06)80309-7. ISSN 01406701. Available from: http://linkinghub.elsevier.com/retrieve/pii/S0140670106803097
13. MAGEN ECO-ENERGY. Available from: <http://www.magen-ecoenergy.com/Products-Magen-Eco>
14. CHEN, L., LI ZH., GUO Z.Y. Experimental investigation of plastic finned-tube heat exchangers, with emphasis on material thermal conductivity. *Experimental Thermal and Fluid Science*. 2009, **33**(5), 922-928. DOI: 10.1016/j.expthermflusci.2009.04.001. ISSN 08941777. Available from: http://linkinghub.elsevier.com/retrieve/pii/S0894177709000570
15. LIU, W., DAVIDSON J. MANTELL S. Thermal Analysis of Polymer Heat Exchangers for Solar Water Heating: A Case Study. *Journal of Solar Energy Engineering*. 2000, **122**(2), 84-. DOI: 10.1115/1.1288027. ISSN 01996231. Available from:http://SolarEnergyEngineering.asmedigitalcollection.asme.org/article.aspx?articleid=1455995
16. SCHEFFLER, T.B., LEAO A.J. Fabrication of polymer film heat transfer elements for energy efficient multi-effect distillation. *Desalination*. 2008, **222**(1-3), 696-710. DOI: 10.1016/j.desal.2007.02.076. ISSN 00119164. Available from: http://linkinghub.elsevier.com/retrieve/pii/S0011916407008272

17. HORNUNG, H., HALLMARK B., HESKETH R.P. MACKLEY M.R. The fluid flow and heat transfer performance of thermoplastic microcapillary films. *Journal of Micromechanics and Microengineering*. 2006, **16**(2), 434-447. DOI: 10.1088/0960-1317/16/2/030. ISSN 0960-1317. Available from: http://stacks.iop.org/0960-1317/16/i=2/a=030?key=crossref.d33fac9d17b0466b7987a4e01675cb2e
18. HALLMARK, B., HORNUNG H., BROADY D., PRICE-KUEHNE CH., MACKLEY M.R. The application of plastic microcapillary films for fast transient micro-heat exchange. *International Journal of Heat and Mass Transfer*. 2008, **51**(21-22), 5344-5358. DOI: 10.1016/j.ijheatmasstransfer.2008.01.036. ISSN 00179310. Available from: http://linkinghub.elsevier.com/retrieve/pii/S0017931008001658
19. DORFLING, C., C.H. HORNUNG, B. HALLMARK, R.J.J. BEAUMONT, H. FOVARGUE a M.R. MACKLEY. The experimental response and modelling of a solar heat collector fabricated from plastic microcapillary films. *Solar Energy Materials and Solar Cells*. 2010, **94**(7), 1207-1221. DOI: 10.1016/j.solmat.2010.03.008. ISSN 09270248. Available from: http://linkinghub.elsevier.com/retrieve/pii/S0927024810001261
20. EL-DESSOUKY, T., M. ETTOUNEY. Plastic/compact heat exchangers for single-effect desalination systems. *Desalination*. 1999, **122**(2-3), 271-289. DOI: 10.1016/S0011-9164(99)00048-X. ISSN 00119164. Available from: http://linkinghub.elsevier.com/retrieve/pii/S001191649900048X
21. ZAHEED, L., JACHUCK R. Performance of a square, cross-corrugated, polymer film, compact, heat-exchanger with potential application in fuel cells. *Journal of Power Sources*. 2005, **140**(2), 304-310. DOI: 10.1016/j.jpowsour.2004.08.024. ISSN 03787753. Available from: http://linkinghub.elsevier.com/retrieve/pii/S0378775304009012
22. BURNS, J.R, JACHUCK R. Condensation studies using cross-corrugated polymer film compact heat exchanger. *Applied Thermal Engineering*. 2001, **21**(4), 495-510. DOI: 10.1016/S1359-4311(00)00063-6. ISSN 13594311. Available from: http://linkinghub.elsevier.com/retrieve/pii/S1359431100000636
23. HAZAMI, M., KOOLI S., LAZAAR M., FARHAT A., KERKANI CH., BELGUITH A. Capillary polypropylene exchangers for conditioning of museum aquariums (Tunisia). *Desalination*. 2004, **166**, 443-448. DOI: 10.1016/j.desal.2004.06.099. ISSN 00119164. Available from: http://linkinghub.elsevier.com/retrieve/pii/S0011916404003273
24. ZARKADAS, D., SIRKAR K.K. Polymeric Hollow Fiber Heat Exchangers: An Alternative for Lower Temperature Applications. *Industrial*. 2004, **43**(25), 8093-8106. DOI: 10.1021/ie040143k. ISSN 0888-5885. Available from: http://pubs.acs.org/doi/abs/10.1021/ie040143k
25. CHRISTIAN, S. Investigation of Solid Polymeric Hollow Fiber Heat Exchange Devices for Use in Thermally-Driven Desalination. M.S. Thesis. Otto H. York Department of Chemical Engineering, New Jersey Institute of Technology, 2005.
26. SONG, L., LI B., ZARKADAS D., CHRISTIAN S., SIRKAR K.K. Polymeric Hollow-Fiber Heat Exchangers for Thermal Desalination Processes. *Industrial*. 2010, **49**(23), 11961-11977. DOI: 10.1021/ie100375b. ISSN 0888-5885. Available from: http://pubs.acs.org/doi/abs/10.1021/ie100375b

27. QIN, Y., LI, B., WANG, SH. Experimental Investigation of a Novel Polymeric Heat Exchanger Using Modified Polypropylene Hollow Fibers. *Industrial*. 2012, **51**(2), 882-890. DOI: 10.1021/ie202075a. ISSN 0888-5885. Available from: http://pubs.acs.org/doi/abs/10.1021/ie202075a
28. ZHAO, J., LI B., LI X., QIN Y., LI CH., WANG SH. Numerical simulation of novel polypropylene hollow fiber heat exchanger and analysis of its characteristics. *Applied Thermal Engineering*. 2013, **59**(1-2), 134-141. DOI: 10.1016/j.applthermaleng.2013.05.025. ISSN 13594311. Available from: http://linkinghub.elsevier.com/retrieve/pii/S1359431113003876
29. YAN, X., LI B., LIU B., ZHAO J., WANG Y., LI H., Analysis of improved novel hollow fiber heat exchanger. *Applied Thermal Engineering*. 2014, **67**(1-2), 114-121. DOI: 10.1016/j.applthermaleng.2014.03.021. ISSN 13594311. Available from: http://linkinghub.elsevier.com/retrieve/pii/S1359431114001963
30. RAUDENSKY M., DOHNAL M., (2012), Large scale capillary based plastic heat exchangers, *Chemical Engineering Transactions*, 29, 1477-1482
31. PARTZSCH, A., Kunststoffhohlfasern und ihre Eignung in Wärmetauschern.-2007-68 S. Leipzig, Hochschule Mittweida (FH), Fachbereich Mathematik, Physik, Informatik; Diplomarbeit, 2007 (In German language)
32. GALLIK R., Výskum tepelných výmenníkov z polypropylénových vlákien. Písomná časť k dizertačnej skúške. Košice: Technická univerzita v Košiciach, Strojnícka fakulta, 2013, 117 s. (In Slovak language)
33. WEIß K., Untersuchung des konvektiven Wärmeübergangs und des strömungstechnischen Verhaltens von Kunststoffhohlfaserwärmeübertragern, Masterarbeit, Fakultät für Maschinenbau und Verfahrenstechnik, Hochschule Augsburg, Germany, 2014. (In German language)
34. SCHMIDT M., Leistungsoptimierung eines Photovoltaikmoduls durch Kühlung mittels Kunststoffhohlfaserwärmeübertrager, Masterarbeit, Fakultät für Maschinenbau und Verfahrenstechnik, Hochschule Augsburg, Germany, 2014. (In German language)
35. Thermally Conductive Plastics For Heat Exchangers. Available from: <http://www.coolpolymers.com/heatexchangers.asp>
36. T'JOEN, C., Y. PARK, Q. WANG, A. SOMMERS, X. HAN a A. JACOBI. A review on polymer heat exchangers for HVAC. *International Journal of Refrigeration*. 2009, **32**(5), 763-779. DOI: 10.1016/j.ijrefrig.2008.11.008. ISSN 01407007. Available from: http://linkinghub.elsevier.com/retrieve/pii/S0140700708002272
37. HERWIG H., Flow and Heat Transfer in Micro Systems: Is Everything Different or Just Smaller? ZAMM - Journal of Applied Mathematics and Mechanics / Zeitschrift für Angewandte Mathematik und Mechanik. Volume 82, Issue 9, pages 579–586, September 2002
38. YARIN L.P., MOSYAK A., HETSRONI G., (2009) Fluid Flow, Heat Transfer and Boiling in Micro-Channels Berlin: Springer
39. TSO, C.P., S.P. MAHULIKAR. Experimental verification of the role of Brinkman number in microchannels using local parameters. *International Journal of Heat and Mass Transfer*. 2000, **43**(10), 1837-1849. DOI: 10.1016/S0017-9310(99)00241-0. ISSN 00179310. Available from: http://linkinghub.elsevier.com/retrieve/pii/S0017931099002410

40. GAD-EL-HAK, M. Comments on "critical view on new results in micro-fluid mechanics". *International Journal of Heat and Mass Transfer*. 2003, **46**(20), 3941-3945. DOI: 10.1016/S0017-9310(03)00191-1. ISSN 00179310. Available from: http://linkinghub.elsevier.com/retrieve/pii/S0017931003001911
41. OWHAIB, W., PALM, B. Experimental investigation of single-phase convective heat transfer in circular microchannels. *Experimental Thermal and Fluid Science*. 2004, **28**(2-3), 105-110. DOI: 10.1016/S0894-1777(03)00028-1. ISSN 08941777. Available from: http://linkinghub.elsevier.com/retrieve/pii/S0894177703000281
42. HERWIG, H., HAUSNER, O. Critical view on "new results in micro-fluid mechanics": an example. *International Journal of Heat and Mass Transfer*. 2003, **46**(5), 935-937. DOI: 10.1016/S0017-9310(02)00306-X. ISSN 00179310. Available from: http://linkinghub.elsevier.com/retrieve/pii/S001793100200306X
43. MORINI, G. L. Viscous heating in liquid flows in micro-channels. *International Journal of Heat and Mass Transfer*. 2005, **48**(17), 3637-3647. DOI: 10.1016/j.ijheatmasstransfer.2005.01.011. ISSN 00179310. Available from: http://linkinghub.elsevier.com/retrieve/pii/S0017931005000888
44. MARANZANA, G., PERRY I., MAILLET, D. Mini- and micro-channels: influence of axial conduction in the walls. *International Journal of Heat and Mass Transfer*. 2004, **47**(17-18), 3993-4004. DOI: 10.1016/j.ijheatmasstransfer.2004.04.016. ISSN 00179310. Available from: http://linkinghub.elsevier.com/retrieve/pii/S0017931004001541
45. PETUKHOV, B.S., Heat Transfer and Friction in Turbulent Pipe Flow with Variable Physical Properties, 503. DOI: 10.1016/S0065-2717(08)70153-9. Available from: http://linkinghub.elsevier.com/retrieve/pii/S0065271708701539
46. INCROPERA, F.P. *Fundamentals of heat and mass transfer*. 6th ed. /. Hoboken, NJ: John Wiley, c2007. ISBN 978-047-1457-282.
47. ZARKADAS, D.M., SIRKAR, K.K., Incremental heat transfer number for laminar flow in circular tubes with the boundary condition of the third kind and simple design formula for shell and tube laminar flow heat exchangers with constant external resistance. *Int. J. Transp. Phenom.* 7 (4), pp. 297–306.
48. CELATA, G.P., CUMO, M., MARCONI, V., MCPHAIL S.J., ZUMMO, G., Microtube liquid single-phase heat transfer in laminar flow. *International Journal of Heat and Mass Transfer*. 2006, **49**(19-20), 3538-3546. DOI: 10.1016/j.ijheatmasstransfer.2006.03.004. ISSN 00179310. Available from: http://linkinghub.elsevier.com/retrieve/pii/S001793100600189X
49. MARK, J.E. *Polymer data handbook*. 2nd ed. New York: Oxford University Press, 2009. ISBN 01-951-8101-8.
50. HETSRONI, G., MOSYAK, A., POGREBNYAK, E., YARIN, L.P. Fluid flow in micro-channels. *International Journal of Heat and Mass Transfer*. 2005, **48**(10), 1982-1998. DOI: 10.1016/j.ijheatmasstransfer.2004.12.019. ISSN 00179310. Available from: http://linkinghub.elsevier.com/retrieve/pii/S0017931005000244
51. MALA M., LI G.D. Flow characteristics of water in microtubes. *International Journal of Heat and Fluid Flow*. 1999, **20**(2), 142-148. DOI: 10.1016/S0142-727X(98)10043-7. ISSN 0142727x. Available from: http://linkinghub.elsevier.com/retrieve/pii/S0142727X98100437

52. GUO, Z.Y., LI, Z.X. Size effect on microscale single-phase flow and heat transfer. *International Journal of Heat and Mass Transfer*. 2003, **46**(1), 149-159. DOI: 10.1016/S0017-9310(02)00209-0. ISSN 00179310. Available from: http://linkinghub.elsevier.com/retrieve/pii/S0017931002002090
53. NIKURADSE J., Strmungsgesetze in rauhen rohren, V.D.I. Forschungsheft 361 (1933) 1–22 J. NIKURADSE, Strömungsgesetze in rauhen Rohren. Forschungsheft 361, VDI-Verlag, Berlin 1933.
54. MOODY L.F., Friction factors for pipe flow, *Trans. ASME* 66 (1944) 671–684.
55. WEISS K., ASTROUSKI I., REPPICH M., RAUDENSKÝ M. Polymeric hollow fiber bundle as immersed heat exchanger (in press)
56. JAMES M. (1999) Polymer Data Handbook. Oxford University Press, Inc.
57. JETER S. M. Effectiveness and LMTD Correction Factor of the Cross Flow Exchanger: a Simplified and Unified Treatment. 2006 ASEE Southeast Section Conference
58. BOTT, T. R., 1995, *Fouling of Heat Exchangers*. Elsevier, Amsterdam.
59. GRANDGEORGE, S., C. JALLUT a B. THONON. Particulate fouling of corrugated plate heat exchangers. Global kinetic and equilibrium studies. *Chemical Engineering Science*. 1998, **53**(17), 3050-3071. DOI: 10.1016/S0009-2509(98)00128-6. ISSN 00092509. Available from: http://linkinghub.elsevier.com/retrieve/pii/S0009250998001286
60. WICAKSANA, F., FANE, A.G., CHEN V. Fiber movement induced by bubbling using submerged hollow fiber membranes. *Journal of Membrane Science*. 2006, **271**(1-2), 186-195. DOI: 10.1016/j.memsci.2005.07.024. ISSN 03767388. Available from: http://linkinghub.elsevier.com/retrieve/pii/S0376738805005569
61. ASTROUKI, I., RAUDENSKY, M., DOHNAL, M. Particulate Fouling of Polymer Hollow Fiber Heat Exchanger, in: Heat Exchanger Fouling and Cleaning, M.R. Malayeri, H. Müller-Steinhagen and A.P. Watkinson (eds.), Budapest, 2013, pp. 233–239.
62. CHEMSOF LMTD Correction Factor Charts Available from: <http://www.chemsof.com/lmtd/lmtd.htm>
63. RAMM-SCHMIDT, L. Taking the heat. 2006. Available from: <www.chemitec.fi/uploads/files/783heat1.pdf>
64. HEPBASLI A., BIYIK E., EKREN O., GUNERHAN H., ARAZ M. A key review of wastewater source heat pump (WWSHP) systems. *Energy Conversion and Management*. 2014, **88**, 700-722. DOI: 10.1016/j.enconman.2014.08.065. ISSN 01968904. Available from: http://linkinghub.elsevier.com/retrieve/pii/S0196890414007900
65. CHEN, Z. F., YAN, Z. S. (2006). Application analysis of plastic heat exchanger in sewage source heat pump systems [J]. *Journal of Harbin University of Commerce (Natural Sciences Edition)*, *3*, 016.
66. CHEN Z.F. Application prospect of plastic heat exchanger in sewage source heat pump systems. *MSIE 2011*. IEEE, 2011, 1184-1187. DOI: 10.1109/MSIE.2011.5707631. ISBN 978-1-4244-8383-9. Available from: http://ieeexplore.ieee.org/lpdocs/epic03/wrapper.htm?arnumber=5707631